VELOCITY PROFILES AND TURBULENCE IN THE AORTA:

A STUDY BY HOT-FILM ANEMOMETRY

A Thesis submitted to the University of London for the Degree of Doctor of Philosophy in the Faculty of Medicine, 1972.

by William Anthony Seed

Physiological Flow Studies Unit,
Imperial College,
London.

ABSTRACT

This thesis describes experimental observations on the form of velocity profiles and the incidence and nature of flow disturbances and turbulence in the aorta.

The work is presented in two parts. In the first, the technique of constant temperature hot-film anemometry, and its possible application to measurement of point blood velocity in arteries, is discussed. The development and evaluation of a probe designed for intra-arterial use is described, and the performance of the probe and anemometer system in steady, unsteady and turbulent flows of water and blood are evaluated. The system is shown to be capable of registering arterial point velocities with acceptable limitations of accuracy and frequency response.

The second part describes measurements made with this system in the aorta of dogs. Velocity profiles in the thoracic and abdominal aorta are shown to be blunt, with boundary-layers estimated to be less than 2 mm. thick throughout the cycle; significant skews are demonstrated, the explanation for which appears to lie in the influence of local geometry on the flow. A study of flow disturbances in the aorta, based on visual observation of instantaneous velocity waveforms and frequency spectral analysis, is also reported. Turbulence is shown to occur, its appearance being related to peak

Reynolds number and the frequency parameter α ; its possible origins are considered.

The physiological significance of the observations, their applicability to normal conditions in the conscious animal and man, and their possible implications in terms of arterial wall pathology and vascular sound production are discussed. Worthwhile further applications of the technique are outlined.

CONTENTS

INTRODUCTION

The main object of this study has been to extend the very sparse information previously available on the form of blood velocity profiles within the aorta during the cardiac cycle, and to examine the nature and extent of any high-frequency disturbances, and particularly turbulence, which might occur in the aorta under physiological conditions. An arterial flow velocity probe with good spatial discrimination and a high frequency response was therefore developed, and used to examine instantaneous velocity waveforms from point to point within the aorta of the dog.

Apart from their intrinsic interest, such measurements are relevant to a number of questions in cardiovascular physiology. It has been demonstrated that both the endothelial surface (Fry, 1968) and the arterial wall (Roach, 1963) are sensitive to local hydrodynamic events, and recently Caro, Fitz-Gerald & Schroter (1970) have postulated that low wall shear rates are important in dictating sites of atherogenesis. Similarly, flow regimes are of interest in terms of their influence on mixing and mass transfer processes, pressure-flow relations, and the generation of audible sounds. In addition, many techniques which have been used to measure instantaneous volume flow rate (or the related quantity, instantaneous cross-sectional mean velocity) depend for their accuracy on some assumption about the velocity profile. For

example, the pressure gradient technique used by Fry, Mallos & Casper (1956), mentioned below, assumed entry conditions with a uniform velocity distribution; and the assumption of an axisymmetric velocity profile is inherent in the use of cuff electromagnetic flowmeters (Shercliff, 1962). Similarly, catheter-tip velocity transducers tend to register the velocity close to them and may therefore be sensitive to the velocity profile. The quantitative use of some ultrasonic Doppler techniques for blood velocity measurement also involves some assumption about the form of the velocity profile.

Many of these techniques are applied in the proximal aorta, where it has been universally assumed that entry conditions exist, with a very thin boundary layer surrounding a broad fluid core which moves with uniform velocity. This assumption needs confirmation; Kuchar & Ostrach (1967) have pointed out that whilst entry conditions almost certainly exist in the ascending aorta, it is not certain whether conditions upstream (in the left ventricle and at the aortic valve) will produce a uniform velocity profile. Furthermore, the proximal aorta is not a straight pipe, and asymmetries might therefore be expected in the region of the bends, their shape depending on the presence or absence of viscous shear, and its form. In a viscous flow with relatively thick boundary-layers, the centrifugal pressure gradient which occurs in a bend produces a helical

motion, the faster moving core streamlines being swept to the outside of the bend (Goldstein, 1938). In an inviscid flow, with a flat velocity profile, there would be no such secondary motion; in this case the pressure gradient would be balanced by an acceleration of the streamlines near the inside wall. An inlet flow with thin viscous boundary layers and an inviscid core represents an intermediate situation and thus the flow patterns there depend strongly upon boundary layer growth and local geometry.

Although direct measurements of the axial components of velocity (the object of this study) clearly cannot describe the time-varying and three-dimensional flows to be expected in such a system, they should yield useful information about the relative importance of viscous and inertial factors, the form of the inlet flow, and the major geometric influences. In particular, there appears to be a lack of information, either theoretical or experimental, about oscillatory flow superimposed upon a steady flow in curved pipes.

Direct evidence about turbulence in arteries is also of interest. Both practical and theoretical difficulties have retarded the study of arterial flow disturbances and the possible transition to turbulence. In general, engineering studies have examined turbulence and transition primarily in steady flows, and there have been few studies of the stability of pulsating pipe flows. Those which have

been carried out (Yellin, 1966; Sarpkaya, 1966) centred primarily around the growth and decay of disturbances in sinusoidally accelerating and decelerating flows, but the conditions differed considerably from those to be expected in large arteries, since the boundary layers were thick, and the oscillatory components of the flow were small compared with the mean. This corresponds to domination of transition by the mean flow properties, and thus discussion of the onset of turbulence in arterial flow has been largely speculative, based on comparison with steady flow regimes. Such speculation has suggested that turbulence might occur in larger arteries during systole. The few attempts which appear to have been made to examine arterial flow in vivo, either by direct cinematography of injected dye (McDonald, 1952) or by cineradiography (Ohlsson, 1962) have tended to bear this out. Flow visualisation techniques are, however, difficult to interpret in phasic flow, since they are observed locally and for short periods, and almost any disturbance (vortex streets, secondary motion) may affect the dyestream and look like turbulence. Similarly, the standard technique, that of demonstrating the breakdown of the Poiseuille pressure-flow relationship, is inapplicable, and therefore point velocity measurement, with an instrument capable of following high frequency fluctuations, becomes extremely attractive.

At the outset of this work there was no satisfactory method available for the measurement of velocities from point to point within arteries. Attention had been largely concentrated on the measurement of volume flow, or of a cross-sectional average velocity from which volume flow could be derived. Thus although Frank (1928), and later Müller (1954), in attempting to apply the principle of the Pitot flowmeter for arterial measurements, pointed out that local velocity measurements were of considerable intrinsic interest, most physiologists considered that the existence of the velocity profile would merely complicate the derivation of the really important parameter, volume flow, from measurements of point velocity. Partly because of the small pressure differences between the dynamic and static tappings of a Pitot probe within an artery, and partly because of difficulties due to the non-linear calibration characteristics of such devices, neither Frank nor Müller derived quantitative data in arteries. Baxter & Pearce (1951) did obtain calibrated velocity records with this technique in the pulmonary artery of the cat. The waveforms are probably distorted, since the differential pressure signals were linearised electronically on the basis of the steady flow Bernoulli equation, pressure drops due to local inertia being ignored. This would not affect peak velocities and the quoted values (50-80 cm/sec) should be reliable. This paper is of historical interest, since it presents probably the earliest measurements of

phasic velocity ever made in the pulmonary artery, and the only successful application of the Pitot technique in arteries; however no attempt was made to explore velocity profiles, the probe being rigidly mounted on the centre-line of the(cannulated) vessel.

The Pitot technique has also been used in veins (Mixter, 1953), and has recently been revived for studies of flow within the heart (Taylor & Whamond, 1972).

A number of other pressure gradient techniques have been used to derive instantaneous point velocity in arteries. Fry, Mallos & Casper (1956), and later Porje and Rudewald (1961),employed the longitudinal pressure gradient within a vessel, but a necessary assumption in this technique was that viscous energy losses were very small, so that it can only be applied in inviscid flow such as entry regions with flat velocity profiles; it does not permit the exploration of boundary layer regions where viscous effects become important. The basic equations of fluid motion were applied much more fully by Womersley (1955) to oscillatory pipe flow. Here, viscous terms were not approximated, and the solutions allow the derivation of both velocity distribution and instantaneous cross-sectional average velocity from the pressure gradient. McDonald (1955) shows good agreement between velocity waveforms measured directly in the femoral artery of the dog by high speed cinematography of injected air bubbles and calculated by means of Womersley's equations from the

pressure gradient measured at the same time. However, restrictive simplifications (assuming rigid walls and a straight pipe far from entrance conditions) limit the application of this method also, and these techniques, which dropped out of use largely because of the demands they make on manometer performance and experimental technique, all involve the assumption of laminar flow and are incapable of detecting turbulence. For all these reasons they are inherently unsuitable for exploratory studies of arterial velocity patterns.

The catheter-tip form of electromagnetic flow probe (Mills, 1966; Mills & Shillingford, 1967) provides some degree of spatial discrimination, apparently responding to flow velocity within approximately one radius (1.25 mm.) of its surface. The signal is therefore effectively derived from a circular region of the flow cross-section approximately 5 mm. in diameter, which gives it only coarse discriminatory ability in a sheared flow, and prevents its use close to vessel walls. It will also be insensitive to eddies and velocity fluctuations on a scale much smaller than 5mm., even if they are convected past it slowly enough for the perturbation to lie within its frequency response (up to approximately 80 Hz). Thus it is also unsatisfactory for the examination of flow disturbances and turbulence.

A number of attempts have been made to develop heat transfer techniques for the measurement of blood flow

velocity. The earliest work appears to be that of Machella (1936), who used a fine wire stretched across the diameter of the vessel and heated it by constant current. Such a system measures some function of cross sectional average velocity and is liable to errors due to strain-gauging of the wire - i.e. stretching, and therefore resistance changes, due to inertial and drag forces; this may be non-linearly related to velocity. In addition, since the wire has a finite mass whose temperature is allowed to vary, frequency response is limited; as McDonald (1960) points out, Machella's records show appreciable phase lags, which are probably a reflection of this. Like other heat transfer techniques, the method is non-directional, so that all signals are registered with the same polarity. Machella does not discuss this, and appears to have assumed that arterial flow was unidirectional; nonetheless his measurements clearly demonstrated the pulsatility of arterial flow and the magnitude of the velocities involved and have particular relevance here, since the constant current anemometer he employed was the direct precursor of the constant temperature anemometer to be described in this thesis.

Heated thermistors have also been employed for the measurement of blood flow velocity. Katsura, Weiss, Baker & Rushmer (1959) developed a constant-temperature heated thermistor probe, but found its frequency response inadequate for arterial measurements because of its thermal mass.

A catheter tip probe operated on the same principle, but employing miniature thermistors to improve frequency response, was described by Grahn, Paul & Wessel (1968, 1969), but intravascular measurements were not presented and only qualitative evidence about the frequency response was offered. This type of device, which operates on exactly the same principle as the hot film system to be described here, clearly has the potential for good spatial discrimination.

Constant current anemometry, the technique used by Machella, has a long history; the basic equation governing heat transfer from a fine wire by forced convection was published by King in 1914, and the system found many applications in aeronautical engineering, despite the limitations of frequency response and the extreme fragility of the very fine wires needed for good spatial discrimination. These drawbacks were in good part overcome by the development of constant temperature hot film anemometry (Ling, 1960) in which the wire was replaced by a thin metallic film mounted on a rigid supporting substrate, and the frequency response, greatly degraded in the constant current mode by the presence of the substrate, was improved by operating the film at constant temperature.

There were a number of features which made the hot film constant temperature system attractive as a starting point for a technique to measure point velocity within arteries. It appeared feasible to miniaturise the sensor element on

a needle probe; appropriate electronic circuits for controlling the sensor had reached a high degree of development, and were available commercially; and on theoretical grounds a system of this kind could be predicted to have a good frequency response when used in a liquid like water or blood.

The text which follows describes the development of a needle-mounted probe of this type and measurements made with it of blood flow velocity in the aorta of the dog.

During the period in which the work described in this thesis was carried out, two other groups (Ling et al, 1968; Schultz et al, 1969) have applied the same principle for arterial measurements, though with considerable differences in detailed technique. These, and the respective experimental results, will be assessed in the text. The literature on arterial hot film measurements appears to be still growing, and recently, another laboratory has adopted the technique (Francis, Kiser & Falsetti, 1972). Accounts of the work described in this thesis have also been published and are listed at the end of the references.

SECTION 1: DEVELOPMENT AND EVALUATION OF HOT-FILM SYSTEM

GENERAL CONSIDERATIONS

Principle of constant temperature hot-film system

A constant temperature anemometer circuit (Fig.1) consists of a Wheatstone bridge in the feedback loop of a high gain DC amplifier. The sensor is connected as one arm of the bridge; in the opposite arm is a variable reference resistance, usually in the form of a set of series resistance decades. The bridge output is applied as the input to the amplifier, and the amplifier output is in turn used to power the bridge. The sensor, in the case of film probes, is an extremely small resistive metallic strip mounted on a rigid insulating substrate (usually pyrex glass) and built into a probe which is connected to the anemometer by a cable.

The instrument is set up under open-loop conditions, by matching the variable resistance exactly to that of the film and then increasing it by a fixed proportion - the overheat. When the loop is closed, this preset bridge imbalance produces an imbalance at the input to the amplifier, and thus an output voltage across the arms of the bridge. The film therefore heats up, and since it has a positive temperature coefficient of resistance, this brings the bridge into balance. Thereafter, provided the frequency response of the anemometer is flat over a sufficient range

to keep the film temperature constant, heat loss from the film is proportional to the power supplied to the bridge.

Steady flow response

The voltage output from the amplifier, V, is approximately related to fluid velocity past the film, u, by:

$$V^2 = V_0^2 + Bu^{\frac{1}{2}} . \Delta T$$

(King, 1914), where V_0 is the signal at zero flow, B is a constant depending on fluid properties, probe shape and dimensions and bridge ratio, and ΔT is the temperature difference between the film and environment, dictated by the overheat. Intrinsically, the system does not distinguish forward from backward flow, and, for physiological measurements, means must be provided for this.

Obviously, ΔT has a strong influence on the sensitivity of the system, and in engineering applications the films are operated as hot as possible. In blood, excess temperature must be limited, both to prevent the accumulation of fibrin and platelets on the film, and to prevent damage to blood constituents. Fibrinogen, the most thermolabile constituent of plasma (Mcfarlane, 1960), is denatured above 47°C, and above 48°C red cell damage also occurs (Ham, Shen, Fleming & Castle, 1948). Except where specifically stated, overheat has been limited in this study to 1%, which yields an excess temperature of approximately 5°C in the gold and platinum films used.

The relationship between flow velocity and anemometer voltage output described by King's equation is obviously non-linear; its form can be seen in Figs. 3 and 9a, for example. Linearisation of the voltage-velocity relationship can be achieved over almost all the range of interest with commercially available linearising circuits; this technique was employed in all the animal studies presented here. In probe evaluation studies the anemometer output was recorded direct, since King's equation does not hold rigorously during transition from free to forced convection at very low velocities and linearisation becomes approximate below about 5 cm/s. Direct outputs were therefore necessary for assessment of the zero stability of the system and for direct comparison of signals obtained in steady and unsteady flow at very low velocities.

Unsteady flow response

A number of influences can cause departure from King's law in unsteady flow, and analysis of these effects is crucial where oscillatory flows are to be measured. Fourier analysis of flow waveforms in major arteries shows that harmonics up to the eighth may have significant amplitude (Ferguson & Wells, 1959; Bergel & Gessner, 1966); thus the velocity waveform in the dog aorta may be expected to contain components of significant amplitude up to approximately 25 Hz; if present, superimposed flow disturbances, particularly turbulence, will reach much higher frequencies. In fully developed turbulence, the maximum

amplitude will occur at some 'centre' frequency which will be of the order of $\frac{u}{L}$, where u is velocity and L is an appropriate dimension such as vessel diameter. About this centre frequency, amplitudes decay progressively to zero. Thus at a systolic velocity of 100 cm/s, in a vessel 1 cm. in diameter, frequencies well over 100 Hz will occur in turbulent flow.

The ideal instrument will have a flat frequency response. In practice, three sources of disturbance must be considered with hot film systems:

1. Fluid dynamic effects

Heat transfer from a body exposed to fluid flow depends on the form of the velocity and temperature gradients - that is, boundary layers - which develop at the surface. In steady conditions, and in unsteady conditions where velocity perturbations are small compared with the mean (Lighthill, 1954), the relationship can be examined theoretically; but where perturbations are large, and particularly where flow reversal occurs, it is difficult to apply existing theory rigorously. It is clear, however, that a change in stream velocity has to modify the boundary-layer growing along the probe from its tip before the hot film can respond. With a tip-to-film distance of x cm., and stream velocity u, the time taken to modify the boundary-layer will be of the order of x/u; and this must be small in comparison with the cycle-time (1/f, where f is frequency) if the film response is to 'keep up' with

the velocity oscillation. Thus the ratio fx/u must be small compared to unity if steady heat-transfer conditions and calibrations are to hold. Near zero velocity, this requirement inevitably breaks down, and the situation is further complicated by rectification of the signal, which introduces higher harmonics than are present in the flow waveform. Figure 2 illustrates the effect this may have. The ideal and predicted hot film responses are superimposed upon a velocity waveform redrawn from an electromagnetic flowmeter record; as fx/u becomes large, the probe cannot respond fast enough to give a zero signal at zero flow. This reinforces the need for a means of direction sensing which will allow reconstruction of the true velocity history, and indicates that body length is an important feature of probe design.

2. Thermal dynamic effects

Part of the heat generated by the film will be conducted into the substrate on which it is mounted. In unsteady flow, fluctuating thermal gradients may be set up in the substrate whose time course is different from the flow fluctuations, and which may therefore distort the flow signal. This problem has been treated by Bellhouse & Rasmussen (1968), who analysed mathematically heat conduction in a one-dimensional film-substrate model. This is a simplified situation, but they concluded that again errors would increase with diminishing velocity, and also with increasing frequency and substrate dimensions. They also

concluded that these effects should be slight in fluids such as water and blood, whereas the frequency response would be greatly degraded in air.

3. Electrical effects

These are extremely difficult to assess, since the overall behaviour of the system depends on a number of interacting factors. High current-generating capacity (transconductance) in the anemometer amplifier is an obvious prerequisite, since it is the power source which heats the film; and amplifier loop-gain must also be high if the changes in film temperature which produce the input voltage are to be kept small and corrected rapidly. These are characteristics of commercially available anemometers. However, the rapidity of the response is controlled in part by the small but finite thermal inertia of the film, and the amplitude by the temperature coefficient of resistance. These characteristics interact with the purely electrical properties of the circuit in a manner which cannot be calculated accurately.

In summary, these theoretical considerations imply that fluid dynamic effects are likely to distort the signal at high frequency and/or low velocity, but the electronic and thermal properties of the system are not predictable. There is therefore a clear need to examine the frequency response experimentally, by direct comparisons between calibrations performed in steady and unsteady flow.

CALIBRATION TECHNIQUES

A number of different flow regimes proved necessary to examine all relevant aspects of probe performance. The majority of tests were carried out using steady motion of the calibrating fluid on a turntable apparatus, with or without superimposed sinusoidal motion of the probe. Poiseuille flow was generated in a steady flow pipe rig to examine the spatial discrimination of the probe and the effects of wall proximity, and fully developed turbulent flow was generated in the same rig to examine the response to turbulence. An oscillating pipe flow was used to examine wake effects in a bounded flow; and finally an indirect (electrical) test was developed for rapid frequency response assessment.

Steady flow

Turntable

For routine use channel and pipe flows proved unsatisfactory, because the higher velocities were disturbed by eddies and turbulence, and because temperature fluctuation in the liquid was difficult to avoid. Free jets from a still reservoir were ruled out because theoretical calculation of jet velocity is only accurate if a considerable pressure head is present; this makes it an unreliable method for velocities below 100 cm/s, and therefore a turntable device, which proved extremely convenient, was adopted.

This consisted of a commercial transcription gramophone turntable (Goldring G99) having continuously variable speed from 16 to 80 rpm set by a built-in stroboscope, on which was mounted an open cylindrical container, of 30 cm. diameter, for the calibrating liquid. To ensure balance of the rotating mass, containers were machined from solid perspex or dural.

Flow in the container immediately after starting rotation is complicated, but steady conditions, with solid body rotation, are achieved after a half to one minute depending upon rotational speed. The velocity at any point in the fluid is then known from radial position and revolution rate.

Tests were made to check that immersion of the probe did not disturb solid body rotation, and that the wake behind the probe, which will of course rotate with the container, did not give rise to an artefact. The probe was plunged into the fluid after establishment of solid body rotation, and the signal monitored for any disturbance at the end of the first revolution after immersion. No change in the mean signal occurred, and it was concluded that the centrifugal force due to rotation caused secondary motion in the wake, which either displaced the wake away from the locus of the probe, or caused it to be damped within one revolution. At some combinations of radius and rotation rate, minor unsteadiness was present in the signal from water, but not from more viscous fluids like glycerine and

blood. This might be a vestigial wake effect, or it might be due to surface waves (see below). Subsequently, a check on the validity of the assumption of solid body rotation was made by comparing calibrations made on the turntable and in a towing tank. The results are shown in Fig.3. There is no systematic difference between the calibrations, the scatter being attributable to dust contamination and local temperature variations within the fluid, both of which affect heat transfer from the film and are almost impossible to eliminate completely.

The liquid surface during rotation is paraboloidal, the depth h at radius r being given by:

$$h = H_0 + \frac{\Omega^2}{2g}\left(r^2 - \frac{R^2}{2}\right)$$

where H_0 is initial depth of filling, R is radius at the rim, Ω is the angular velocity of the turntable, and g is acceleration due to gravity (Prandtl, 1952). Initially, the container was made with a second inner rim, at 8 cm. radius, to avoid making it too deep (at 80 rpm the depth at the centre would be zero for a rim height of 8 cm.). For studies on blood, a second dish was made; this had two annular channels, each 1 cm. wide, with centres at radii at 7.3 and 15 cm. The remaining spaces of the dish were filled with water, into which dipped supply and return pipes from a thermostatically controlled water heater and circulator (Churchill). After appropriate adjustment of

the heater, it was possible to maintain fluid in the annular channels at 37°C (± 0.2°C), and to carry out a steady flow calibration in small steps from 0-120 cm/sec, using a total volume of 150 ml. blood.

The presence of the probe can cause surface waves in the rotating fluid, which can propagate around the container and perturb the velocity field around the probe. Such disturbances should decrease exponentially in amplitude with increasing depth (Stoker, 1957), but might be a source of signal instability near the surface. This was examined empirically using various depths of liquid and probe in a 20 cm. deep container, and it was found that for a probe with a 1 mm. diameter shaft, signal disturbance from this source was insignificant if the probe was immersed to a depth of 1 cm. or more. The actual depth of the calibrating fluid beyond this was not important.

A rotating calibrating system gives rise to a centrifugal force which might cause concentration gradients in fluids such as blood, which contains suspended particles. The outward acceleration is $R\Omega^2$, which in this case is almost exactly 1g at 80 rpm. Thus the outward movement of particles is no greater than the sedimentation rate, and in any case the fluid can be regularly stirred to ensure homogeneity.

Pipe-rig

This consisted of a fixed-head water reservoir (containing honeycombing, fine mesh screens, and small glass spheres for flow smoothing), with a carefully radiused and polished 'trumpet' orifice which was connected, via a short perspex test section, to a 400 cm. straight stainless steel pipe with a polished bore, 1.68 cm. in diameter. At the downstream end of this was fixed a second perspex test section. Both test sections were cylindrical, and exactly the same bore as the pipe; each one had a single small entry port drilled through it and covered with a rubber membrane through which the probe could be pushed into the flow.

The length of the pipe was selected to be greater than the entry length at Reynolds numbers up to approximately 2500* so that all laminar flows would have fully developed (Poiseuille) velocity profiles at the downstream test section. In practice, traverses with a Pitot probe showed that departure from the expected parabolic form was detectable

---

*Entry length x in a pipe of radius r is given by

$$x \simeq .06.Re.r \qquad \text{(Goldstein, 1938)}$$

Re is Reynolds number, defined as $\frac{u.d}{\nu}$; u is mean velocity, d is pipe diameter, and ν is kinematic viscosity.

at Reynolds numbers above 2300. At higher Reynolds numbers, flow through this test section was turbulent. The upstream test section provided access to entry type flows with blunt velocity profiles. Flow rates in the pipe were controlled with a valve at the outlet, and measured with stopwatch and measuring cylinder.

Unsteady flow

Probe oscillation

Sinusoidal probe motion was generated by mounting the probe on an arm connected to a yoke which was driven by an electric motor and executed true simple harmonic motion at frequencies up to about 12 Hz (Fig.4). The linear amplitude of the motion could be varied between about 0.5 and 3 cm. When probe oscillation was used in conjunction with steady flow at small radii on the turntable, the stroke of the oscillation had to be limited to minimise the mean velocity variation due to the shift in radial position of the probe, produced by the tangential motion. For example, the peak to peak movement should be no greater than 1 cm. at radius of 3 cm., or 2 cm. at a radius of 7 cm., to limit the velocity error to 1% of the mean.

The oscillatory velocity of the probe was measured continuously with a Sanborn linear velocity transducer (6LV 3-N), which was attached to the probe clamp. The signal from this was recorded on ultra-violet paper alongside the probe velocity signal. Its calibration, which was

very stable, was checked in each experiment.

For sinusoidal motion, the instantaneous velocity of the probe $\tilde{u}$, is given by

$$\tilde{u} = a\omega . \sin \omega t$$

where a is the half-stroke amplitude, and ω is the angular frequency of oscillation. Peak oscillatory velocity is therefore $a\omega$, or $2\pi af$ where f is frequency in Hz. If a steady motion, of velocity $\bar{u}$, is added, then the probe velocity is given by

$$u = \bar{u} + a\omega . \sin \omega t$$

and peak forward velocity, $\hat{u}$, by

$$\hat{u} = \bar{u} + 2\pi af$$

The total range of peak oscillatory velocity available from the shaker rig was approximately 2-100 cm/sec.

This combination of probe motion and liquid motion is exactly equivalent to a composite motion in the liquid along; the coordinates have merely been transferred between the probe and the liquid. Where a calibration system of this sort does depart from the situation in an artery is in the absence of wall constraint and friction, which might modify the wake. This was briefly examined in oscillating pipe-flow.

Oscillatory pipe-flow

A brass pipe, 1.1 cm. diameter and 3 m. long, was mounted vertically (to avoid bubbles) and filled with water. This was moved in simple harmonic motion at frequencies from 1-5 Hz by a piston. The probe was inserted midway from the ends and aligned on the centreline. The pipe length was chosen so that flow past the probe was fully developed. For oscillatory flow under these conditions, the velocity profiles can be calculated exactly (Schlichting, 1968), and the relation between the (monitored) piston velocity and centreline flow velocity at the probe can be derived.

Indirect calibration method

The frequency response of the anemometer in its operating mode was also examined by coupling an oscillator across the film, as shown in Fig.5, and injecting a sinusoidal voltage of small amplitude under the conditions recommended for the square wave frequency response test in the anemometer handbook. This produced a sinusoidal anemometer output, the amplitude of which could be plotted against the frequency of the (constant amplitude) input signal to yield an 'electrical' frequency response.

This technique is easy to use, but has theoretical disadvantages as a method of assessing the instrument frequency response, since the signal disturbs the temperature of the film as well as the input voltage to the amplifier, and this represents a departure from normal operating

conditions. This temperature perturbation is very small, and as long as temperature distribution in the film is nearly uniform, requiring that conduction in the substrate should be in one dimension only (i.e. down into the substrate, and not spreading sideways to create spanwise or lengthwise temperature gradients under the film) the method should be valid. For these films, this requirement holds down to about 3 Hz.*

In fact it will be shown that the frequency response measured electrically reflects closely that inferred from direct flow calibrations, and the method has been valuable in comparing the response characteristics of different constant temperature circuits and overheat settings, and in monitoring the effect of necessary modifications.

---

*One dimensional heat conduction will occur if the depth of penetration of thermal waves into the substrate is small compared with the smallest dimension of the film. The depth of penetration of thermal waves is given by $\left(\frac{K}{\omega}\right)^{\frac{1}{2}}$, where K is thermal diffusivity (approximately 6×10^{-3} cm^2/sec for pyrex). Smallest film dimension is less than 0.02 cm. This becomes equal to $\left(\frac{K}{\omega}\right)^{\frac{1}{2}}$ at a frequency between 2 and 3 Hz.

PROBE FABRICATION

Resistive metallic films can be deposited on a glass surface by vapour deposition in vacuo, by electroplating, or by application of paints which deposit a metal layer when fired to high temperatures. All these techniques were investigated, but the first two were abandoned because in preliminary trials the films had unpredictable resistances (probably because of uneven deposition on the curved substrates); they also required sophisticated equipment.

The painting technique is comparatively simple, and was eventually used to construct all the thin film circuits. It is an old technique, originally (and still) used to decorate pottery; commercially available gold or platinum paints (Hanovia Liquid Bright Platinum, OX5, and Liquid Bright Gold, KA12 - Engelhard Industries), which contain the metal in solution as an organic salt, are applied to the substrate by brush, or dip-coating, and then baked in an oxidising atmosphere. This breaks down the salt to yield the free metal and volatile side-products which evaporate. If the temperature is elevated to the softening temperature of the glass, the metal film bonds firmly to its surface.

In practice, a high temperature laboratory oven, ventilated with a trickle of air vented from a domestic hair dryer, was used initially. Later, when probe design problems had been solved and all the films were being laid

down on standardised tiny glass beads, a small bench-mounted heating coil was used. Sufficient air flow through the coil occurred by convection, and the glass steadily heated to its softening temperature (approximately 670°C for pyrex). The whole process took only about 30 seconds; thus large batches of films could be made, and the uniformity and abrasion resistance greatly improved with the use of multiple thin coatings.

The properties of both gold and platinum films were examined. Platinum films proved extremely tough and adherent, with resistances in the region of 10 Ω/sq. cm., and positive temperature coefficients of resistance of 0.2% per °C. This value was highly reproducible, and constant over a wide temperature range. All these properties were desirable, as was the fact that wires can be soldered directly to the metal surface. Gold films had similar electrical properties, but were, predictably, softer. They were also less adherent to the glass and were soluble in solder; thus an intermediate step was necessary in soldering, to cover the gold surface in the soldering region with a thin layer of heat-fused silver paste. Despite these disadvantages, it proved necessary to use gold for most of the probes because more than one film was necessary on each probe for direction sensing (q.v.). This involved a masking and etching process to register the films with sufficient precision and platinum is extremely resistant to

both chemical and electrolytic attack; gold dissolves in seconds in a solution of iodine in potassium iodide.

The first step in this process was to coat the whole glass bead with gold by dip-coating and firing, as described above. Definition of the required film pattern was then achieved by chemical etching of excess areas of this gold film after the application of an adherent mask made with photoresist (KPCR, Kodak).

The metal-clad substrate was dip-coated with photoresist and dried. A negative photographic film image of the required metallic film pattern, life size, was then applied to the surface, and the photoresist layer exposed, through this mask, to ultraviolet light. The negative was removed and the bead immersed in photoresist developer, which hardened the exposed areas of photoresist, and dissolved away the remainder, exposing the excess gold, which was etched off. The photoresist was then removed with solvent.

Really sharp definition of this etched pattern depends upon intimate contact between the resist-coated substrate and the photographic negative. Photographic film which is sufficiently thin, flexible and dimensionally stable to be used as a negative is available in the form of 'stripping film' (Kodak Transparent Stripping Film, type 3), in which the emulsion layer (approximately 0.01 mm. thick) can be peeled off its backing after exposure and development and handled separately. Thus the mask is made in one step by

photographing on to stripping film a scaled-up image, in black and white, of the circuit layout required on the probe. After development the film is stripped from its backing, and folded round, or glued against, the substrate. It proved possible with this technique to systematically define up to three gold films 0.2mm. wide, and separated by 0.1 mm., on the surface of glass beads 1-1.5 mm. in diameter.

Small areas at each end of each film were covered with silver by fusing on a silver paste preparation (Hanovia Silver Paste No.38). Fine, epoxy-lacquered wires were soldered to these points; the solder joints were reinforced with epoxy resin (Araldite Twinpack), the wires then threaded through a pre-shaped hypodermic, and the glass bead cemented into position with more resin.

The final design of probe, which was used in all the animal studies, and whose performance is to be described, carried three films, each electrically independent (Fig.6). The films were aligned at right angles to the axis of the needle, and thus at right angles to the axis of the flow. The upstream and downstream films were used for sensing flow direction (q.v.); the central film was connected to the anemometer and used for measurement of flow velocity.

Although miniaturisation of these probes was obviously desirable on all counts, the detailed shape represents a compromise between the practical needs of arterial puncture and fluid dynamic requirements. A very wide range of

shapes and film orientations was tested originally. Most were discarded because incipient or actual flow separation in the neighbourhood of the film led to noisy or poorly-reproducible velocity signals. Others had very different sensitivity to forward and backward flow. Some other theoretically attractive shapes were either difficult to build, or difficult to insert into an artery without gross haemorrhage.

ANEMOMETERS

Commercially available circuits were used throughout this work. A number of these are available, all primarily intended for aeronautical application, particularly turbulence measurements with hot wire probes run at very high temperatures. None of them had entirely satisfactory performance when used at low overheats, the main failing being in frequency response. The DISA 55D01, which is a transistor design, caused least distortion of high frequency signals and was therefore adopted. Two modifications were made to it (Fig.5) to improve the accuracy of bridge balancing and overheat setting:

1) An additional series resistance decade was inserted in the balancing arm of the bridge. This allowed balancing to .001 rather than .01 ohms.

2) A switched resistor was inserted in parallel with the upper arm of the bridge adjacent to the decades. The value of this was chosen so that it reduced the resistance of that arm by 1%. Closing the switch then automatically provided 1% overheat.

LINEARISATION AND RECORDING

As described earlier, the relationship between anemometer output and flow velocity is non-linear. It is convenient visually, as well as for derivation of average values, integrals, and derivatives, to linearise this

voltage-velocity relationship; this can be done with a commercial analogue circuit (DISA D10 lineariser) which accepts the output from the anemometer and is set up during calibration of the probe. It was used in all the animal studies reported here.

During development and evaluation studies, the anemometer output was recorded using an ultraviolet recorder (S.E. Laboratories, 2005) with 450 Hz galvanometers. Appropriate zero adjustment, gain control, and impedance matching were interposed via operational amplifier circuits of the type described by Gordon (1972).

PROBE PERFORMANCE

The results which follow apply to probes of the form shown in Fig.6, which was the design used for all the animal experiments. Behaviour in steady flow is described first; performance is then assessed in unidirectional and reversing oscillatory flow, and in turbulent flow.

This section is necessarily fairly long, because many aspects of probe performance are relevant to intra-arterial use. It has been condensed as much as possible, and summarises experience in a long programme of probe development; as will be immediately obvious, it also leans heavily on the knowledge of fluid dynamics supplied by my colleague in this part of the work, Dr. N.B. Wood.

Steady flow

Signal stability

Heat loss from the film in still liquid occurs principally by conduction, since natural convection (buoyancy) and radiation losses are very small at 1% overheat. When the liquid is set in motion, forced convective heat loss is added. Both of these are directly proportional to ΔT, the temperature difference between film and environment which is dependent on both film and fluid temperature. Variations in these were the principal cause of baseline (zero) and gain instability. In still liquid, the fluid temperature is constant; film temperature, however, is a function of bridge resistance, and zero drift occurred if there was any resistance instability in the probe circuit. High quality

leads and plugs between the probe and anemometer were therefore essential, but by far the commonest source of resistance changes lay in the film itself, which was susceptible both to mechanical damage (abrasion) and to AC electrolytic etching by stray potentials in the calibrating fluid. The likelihood of both was greatly reduced by firing on a protective silicon dioxide coating (again applied in the form of paint) during fabrication, as described by Vidal and Golian (1967). Thin epoxy lacquer coatings (Araldite 820) were later shown to be even more satisfactory. Stray EMF's in the calibrating fluid were eliminated by earthing the steel shaft of the probe, and therefore the fluid, to the anemometer bridge earth.

In steady flow on the turntable apparatus, ΔT was also affected by slow cooling of the calibrating liquid due to accelerated evaporation and latent heat losses. However, ΔT is set in the first place by balancing the bridge, which takes only seconds and was therefore repeated for each calibration point.

When these precautions were taken, and the calibration liquid was filtered to eliminate particle contamination, steady flow calibrations for each probe became highly reproducible - typically within $\pm$ 5% in velocity terms over several weeks. Changes were almost always the result of damage to the film, and were easily detected during overheat setting because of a change in resistance.

Short-term temperature drift was never a problem in the aorta. Initial experiments confirmed the observation of Wessel, James & Paul (1966), who found that short-term temperature fluctuations in the aorta are negligible. Slow drifts downwards, due to body cooling, occurred in long experiments; the effect of these was easily circumvented by regularly checking and, where necessary, resetting the overheat.

Linearity

Linearisation of probe response on the basis of King's law involves certain approximations. First, the value of the velocity exponent is weakly dependent on probe geometry, and the value of 0.5 strictly applies only to a cylindrical body. Second, the zero flow signal depends on both convective and conductive heat loss, and their absolute and relative magnitudes will be influenced by geometry, ΔT, and the thermal properties of the calibrating liquid and probe. Thus V_0^2 may not always be a precise zero flow intercept.

The magnitude of these approximations was examined by numerical linearisation of directly recorded anemometer outputs from steady flow calibrations. A velocity exponent of 0.5 gave very good linearisation through the steady flow points, but the extrapolated zero intercept frequently differed slightly from the measured zero flow voltage. Thus linearisation, whether calculated or set up on an electronic circuit, involved errors at very low velocities,

since the slope of the calibration effectively changed somewhere in the region of 5 cm/sec. This was considered acceptable in practice, since other errors occur at these low velocities in unsteady flow (see below). The stability and frequency response of the electronic lineariser used in the animal experiments were separately tested and shown to be satisfactory.

Relative sensitivity in water and blood

There were obvious attractions in using water for calibrations if the results were valid for blood. Heat transfer theory for homogeneous liquids predicted that flow sensitivity would be strongly influenced by viscosity, which implied not only a difference between water and blood calibrations, but possible dependence of the blood calibration on haematocrit. At this time, preliminary reports on the use of hot film systems in arteries were appearing from other laboratories, with conflicting statements on this point, which it seemed important to clarify.

Serial calibrations were therefore carried out, at 37°C, of water and of samples of blood, freshly drawn and anti-coagulated with heparin, 10 units per ml. To examine the influence of red cell concentration on sensitivity, extra samples of blood were taken and centrifuged; the resulting cells and plasma were then mixed in different proportions to obtain variations in haematocrit, and the probe was again calibrated in this reconstituted blood.

A typical result is shown in Fig.7. Sensitivity to flow (slope)was very similar; zero sensitivity differed considerably. Over a fairly wide range, haematocrit was unimportant. These results were highly reproducible with different probes and blood samples.

The close correspondence of the forced convection response of the probe in water and blood leads to the possibility of simplifying a linearised calibration by using water, since only a zero offset is required to make the two responses identical (Schultz et al, 1969). The lineariser gain could be set up with a water calibration and the zero then reset with the probe immersed in a small, stationary sample of blood. There are, however, drawbacks to this, since the linearising circuit has the inherent property that any error in zero setting seriously changes the gain also. For this procedure to be valid, therefore, the difference between the forced convection signals must be exactly the same as that between the zero signals; this did not prove to be the case for all probes. This technique has the further disadvantage that the calibration depends on the accuracy of setting of one point. The technique was tested on a number of occasions by calibrating in water and then transferring to blood, resetting zero, and examining the flow sensitivity in blood. On only one out of four occasions was this within 20% of that predicted from the water calibration, and the method was abandoned. The standard procedure was to calibrate the probe, in blood from the animal, at the beginning of each experiment.

Spatial discrimination and blockage effects

Two possible sources of error could not be evaluated in the open channel of the turntable apparatus. The first was the progressive blockage effect which might occur, and might distort the measured profile, as the probe was advanced across the diameter of a closed pipe. The second arose because the film was offset sideways from the tip position, as well as downstream, and in a sheared flow neighbouring streamlines with different velocities impinged on the probe, contributing to the growing boundary layer ahead of the film and possibly 'weighting' the response. This might appear as a distortion of the profile or as an offset of the measured profile in relation to the probe-tip position.

Steady pipe flow was used to assess these sources of error. Probes were traversed across a diameter of the pipe, after calibration in water on the turntable apparatus. Two sites were used; the first was 10 cm. from the entrance, where the (blunt) velocity profiles could be predicted from the volume flow rate, using the experimental data of Nikuradse (1934). The second site was 400 cm. from the entrance, where the flow was fully developed.

Results are shown in Fig.8. In the entrance region (Fig.8a) measurements made at three flow rates are compared with the predicted velocity profiles (full lines). At the downstream site (Fig.8b) measurements made at a Reynolds number of 1070 are compared with a parabolic velocity profile calculated from the measured volume flow rate.

Blockage effects are clearly negligible. This was expected since the film is mounted about 5 mm. ahead of the probe shaft. Potential flow theory predicts that the velocity perturbation round an obstacle falls off as the square of the ratio of obstacle size to distance from it. In this experiment, with an area blockage at the plane of the shaft of 13%, the perturbation in velocity at the plane of the film should be under 1%. The worse physiological case, in the distal aorta, would give an area blockage of 20%. In the ascending aorta, blockage would be less than 10%.

The profiles demonstrate that 'weighting' of heat transfer does occur in sheared flows; first, offsetting the profile, in relation to the probe tip position, by 0.5-1 mm. towards the film position, and second, distorting the measurements close to the near wall. These results can be summarised as follows: this type of probe is unsatisfactory for making measurements within 2 mm. of the point of insertion through a wall; further out than this, velocity profiles can be registered within $\pm$ 5% (calibration accuracy) by taking a point midway between probe tip and film as the measurement position. Aortic profiles presented in this thesis were constructed accordingly from the measurements made in the vessels.

Unsteady flow

Direct testing of the behaviour of the system in oscillatory flow was possible up to about 12 Hz; above this

the motion of the probe was distorted by backlash and high frequency vibration in the shaker rig.

A fairly standard procedure was adopted for the unsteady flow tests. For each run, a particular amplitude of oscillation was set on the shaker rig, and the frequency increased in steps from about 0.5 Hz upwards. At each step, probe and velocity transducer signals were recorded on the ultraviolet recorder. The peak probe signal during the forward stroke at each frequency was then measured, and plotted unlinearised against instantaneous velocity for comparison with the steady flow calibration.

A number of such runs were normally made, each with a different steady velocity set on the turntable; a run was also made with the turntable stationary. Steady flow calibrations were carried out before and after the unsteady runs. Water was normally used, for convenience; similar results were obtained when the tests were repeated using blood.

Initially, attention was focussed on the peak signal for two reasons. First, it was easier to read, and gave the best signal to noise ratio. This minimised scatter, which was important since it was deviations of this signal from the steady flow signal at the same velocity which were of interest - i.e. a potentially small difference between two large signals, both subject to scatter and measurement errors. Second, it was least likely to be distorted by fluid dynamic artefacts, as discussed earlier.

The behaviour of the system in unsteady flows at 1% overheat was initially extremely confusing, because both artefacts in the flow, and distortions in the probe response, were present in proportions which depended upon the particular flow conditions. The situation is simplified if the behaviour in unidirectional oscillatory flow - which reveals the frequency response of the system - is examined first, and observations made in reversing flow - which reveals the fluid dynamic sources of signal distortion - are deferred until the frequency response has been examined.

Frequency-response

At frequencies and amplitudes too low to cause flow reversal, the unsteady responses were consistently above the steady calibration (Fig.9a). In Figure 9b, the results of these and a number of other, similar tests are plotted in frequency-response form. It seems clear, despite the scatter, that the effect is frequency-dependent, but is independent of both amplitude of oscillation and absolute velocity. Electrical testing at low frequency also revealed a response that rose with frequency at 1% overheat (Fig.10). All this suggested that the behaviour of the system rather than any fluid dynamic artefact was responsible for the flow result. Flow tests were therefore repeated at 5% overheat, since in this condition the electrical response was virtually flat at low frequencies (Fig.10). The results are summarised in Fig.11. With the single exception of oscillation in still liquid (see below), the discrepancy between steady and unsteady signals was eliminated.

An overheat of 5% means a film which is approximately 25°C hotter than the surrounding fluid, and this is at least 15° too hot for use in blood. At 2% overheat, the maximum feasible for blood, the system performed only marginally better than at 1%. An alternative means of improving the frequency response was therefore sought.

The most satisfactory solution would be to improve the design of the anemometer. This was not attempted, because at best it only offered a long-term solution; anemometer feedback theory is inexact and extremely complex, since the purely electrical amplifier and bridge characteristics interact with the thermal properties of the probe. Instead the simplest solution which suggests itself - a filter - was adopted.

A single-stage resistance-capacitance filter at the anemometer output proved satisfactory. Since the amount of attenuation, and the exact frequency range over which it was needed varied between different probes, the filter was built with adjustable components, and was set up (using the electrical frequency response test) for each probe before measurements or calibrations were performed. The filter was in the form of a frequency-sensitive voltage divider (Fig.12a); the upper arm is a non-inductive resistor R_1 and the output is picked off across the lower arm, which contains a resistance R_2 in series with a capacitor C. In Figure 12b, its amplitude and phase characteristics are

shown for two levels of attenuation (set by adjusting R_1) at a single frequency setting. As can be seen, it gives progressive attenuation over approximately one decade of frequency.

In Figure 13 is shown the electrical frequency-response of the system with the probe exposed to two steady flow velocities. This figure is directly comparable to Fig.10, though it is taken to much higher frequencies; over the range 1-25 Hz, the filter allows correction to within about 5%.

In Figure 14 the results of unsteady, unidirectional flow tests with the filtered system are shown; this figure is directly comparable to Fig.9b. Again the scatter is rather wide, but the rising response characteristic has been neutralised. Over a number of such tests, the response appeared flat within $\pm$ 5% at low frequency. Using the electrical test to higher frequencies showed that the response was flat within $\pm$ 10% up to 500 Hz (Fig.13); this was considered satisfactory.

Reversing oscillatory flow

If the maximum oscillatory velocity achieved by the probe exceeds the steady velocity imposed by the turntable, flow over the probe will be reversed for some part of the 'backstroke', and the probe will move through its own wake. In addition, it will, twice per cycle, pass through the 'high frequency low velocity' conditions predicted above, from

fluid dynamic considerations, to distort the response. To assess these sources of error, and to examine the relative sensitivities of probes to forward and backward flow, the unsteady flow studies were extended to include reversing flow and the extreme case of zero mean flow, when the probe is continuously in its own wake.

a) Wake effects

Figure 15a shows a steady flow calibration together with signals obtained when the probe was oscillated in still water at frequencies up to about 12 Hz. Two sets of results, at different amplitudes of oscillation, are shown. In Figure 15b, these results, combined with those from other runs, are plotted in frequency-response form. The results demonstrate a repeatedly observed feature: that for a given instantaneous velocity, the dynamic response was higher than the steady response.

In this example the effect is partly due to rising frequency response of the electronic system, which was operating, unfiltered, at 1% overheat. However, the effect was constantly present, even with a flat frequency response; this is shown, for example, in Fig.11, where the frequency response was corrected by running the system at 5% overheat. Very similar results were obtained when the probe was exposed to flow oscillating sinusoidally with zero mean velocity in a pipe.

The effect was not frequency dependent. As shown in Figure 15, the discrepancy increased as amplitude of

oscillation decreased, and magnitude was also influenced by the position of the film on the probe surface. This was not explored systematically, but it was noted that on one multi-film probe, one film gave signal augmentation of 20% over the steady calibration; a second film, situated 15% nearer the tip of the probe, gave signal augmentation of 6%. This dependence on geometry was very suggestive of a fluid-dynamic origin of the effect. When aluminium powder was sprinkled on the surface of the water for flow-visualisation, a steady streaming motion was seen in the initially still liquid when the probe was set in motion; the form of this is sketched in Fig.16. Such secondary streaming motion was described, and examined theoretically, by Schlichting (1932); it stems from an interaction between viscous and inertial forces. On each stroke, the probe induces motion in the fluid through which it passes (which becomes the wake) by viscous drag. As the probe slows and then reverses its direction, the wake, with its newly acquired inertia, continues in motion. Thus the probe acts as a pump and a streaming motion is set up. Such motion, which has been shown by Richardson (1967) to increase heat transfer from the oscillating body, appeared to be the cause of the increased signals seen under these conditions.

Oscillatory probe motion is of course analogous to oscillatory motion of the liquid with zero mean flow about a stationary probe; even then it would seem to have little direct relevance to the motion of blood within an artery.

However, it merely represents an extreme condition whose essential feature is reflux of the wake over the probe. Since transient flow reversal in diastole is a common feature of flow in large arteries, this effect might be a source of error. Therefore, once the effect had been identified, a series of calibrations were performed with a steady velocity set on the turntable, and the frequency of oscillation of the probe increased, as before, in steps, but arranged so that flow-reversal occurred, its magnitude increasing with each step in frequency. The results of a series of such runs are presented in Fig.17, where probe responses are plotted against λ , the ratio of unsteady to steady velocity components of the flow. Flow reversal occurs in any flow where λ is greater than unity, and lasts for a longer fraction of the flow cycle (approaching one half cycle) as the value of λ increases; it occupies a third of the cycle at $\lambda = 2$. It can be seen that a significant elevation of the probe response above unity, implying some wake effect, does not occur till λ exceeds 2. This is not likely within a large artery, and thus velocity measurements within the aorta should be free of distortion by wake effects.

There will be an error, however, if probes are calibrated by oscillation in still liquid, which, as a quick and convenient method, was used by both Schultz et al (1969) and Ling et al (1968). The effect would be to distort the calibrations so that arterial flow velocity was underestimated by an amount dependent on amplitude of oscillation,

probe geometry, and possibly other factors. The magnitude of this effect cannot, in general, be predicted; if the calibrations shown in Fig.15 were used, for example, arterial velocities would be measured 7-17% below their true value. If no direct comparison is made with a steady flow calibration, an oscillatory calibration of this sort will appear satisfactory, since it will linearise satisfactorily, and give the impression that the overall frequency response of the system is flat, as shown in Fig.15b. It appears to be for this reason that the method was accepted by Schultz et al and Ling et al.

b) Relative sensitivity to forward and backward flow

This proved to be the most difficult feature to control in probe design, since the velocity field very close to the probe surface - i.e. the boundary layer - is influenced by probe geometry and it is this that governs heat transfer from the film. It follows that identical sensitivity to forward and backward flows requires exact symmetry of the probe upstream and downstream of the film position.

In practice, this was unattainable with needle-probes because of the shaft (see Fig.6) and because very precise alignment of the films during construction was difficult. Furthermore, calibration trials showed that with transient periods of flow reversal, films had different sensitivity for steady and unsteady reversed flow. This was presumed to be due to changes in the form of the boundary layer, together with, or due to, the presence of wake disturbances.

In practice, therefore, each completed probe was tested in steady forward flow and unsteady reversing flow. Where there was severe divergence (greater than 20%) between the sensitivity to steady forward flow and unsteady reversed flow, the probe was discarded. Initially this led to a good deal of wastage; later, with further miniaturisation, it became less important. The results of one such calibration are shown in Fig.18; in this case the probe was considered satisfactory.

c) Probe boundary-layer effects

The final source of error to be examined was boundary layer phase-lags, which were expected on simple theoretical grounds as the parameter fx/u approached unity - i.e. at high frequency and/or low velocity. Their importance was assessed by measurement of full cycles of oscillatory flow, both with and without flow reversal, using a probe which had very nearly equal sensitivity to forward and backward flow, and a frequency response corrected by means of the output filter described earlier.

Figure 19 shows typical results, (a) for unidirectional flow and (b) for reversing flow. For an individual cycle, since f and x are fixed, the errors appear during low velocity periods of the cycle. The results from many complete cycles analysed in this way and plotted as a function of fx/u are shown in Fig.20. It can be seen that fidelity falls off rapidly as fx/u exceeds about 0.2.

Nonetheless, absolute errors from this source (which can be read off Fig.19) are less than 4 cm/sec except at instants of zero flow. The latter error, which shows as a 'lifting-off' of the rectified signals from the zero velocity base-line - e.g. Figs. 24D and 25 (upper trace) - is reduced by an order of magnitude by extrapolation through zero during reconstruction of the unrectified waveform - e.g. Fig.25 (lower trace). Of course, at the instant of zero velocity, any correlation involving velocity becomes meaningless. In fact, measurements of zero 'lift-off' for three probes with similar film and substrate dimensions but different overall streamwise lengths (i.e. different values of x) were found to correlate with frequency only (Fig.21); it is thus likely that 'lift-off' is a substrate conduction effect, and is independent of convective heat transfer.

Detection of turbulence

Earlier in this section, it was pointed out that if turbulence occurred within the aorta, it would cover a wide frequency range - certainly extending above 100 Hz. Since it proved impossible to generate known oscillatory flows at high frequency, the response of the hot film system to turbulence was difficult to assess quantitatively. The absolute upper frequency limit would be set by the dimensions of the film, since it could not detect an eddy much smaller than itself (i.e. of the order of 1 mm.). Eddies of this size, convected past the film at 100 cm/sec, represent a frequency of 1000 Hz. From electrical frequency response

ing (e.g. Fig.13) it seemed that the system should be le of responding up to at least 500 Hz. Boundary layer derations (see over) would at first sight suggest a limit; taking a tip-to-film length of 3 mm. (a typical for these probes), assuming again that the turbulent city fluctuations would be superimposed upon a systolic city of 100 cm/sec, and using the results in Fig.20, distortion due to boundary layer phase-lags might be cted to become significant above approximately 70 Hz. act, this is certainly too low, because the boundary r would itself be greatly modified by the presence of ulence, becoming thinner, and therefore reacting er to velocity fluctuations. Pedley (1972) has ntly published an analysis of the behaviour of probes his type in unsteady flow, using boundary-layer theory redict heat-transfer. His results, which give good itative agreement with the experimental observations ribed here for oscillatory flow, predict that turbulent city fluctuations will be registered within 5% up to Hz when they are superimposed upon flows with cities of 100 cm/sec or more.

It was of course extremely simple to show that the em was capable of registering turbulence, by exposing probe to turbulent flow in the pipe rig; Fig.22 strates this. It was also possible to extend this test nd simple visual observation, since the measurements made at the downstream end of the pipe rig, where

turbulence was fully-developed and could therefore be compared with observations on developed turbulence made with hot wire probes of known high frequency-response (e.g. Laufer, 1954). Such experimental results bear out theoretical predictions that spectral energy content (measured with the spectrum analyser and expressed as $\overline{u'^2}/U^2\Delta f$ - see Appendix A) decays with increasing frequency in a predictable fashion, such that $\frac{\overline{u'^2}}{U^2.\Delta f} \propto \frac{1}{f^{5/3}}$; thus a logarithmic plot of spectral energy distribution, against frequency, should be a straight line with slope -1.67. Figure 23 shows such a plot for the probe, with a line through the points which has a slope of -1.67. This is obviously close to a best fit, and thus the circumstantial evidence is strong that these probes will register turbulent velocity fluctuations faithfully up to at least 500 Hz.

Direction-sensing

Early trials showed that a second film, placed close to the heated film, and acting as a resistance thermometer, could be used to detect flow reversal. When it lay downstream, its resistance increased; flow reversal was accompanied by a drop in resistance. This effect does not appear to be due to heat convected by the flow, but to biassing of the surface temperature distribution created in the glass substrate by the heated film, since a 'heat-pulse' applied to one film intermittently was detected after an equal delay by the second film, regardless of whether it lay upstream or downstream.

The clarity of the direction signal was greatly improved by mounting films on either side of the heated film, and connecting them as two arms of a Wheatstone bridge. The amplified output of this bridge gave an unequivocal direction signal, since 'common-mode' signals due to noise and flow sensitivity were largely cancelled out, and flow reversal was signalled by polarity change. The performance of this system in the calibration rig is shown in Fig.24.

Probes with twin direction-sensing films were used in all the animal experiments. The Wheatstone bridge was run at low power (less than 1% of velocity film power) and the amplified output displayed, or recorded, with that of the heated film. The bridge balance position was set up and recorded during calibration. Figure 25 demonstrates the performance of this system in vivo.

In the majority of experiments, both velocity and direction signals were recorded on magnetic tape, and it was then possible to 'reconstitute' the unrectified velocity signal electronically at playback. The velocity signals were played through a unity-gain switched amplifier; the direction signal was used to generate switching pulses in a comparator, and these pulses controlled the polarity of the switched amplifier output. Thus the part of the (rectified) velocity signal which corresponded to reverse flow was automatically inverted, and the switched amplifier output was an unrectified velocity signal. Figures 27, 28,

32, 42, 43 and 44 show examples of such automatically processed signals; the discontinuities at the instants of switching are occasionally visible.

SUMMARY

The needle-mounted probes in the form shown in Fig.6, used in conjunction with a commercially available anemometer and lineariser at 1% overheat, have the following characteristics:

1) Adequate signal stability, provided temperature variation in the environmental fluid is small, or overheat is adjusted frequently. Repeated steady flow calibrations then reproduce $\pm$ 5% unless the films are mechanically damaged - which is immediately detectable as it produces a resistance change.

2) A frequency response which rises at low frequency; this can be considerably improved by a simple output filter. The frequency response extends upwards to at least 500 Hz. The system will register turbulent velocity fluctuations up to this frequency when they are superimposed on high mean velocities; indirect evidence suggests that there is little amplitude distortion even at the top end of this range.

3) In unsteady reversing flow, ancillary direction-sensing films will signal reverse flow unequivocally, and this signal can be used to activate switching circuits which correct the polarity of the velocity signal automatically.

4) At the instant of flow reversal in such flow, the

velocity signal is subject to severe errors due to phase-lags in substrate heat conduction. This cannot be prevented, but is unimportant if direction-sensing is available to correct the polarity of the velocity signal.

5) At low velocity and/or high frequency, velocity signals are distorted by boundary layer phase-lags over the probe, leading to an over-estimate of velocity. This is also inevitable, though it can be minimised by probe miniaturisation. The errors introduced in calibration studies were large in percentage terms, but in absolute terms were always less than 4 cm/sec. As an instantaneous error, this might be larger in the ascending aorta with the very rapid flow reversals which occur at high heart rates; elsewhere in the circulation it is unlikely to be exceeded.

6) A further error is present with some probes at very low velocities (less than 5 cm/sec) because the velocity-voltage relationship which is assumed in setting up the linearisation circuit breaks down near zero flow. This will act in the opposite direction to the error in (5).

7) Equal sensitivity of probes to forward and backward flow is difficult to achieve because it depends upon very rigorous control of probe geometry. In this work, probes with sensitivities within 20% of each other for forward and backward flow were tolerated.

8) Calibrations in regimes of unsteady flow which include considerable degrees of wake reflux over the probe

will be influenced by secondary motion. The extreme case - oscillation of the probe in initially still liquid - introduced errors of up to 17%. Calibration in unidirectional oscillatory flow, or (far simpler) steady flow, appears most appropriate for arterial work.

9) Calibration should be performed in blood.

Thus with appropriate adjustment of frequency response, followed by steady flow calibration in blood, the system is accurate within $\pm$ 5% (calibration error) during most of the cycle. Velocities between about 5 cm/sec and -5 cm/sec will be unreliable; and larger reversed velocities will only be accurate $\pm$ 20%. Turbulent velocity fluctuations will be registered at least semi-quantitatively up to 500 Hz. The probe can discriminate spatially down to approximately 0.5 mm., but it is not reliable for measurements closer than 2 mm. to a flow boundary.

SECTION 2: ANIMAL EXPERIMENTS

METHODS

Preparation of animals

For the measurements on velocity distribution, adult dogs (mainly greyhounds) weighing 16-30 Kg. were used. Anaesthesia was induced and maintained with intravenous pentobarbitone sodium, with an initial dose up to 30 mg/Kg. Occasionally, intramuscular morphine, 1 mg/Kg, was used as premedication.

In the later series of experiments on flow disturbances and turbulence, dogs between 3 and 14 Kg. were used, because the detection of highly-disturbed waveforms in the previous experiments, and in studies in other laboratories (Ling et al, 1968; Schultz et al, 1969), had been confined to small dogs. These animals were premedicated with morphine, 4 mg/Kg, and anaesthetised with intravenous pentobarbitone sodium; this combination permits a small dosage of pentobarbitone to be used for induction, and prevents the increase in heart rate which occurs with pentobarbitone alone.

Aortic pressure was measured with a Statham P23Gb strain-gauge transducer, attached to a 30 cm. nylon catheter (1.5 mm. i.d.) introduced into the left carotid artery and later adjusted so that its tip lay in the orifice of the brachiocephalic artery. The system had a damped natural

frequency (pressure transient method, McDonald, 1960) of 100-120 Hz and a damping factor of 0.1-0.2.

An intravenous cannula was inserted into a leg vein for drug and anaesthetic infusions. In the later experiments, one vagus nerve was exposed in the neck for electrical stimulation.

The chest was opened via a left thoracotomy or a sternal split, respiration being maintained by intermittent positive pressure ventilation (Cyclator, British Oxygen Company) via a cuffed endotracheal tube. In early experiments, in which the aorta was encircled with a full collar probe-mounting, it became clear that any distortion of the vessel produced gross skewing of velocity profiles within it. Thereafter, no attempt was made to mobilise the aorta; small areas were locally cleared of overlying fat or pleural reflections, and purse-string sutures sewn into the wall. In some experiments, a left paramedian incision was used to expose the abdominal aorta, which was prepared in a similar fashion.

Calibration and mounting of velocity probe

The velocity probe was calibrated during each experiment. At the time of introduction of the pressure catheter, a sample of blood (approximately 150 ml.) was taken, anti-coagulated with heparin (10 units/ml.) and placed in the turntable dish, where it was maintained at 37°C throughout the calibration. The probe was lowered into the blood and

clamped. The system frequency-response was examined by the electrical method, and adjusted by the output filter attached to the anemometer. The zero and gain settings of the lineariser circuit were adjusted, and a steady flow calibration from 0-125 cm/sec was carried out. Figure 26 shows the quality of linearisation which could be achieved with careful setting up.

The lineariser output signals were recorded on magnetic tape with an FM recorder (Precision Instruments PI-6200). The recording speed was 3.75 i.p.s. which gives a response flat within 1 db to 1 K Hz; this was checked. During the calibration, the Wheatstone bridge containing the twin direction-sensing films on the probe was balanced to give zero volts at zero flow. The output from this, suitably amplified, was recorded on a separate tape channel, as were blood pressure and ECG during the experiment. The inputs to each channel were monitored on a six-channel display oscilloscope (Cardiac Recorders).

At each site in the aorta, the probe was inserted by direct puncture, and the purse-string suture tightened around it just sufficiently to prevent leakage. The probe was aligned on a diameter normal to the vessel, and clipped into the slide of a plastic carrier; the latter was then rigidly clamped to a bar on the operating table, so that as the probe traversed the diameter of the vessel lumen, the slide moved along a millimetre scale on the carrier.

This system was adopted to avoid pressure or constraint on the vessel wall, except at the entry point of the probe.

At each site the internal diameter was established by traversing the probe from the near to the far wall and adding the width of the probe head (2-2.5 mm., depending upon the probe used). The position of the far wall was established as the point at which flat (zero flow) signals were recorded throughout diastole. (As the vessel was unrestrained, a velocity signal was still seen in phase with systolic pressure, due to expansion of the vessel and loss of contact between the velocity film and the far wall.)

Investigation of velocity distribution

After measurement of vessel diameter, the far wall was taken as a datum point, and the probe traversed across the diameter of the vessel in one- or two-millimetre steps. Velocity and direction signals from the probe, aortic arch pressure, and ECG were recorded at each station. Since these sequentially recorded velocity signals were to be used after each experiment for the reconstruction of instantaneous velocity profiles, a great deal of care had to be taken to establish stability, both of probe sensitivity and of cardiovascular behaviour.

Probe sensitivity may be changed by a temperature variation in the blood and by surface deposition in the immediate region of the film - either thermally insulating it, or modifying the boundary layer over it. The effect of

temperature variation was cancelled by repeated checking of film resistance, and, where necessary, resetting of overheat. Probe contamination was prevented by wiping the films against the far vessel wall between recording points. (With some probes, signal amplitude was found to fall off gradually with time. This did not happen in the calibrating apparatus, and examination revealed fibrin deposits which originated in minute discontinuities at the epoxy/metal junctions around the film-bearing glass substrates. Presumably, fragments of tissue were carried into the vessel during wall puncture and initiated clotting by release of tissue thromboplastin.) In later experiments the animals were anticoagulated with heparin as soon as surgical exposure of the vessels was completed.

A number of precautions were taken against variations in cardiovascular parameters which might affect the velocity measurements:

1) Sampling procedure - traverses were made at each site in pairs, inward and outward. Any continuing drift in conditions would thus appear as opposite skew in the profiles. A shorter-term drift which reversed direction might still be masked, and these double traverses were therefore repeated with both long (50-100 beat) and short (less than 10 beat) sampling periods. In addition, records were taken repeatedly at a single reference station during at least one traverse at most sites.

2) Averaging procedure - the only index of changing conditions immediately accessible from the records was heart-rate. Therefore, after each experiment, the ECG signals recorded during each traverse were examined; any traverse during which heart-rate varied more than 5% about a mean value was discarded.

To eliminate beat-to-beat variations, the velocity waveforms recorded at each station were then averaged. The velocity signals were played out through the automatic direction-correcting circuit described earlier. The reconstituted velocity signal was passed to the input of an averaging oscilloscope (Northern Instruments NS-513), which was triggered by the R-wave of the ECG. The time-base of the oscilloscope was set so that during each sweep, one, or sometimes two, complete velocity cycles would be captured. During the sweep, the signal was digitised by the oscilloscope at 512 equal intervals, each value being stored. On the next sweep, the amplitude of each stored signal was compared with that of the new one at the corresponding instant, and the stored signal adjusted up or down according to the discrepancy. The relative emphasis given to the new and stored signal in this adjustment could be varied by the operator. Thus an average could be built up roughly in a few sweeps, or precisely with a large number.

The average velocity waveform for each station on a traverse was built up in this way by playing through the

averaging oscilloscope an equal number of velocity signals recorded on tape at each station. The tape was stopped at the end of the record from each station, and the averaged waveform was recorded on a pen-recorder, having been played out from the oscilloscope, as 512 successively presented analogue (i.e. voltage) signals, at a rate slow enough to lie within the frequency-response limits of the recorder. Figure 27 shows average waveforms retrieved in this way. The probe calibration was played out through the same system. Instantaneous velocity profiles were then constructed by taking values at corresponding instants from the averaged waveforms for each station of the traverse. Subsequently, the waveforms from each station, and the velocity calibration, were replayed again from the tape through an operational amplifier integrating circuit, to provide time-average velocity.

Investigation of flow disturbances

In these experiments the probe was aligned on the centreline of the vessel and clamped. ECG, pressure, velocity, and flow-direction signals were tape-recorded as before. In addition, in five experiments, the velocity signals were passed through a frequency spectrum analyser (see Appendix A). The velocity signal and the spectrum analyser output were recorded simultaneously on an ultra-violet paper recorder (S.E. Laboratories, 2005), using 450 Hz galvanometers.

Changes in heart-rate and peak velocity in these latter experiments were induced by a number of means, either singly or in combination:

1) intravenous isoprenaline infusion at a constant rate of 0.5-1 μg/Kg/min.

2) Single intravenous injections of propranolol, 1 mg/Kg.

3) Single intravenous injections of pentobarbitone sodium, 10-20 mg/Kg.

4) Vagal stimulation at 25-50 Hz using 10 msec. squarewaves.

Following each intervention, recordings were made, and frequency spectral analysis performed. Where possible, the effect of these interventions on the velocity waveforms was examined at more than one site in the same animal.

RESULTS AND DISCUSSION

Velocity distribution

Velocity waveforms were in general comparable to those which had been recorded at similar sites with cuff electromagnetic flowmeters, and at any one site showed little beat-to-beat variation; Fig.28 shows a run of beats recorded in the ascending aorta, together with simultaneous ECG and pressure traces. The phase relationship displayed in this figure is not quite correct, since the pressure signal was recorded downstream of the velocity signal, and there will also be a transmission delay in the pressure catheter. Assuming a wave speed of 500 cm/sec in the ascending aorta, the pressure wave will take about 10 msec. to travel between the two probes, and perhaps 1-2 msec. to traverse the pressure catheter. Advancing the pressure signal 12 msec. will, if anything, improve the 'in-phase' relationship between the two in early systole. This relationship is in itself evidence that viscous forces are small. If wave reflection is ignored, the equation of motion for inviscid flow can be approximated as:

$$\frac{\partial u}{\partial t} = -\frac{1}{\rho} \cdot \frac{\partial p}{\partial x} = \frac{1}{\rho \cdot c} \cdot \frac{\partial p}{\partial t}$$

so that acceleration and temporal pressure gradient are in phase. Of course, at other points in the cycle, this relationship breaks down because of viscous effects, wall

movements and wave reflections, but if it holds in early systole, peak velocity will be approximately $\frac{\Delta p}{\rho . c}$ where Δp is the pulse pressure. In Figure 28, $\Delta p \simeq 35$ mm. Hg, and if c = 500 cm/sec, peak systolic velocity is almost 90 cm/sec, which is close to that measured.

Some waveforms in the ascending aorta had peak reverse velocities higher than those usually observed with EM flowmeters. This is probably a combined effect of the superior frequency-response and inferior reverse flow accuracy of hot film probes. In many of these experiments, cardiac cycles were short because of anaesthetic-induced tachycardia, and reverse flow in early diastole lasted less than 20 msec.; this implies frequency components of 25 Hz and above. Also the spatial averaging which occurs with cuff EM flowmeters might possibly lower their signals in reverse flow; small phase differences in the timing of boundary layer and core flow reversal, for example, would have this effect. In the descending aorta, backflow in early diastole did not always occur (e.g. Fig.29), and never reached the velocities seen more proximally. Fairly typical averaged waveforms for this site, and for the abdominal aorta, are shown in Fig.29; these are not from the same animal, since all sites could not be made accessible in each experiment.

Centreline peak velocities in the ascending aorta ranged from 40 to 200 cm/sec, which must reflect cardiovascular effects of anaesthesia and surgery, as well as

physiological variability. Time-average velocities ranged from 8 to 24 cm/sec.

Velocity profiles recorded at each site in the aorta showed consistent features from animal to animal, despite some scatter. In Figure 30, peak systolic velocity profiles are plotted in non-dimensional form at three sites in the ascending aorta. Each plot is made up of one or more profiles from each of several animals. The lower profiles were measured as near as possible to the aortic valve, with probes inserted just downstream of the sinuses of Valsalva. The profiles therefore represent the region 1-2 cm. from the valve. The next site was 1 cm. downstream from this, and the third (top) a further 1 cm. downstream, approximately 1 cm. proximal to the point of origin of the brachiocephalic artery. In all cases, the probes were aligned as nearly as possible in the plane of the arch, like wheel spokes. In these, and all succeeding profiles, points closer than 2 mm. to the walls have been deliberately excluded; at the near wall because of unreliability of the readings, as described earlier, and at the far wall because the vessel was unrestrained. The thoracic aorta expands and contracts radially by approximately 7% with each pulse (Barnett, Mallos & Shapiro, 1961). While the peak radial wall velocities associated with this were estimated to be only 3-7 cm/sec in the present experiments, the proportional errors in radial position are larger the closer the approach to the wall.

The first obvious feature of these profiles is that the boundary layers are very thin; in nearly all cases, they lie in the unexplored region less than 2 mm. from the walls.

This is in accordance with theoretical predictions. Since the proximal ascending aorta is an 'entrance region', it is possible to make crude estimates of boundary layer thickness in systole from simple theory (Schlichting, 1968). Such estimates only serve to predict the order of magnitude to be expected, since available theory treats situations which are much simpler and more clearly defined than the real one. Nonetheless, they provide useful confirmation that 2 mm. is a realistic upper limit to boundary layer thickness. Two methods can be used:

1) To consider the way a boundary layer over an infinite flat plate grows with time when motion is started impulsively from rest; this treats the time-course of systolic flow acceleration appropriately, and boundary layer thickness δ is given at any point by

$$\delta \simeq 4\sqrt{\nu.t}$$

where t is time elapsed since the onset of motion. If we take t as approximately one-tenth of the cardiac cycle, then δ is 2.5 mm. at a heart-rate of 1 Hz, and 1.5 mm at 3 Hz.

2) To examine the way a boundary layer grows with distance from the leading edge of a flat plate in steady flow; then δ is given by

$$\delta \simeq 4\sqrt{\frac{\nu.x}{u}}$$

where x is distance from the leading edge, and u is free-stream velocity far from the surface. If we assume that x is 2-4 cm., and u is 100 cm/sec, then δ = 1.4 - 2 mm. Boundary layer calculations for further cases, such as an oscillating flat plate, or a steadily accelerated flat plate, give very similar values.

If the boundary layer in the ascending aorta is assumed to be 2 mm. thick, and to be similar in form to that on a flat plate, the radius of the vessel will be effectively diminished by 0.7 mm. (the 'displacement thickness', Schlichting (1968)). A notional cross-sectional area for the flow can be calculated on this basis, and used in conjunction with the mean velocity figures quoted above, give a range of aortic flows between 1.0 and 3.7 litres/min, with a mean of 2.2 litres/min.

These values are reasonable, but must be approximate, since changes in aortic radius during the cardiac cycle are ignored. Radial expansion during systole may effectively cancel the 'displacement' effect of the boundary layer, since it acts in the opposite direction with comparable magnitude. Assuming zero boundary layer thickness gives figures 14-23% higher, the discrepancy getting smaller with increasing vessel radius; it would become less than 10% at a radius of 1.45 cm. In the human aorta, therefore (given axisymmetric flow), it might be possible to derive volume flow from a point velocity measurement with reasonable accuracy.

At the site nearest the aortic valve, the profiles shown in Fig.30 demonstrate reasonable axisymmetry, implying that blood ejected from the left ventricle moves into the aorta with uniform velocity (except very close to the walls). However, this pattern, which is typical of entry flow and has been commonly assumed to hold in the ascending aorta, did not usually hold throughout the cycle. Velocity profiles reconstructed from the averaged waveforms recorded at this site in a single animal are shown in Fig.31 for five phases of the cycle. In this case a marked skew developed in late systole, associated with a peaking of the velocity wave which is progressively more marked towards the anterior wall. The effect is illustrated in Fig.32, which shows individual waveforms near each wall.

The origin of this effect is not clear. It might originate in the ventricle, either as a result of the pattern of contraction, or of flow disturbances - for example the vortex round the mitral valve cusps which Bellhouse (1970) demonstrated in models and Taylor & Wade (1970) observed in vivo. It might be due to flow disturbances generated in the outflow tract; a traverse in this plane lies almost in line with the junction between two valve cusps anteriorly, and is in line with the centre of the third cusp posteriorly. Alternatively, it could be caused by the flow curving into the aorta; the axis of the ventricle lies at an angle to the ascending aorta, and the higher velocity occurred at the

inside of the curve; thus the mechanism described in Appendix B could operate. This seems a less likely origin, since in another animal the effect was present intermittently. A locally generated flow disturbance seems the most probable cause.

The marked early diastolic skew at this site could have similar origins; but its orientation is also consistent with drainage into the left coronary artery, since the posterior end of the traverse lies close to the left posterior sinus of Valsalva. Velocities were close to zero in the latter part of diastole; this was a feature common to most of the waveforms in this region.

The systolic velocity profiles at the two more distal sites in the ascending aorta (Fig.30) show progressive skewing, with higher velocities developing near the posterior wall (inner curvature of the arch). As the profiles show, this skew was consistent, though its magnitude varied from animal to animal.

In Figure 33 instantaneous profiles recorded at the most distal site in one animal are presented; the features they demonstrate, including the systolic skew, were seen consistently and strongly suggest inviscid behaviour in the broad core of the flow, under the influence of a centrifugal pressure gradient, as described in Appendix B. In very early systole the profile is axisymmetric (not shown); centrifugal forces then begin to act, and the skew appears; when flow reverses, the profile becomes a mirror image under the same influence. Thereafter the effect breaks down;

when the second direction change occurs (216°) the profile behaves as if only a uniform axial pressure gradient were acting. This may be because Reynolds numbers are low, as in very early systole, so that the centrifugal effect is inhibited and there is insufficient time for the skew to re-establish. Alternatively, or additionally, the pattern of flow near the aortic arch branches may be relevant; certainly during late diastole (324° onwards) anterior forward flow and posterior backward flow are maintained, suggesting a circulating flow, perhaps draining into the brachiocephalic artery. A further complicating factor is that the impedance offered to the streamlines entering the branches is probably different from that experienced by the flow which continues round the arch.

It was confirmed that the skews measured in this plane were not an artefact caused by progressive changes in flow alignment across the vessel relative to the probe. A probe was constructed with a cylindrical hot film element, which was aligned with its axis perpendicular to both the stream and the traverse; in this orientation it was insensitive to flow direction in the plane of the traverse; similar skews were measured under these conditions.

Instantaneous profiles for a single case at the middle site in the ascending aorta are shown in Fig.34. The systolic profiles in this case show both upstream and downstream influences, inflecting in late systole; during most other parts of the cycle, profiles are fairly symmetrical.

Traverses from left to right (at 90° to the plane of the arch) were only feasible at the distal site in the ascending aorta, since the pulmonary artery overlies the aorta more proximally. Traverses in this plane (Fig.35) also show thin boundary layers; the systolic profiles were always relatively axisymmetric but skews were present during backflow, with higher (backward) velocity towards the left wall; again, this might reflect drainage into the coronary arteries or local circulation of flow.

The growth of the boundary-layer with distance from a pipe entrance has been widely studied for steady laminar conditions, and it is possible to predict the length needed for full development of the profile - the entrance length - with considerable accuracy (see footnote, p.27). However, steady flow theory is obviously inappropriate in the aorta, and a number of attempts have been made to predict realistically entrance lengths in unsteady flow. Atabek & Chang (1961) used the simplified model of unidirectional oscillating flow in a rigid, straight pipe; they found that entrance length would vary with instantaneous velocity, and would be comparable with steady entrance length at the same velocity; thus even at modest velocity, the whole aorta would be an entrance flow. Kuchar & Ostrach (1967) extended the analysis to include the effects of elastic walls, and concluded that there will be an inviscid flow core, with very thin boundary layers, at least as far as the arch; they suggested that elsewhere in the aorta, complexity of the geometry renders the concept of entrance

regions inappropriate. Jones (1970) approached the problem differently, calculating boundary layer thickness in fully developed oscillating pipe flow from Womersley's (1955) solutions (which hold far from the entrance), and matching this to a boundary layer growing from the entrance in quasi-steady fashion. Using conditions appropriate for the proximal aorta, he obtained a matching point only about 1 cm. from the origin of the aorta. Matching results from steady and unsteady flow theory in this way is obviously crude, but the results emphasise one important feature of thoracic aortic flow which applies to both the dog and man - boundary layers are likely to be thin in any region, even away from the entrance.

This prediction is based upon the large values of the parameter α which apply in the thoracic aorta. Womersley first demonstrated the cardiovascular relevance of this frequency parameter, which is defined thus:

$$\alpha = r\sqrt{\frac{\omega}{\nu}}$$

where r is pipe radius, ν is kinematic viscosity, and ω is the angular frequency of the periodic flow oscillation. Since aortic flow is not sinusoidal, α is used approximately, calculated on the basis of heart rate. The simplest interpretation of α is that it represents a ratio between the vessel radius r, and the boundary-layer thickness (which in oscillating flow is proportional to $\sqrt{\frac{\nu}{\omega}}$ (Schlichting, 1968));

more precisely, α^2 represents a ratio between inertial (i.e. local accelerative) forces and viscous (retarding) forces; thus when α is large (e.g. greater than 10), viscous forces become unimportant and the flow is dominated by inertia; acceleration and pressure gradient are then almost in phase and boundary layers are thin in proportion to vessel radius. This is also true for inlet flow, so that although there is a conceptual difference between the two, both have very thin boundary layers.

The governing influence of α on velocity distribution in oscillating pipe flow has been demonstrated in a number of studies, both theoretical and experimental; Womersley's work is usually quoted because he was specifically considering arterial flow, and extended the theory to include complicating features, such as elastic boundaries. Values of α are high in the canine thoracic aorta; Young & Cholvin (1967) collected information on heart-rate and vessel size from the literature, and derived values of α for the thoracic aorta of 8-13, depending on body weight. The more recent literature yields the values plotted in Fig.51, which have a mean of 14.4. In Figure 36, non-dimensionalised velocity profiles, calculated from theory for fully-developed oscillating flow in a straight, rigid pipe at four points in the cycle for $\alpha = 10$ are drawn. The relative narrowness of the boundary layer is well shown, and it is clear that traverses across such a flow with the present probes would reveal little evidence of the boundary layer.

This is precisely what was found experimentally. In Figure 37, groups of peak systolic velocity profiles occurring in the arch and at three points in the descending aorta are plotted. Again, the data at each site is lumped from several animals; single, representative profiles at the upper and lower descending aorta sites are shown in detail in Fig.38 and Fig.39. The values of α for these cases were 12.8 and 15.3 respectively, and the bluntness of these profiles is therefore in keeping with the theoretical predictions. It is difficult to comment further on these profiles, since only one plane (left-right) can be explored in the descending aorta without distortion of the vessel. A skew, with higher velocities towards the right wall, was seen fairly consistently during systole (Fig.37); this is not explicable on the basis of inertial effects, because there is only a very slight curvature in the left-right plane at this level, and its origin must be related to the rotation and splitting of the flow as it traverses the arch. A fuller description of flow in this region would require detailed measurements in more than one plane, together with flow visualisation studies.

Velocity distribution in the lower abdominal aorta was examined in only a few cases because of size limitations. The most notable features here (Fig.40) were blunt and relatively axisymmetric systolic profiles and a lower velocity near the midline during reverse flow. This implies an M-shaped profile, a form which has been demonstrated for

convergent flows in dichotomously branching models at comparable Reynolds numbers by Schroter & Sudlow (1969), caused by the merging of the boundary layers from the inner walls of the daughter branches into the core of the flow in the parent branch. This explanation remains hypothetical, since difficulty of access and size limitation prevented more detailed exploration at this level.

As was mentioned earlier, the hot film technique has recently been used by two other groups for velocity measurements in the aorta (Ling et al, 1968; Schultz et al, 1969), and it is obviously of interest to compare their results with those presented here. Unfortunately this is not straightforward, since detailed technique and methods of data presentation differed in each case from those adopted here.

Ling et al used a simplified, nondirectional probe, and relied on signals from an electromagnetic cuff probe located just downstream to identify forward and reverse components of flow. As they demonstrate, this has a modifying effect on the flow waveform in the segments studied, though they do not describe any effect on the velocity profile. In addition, the probe was carried in a plastic cuff assembly which encircled the aorta at the level of the traverse, so that the vessel wall was constrained and held rigidly; this also introduces the risk of angulation or displacement of the vessel, which distorts the measured profiles. It also seems likely that their calibration was subject to wake artefacts,

as described earlier, since they calibrated probes in an oscillating pipe flow with zero mean flow. Thus absolute values of velocity, and details of the waveforms and profiles, may show some degree of distortion; but their results are still of considerable interest because the immobile vessel wall and the simplified, and therefore very small, probe permitted exploration of flow close to the walls. Their results agree well with those reported here; they show two sets of instantaneous profiles, measured in the descending thoracic aorta of the pig; the α values are 13.3 and 8.1, and the boundary layers have thicknesses of 1.8 and 2.0 mm. respectively.

Schultz et al, using probes of similar form to those described here, examined velocity distribution at a number of sites in the ascending and descending thoracic aorta of the dog. As discussed earlier, their calibration procedure (oscillation in still water) puts in question the reliability of the absolute velocities they record. They also accepted the inherent frequency characteristics of the system, which may have introduced distortion in the higher frequency components of the waveform. However, neither of these effects should grossly distort velocity profiles reconstructed at particular sites, and their results again show blunt profiles in the thoracic aorta. It is only possible to estimate boundary layer thickness roughly, since diameters are not stated (radial co-ordinates being plotted non-dimensionally as fractions), and they have made no

allowance for distortion due to wall movement or probe-wall interaction. Using the data as presented, the blunt core of the flow in the ascending aorta extends in all cases to within 0.15 radii of the wall - say 1.5 mm. for a vessel of 2 cm. diameter. In the proximal descending aorta, the corresponding figure is 0.25 - say 2 mm. for a vessel of 1.6 cm. In a later presentation (Bergel, Clark, Schultz & Tunstall-Pedoe, 1970), they include profiles at the level of the diaphragm, which show appreciable modification towards the parabolic form associated with developed steady or quasi-steady flow. In none of these cases are the α values given.

Their profiles in the upper thoracic aorta demonstrate the skew reported here, and must, of surgical necessity, have been in the same plane. In the ascending aorta, however, they do not report systematic skewing of the profile in the antero-posterior plane of the distal ascending aorta, which was such a consistent finding in the present study. This may be because traverse orientation was not systematically noted - they present 'antero-posterior' traverses which are variously described as 'normal to' and 'in the plane of' the arch - but a more likely reason lies in the way they derived time-averaged values of velocity (from which the majority of their profiles were constructed). Their direction-sensing system did not permit signal polarity switching during reverse flow, and signals from each traverse position were therefore integrated in

rectified form - that is, as if all flow were forward - to give a time-averaged velocity. This does not affect the profile if flow is axisymmetric, but it can cause a considerable transformation if there is skew during back-flow. Figure 41 shows an example drawn from the present work; the lower profile was obtained by integrating the switched signal, so that proper account was taken of reverse flow; the upper profile shows the result when the same waveforms were integrated in rectified form. It can be seen that the true skew is lost.

Confirmation of this effect is given by the one velocity profile which is presented in cyclic, instantaneous form among their results (Fig.12(b), Schultz et al, 1969). It was taken in the antero-posterior plane of the ascending aorta, and shows similar skews in both forward and backward flow to those found in the present study (e.g. Fig.33). Thus the apparent discrepancy between the two groups of results may well be artificial.

Flow disturbances

Some waveforms recorded in the proximal ascending aorta during the preceding experiments showed high frequency velocity fluctuations superimposed on the signal at, or shortly after, the moment of peak systolic velocity. One example, in which the disturbance was systematic enough to skew the velocity profile, has already been presented (Fig.32). In general, however, waveforms were smoother than this, particularly as the recording site moved distally,

and these experiments gave the impression that aortic flow was inherently undisturbed (i.e. laminar) although it might contain disturbances generated upstream of the proximal measuring site, presumably in the ventricle or outflow tract, and decaying with time.

However, in contradiction to this, a waveform showing marked high frequency systolic velocity fluctuations, and strongly suggesting turbulent flow, was recorded in the descending aorta during one experiment (Fig.42). This was the smallest animal in the series (16 Kg.) and was also atypical in that it had been premedicated with morphine and had a slower heart-rate (90 per minute) than the average. Both Ling et al and Schultz et al presented very similar waveforms recorded in the arch; both described this as turbulent flow, and commented that it had been observed rarely, and in smaller dogs only.

In many of these experiments, the Reynolds number in peak systole was of the order of 5000, so that steady flow theory would predict turbulence; a series of experiments was therefore performed to investigate whether true turbulence could ever occur in the aorta, and if it did, whether the governing fluid dynamic conditions could be defined. Because of the observations mentioned above, the experiments were performed in small animals; the procedure used in each case was to record instantaneous velocity waveforms (and in selected cases, their frequency spectra) in the thoracic aorta before and after inducing changes in peak

flow velocity and/or heart-rate by the methods listed earlier.

Under these conditions, flow disturbances were frequently provoked, and it proved possible to classify the velocity waveforms with very little ambiguity into three types - undisturbed, disturbed and highly disturbed. This was, of course, a qualitative judgment, based on visual inspection of the waveforms, but the three types were clearly distinguishable, and only occasional intermediate forms were difficult to categorise. Thus a velocity waveform with negligible high frequency components is termed undisturbed, and representative of laminar flow; a waveform with high frequency components only at peak systolic velocity is termed disturbed, and thought to be representative of a transitional condition; and a waveform with high frequency disturbances persisting all the way through the deceleration phase of systole is termed highly disturbed and is thought to represent turbulence. Examples of each are shown in Fig.43.

Strictly speaking, the presence of turbulence can be proved only by simultaneous demonstration of random velocity fluctuations in more than one plane of a flow. In practice, however, the process has been so well characterised in many fluid dynamic problems that fluctuations in one plane which have an appropriate frequency spectrum can be accepted as evidence of turbulence. In the aorta, the situation is

more complicated, since the unsteadiness of the underlying flow adds its own spectrum, which is inseparable from, and overlaps, that of the flow disturbances, as described in Appendix A. Nevertheless, frequency analysis provided strong evidence of the presence of true turbulence. Typical outputs at selected frequencies from such an analysis, together with the ('highly disturbed') input waveform, are shown in Fig.44, which demonstrates that there are appreciable high-frequency components associated with peak systole and the subsequent deceleration, and that these are damped out in diastole and vary in amplitude and duration from beat to beat. When the spectral energy distribution of such a waveform (calculated as in Appendix A) is compared to that for an 'undisturbed' waveform (Fig. 45), the increasing separation and differing rates of decay with increasing frequency are clearly shown.

These observations are reasonable evidence that true turbulence can occur within the aorta, and prompted two questions. Could the fluid dynamic conditions governing transition to turbulence be defined, and could the origin of turbulence (in the sense of boundary-layer transition or the amplification of upstream disturbances) be identified?

Fluid-dynamic conditions

Conditions governing transition to turbulence in steady flow are well defined; the controlling parameter is Reynolds number, $Re = \frac{UL}{\nu}$, where U is mean velocity, L the

characteristic length scale (diameter in pipe flow) and ν the kinematic viscosity. For small Re (e.g. low velocity, highly viscous fluid) flow will be laminar - that is, the flow will have steady well-defined streamlines, and the transport of material, momentum and energy across the streamlines will occur only by molecular motion; any disturbance initiated in such a flow will be rapidly damped out by viscous action. As Re is increased, the stability of the flow is altered, and the damping of small disturbances is decreased; ultimately, a condition of neutral stability is reached beyond which the amplification of at least some disturbances will take place. This value of Re is called the critical Reynolds number and denoted as Re_{crit}. When $Re > Re_{crit}$, and sufficient time is available, this amplification leads to turbulence, which manifests itself as random fluctuations in velocity, pressure, and other flow properties, superimposed on the mean properties of the flow. The critical Reynolds number for fully developed steady pipe flow, based on mean velocity and pipe diameter, is usually given as approximately 2000. For steady flow over a flat plate, with boundary layer thickness δ, the critical Reynolds number is given by

$$Re_{crit} = \frac{U\delta}{\nu} \simeq 1000 \qquad \text{(Schlichting, 1968)}$$

(these values of course correspond, since in fully developed pipe flow, $\delta = \frac{d}{2}$).

The disturbances that initiate turbulence may come from a number of sources, and their magnitude has a considerable influence on Re_{crit}. However the major difficulties in predicting the stability of aortic flow are due to its unsteadiness, since it is steady-state turbulence that has been primarily examined by fluid mechanicians. First, the appropriate Reynolds number must be chosen, since the mean value is obviously inappropriate in such highly unsteady flows. As the disturbances observed in this and the other hot film studies occurred at or near peak systolic velocity ($\hat{u}$), it is peak Reynolds number, $\hat{Re} = \frac{\hat{u}.d}{\nu}$, that is appropriate here. However, the previously mentioned fact that a finite time is required for small disturbances to grow to turbulence in supra-critical Reynolds number flow implies that $\hat{Re}$ is not the only governing parameter, but that the time course of velocity changes will also be important. The appropriate nondimensional parameter describing frequency is α ; as mentioned earlier, this represents a ratio between inertial and viscous forces in unsteady flow; more importantly in this context, it represents a ratio between the characteristic time for viscous forces to act, $\frac{r^2}{\nu}$, and the time of one cardiac cycle, $\frac{1}{\omega}$.

Thus at low values of α, quasi-steady behaviour will dominate, and Re_{crit} must be expected to approximate to 2000; as α increases, there is a decrease in the time

available in one cardiac cycle, as compared with the time required for amplification of a disturbance. Thus the observed Re_{crit} might be expected to rise with increasing heart-rate.

Thus good theoretical reasons existed for predicting that both $\hat{Re}$ and α would govern transition in aortic flow, and in this series of experiments, the flow state was examined as these parameters were altered. The experimental conditions are given in detail in the Table. In Figure 46 the data for the descending aorta obtained in both these and the previous experiments are summarised in terms of $\hat{Re}$, α, and the extent of the disturbances observed. As indicated in the figure, the shaded points represent highly disturbed or turbulent conditions, the half-shaded points represent disturbed (transitional) conditions, and the open points undisturbed (laminar) conditions. Furthermore, points obtained in the same dog under different conditions are connected by a straight line.

Although there are a number of points where, for a variety of reasons, only one flow condition was observed, it is clear that $\hat{Re}$ alone does not govern flow conditions and that there seems to be a general trend whereby increasing $\hat{Re}$ and/or decreasing α leads to a more disturbed flow condition. The undisturbed and disturbed or highly disturbed conditions can be approximately demarcated by a line having the equation

$$\hat{Re}_{crit} = 250\,\alpha \qquad (1)$$

Below this line, flow is stable and undisturbed; above it, disturbances begin to appear and can grow to turbulence.

Origins of turbulence

Having defined at least two of the main variables governing transition, it was of interest to attempt to define the origin of the disturbances, in the sense of distinguishing between freestream turbulence existing in the blood ejected from the ventricle, and turbulence arising locally in the aorta itself. This can be attempted tentatively be examining the relative energy content of waveforms recorded at different sites, since the time-averaged velocities in these and the previous experiments show that in the majority of cases, blood ejected from the left ventricle reaches the arch in a single beat. In the descending aorta, on the other hand, the flow is of blood which is in its second pulse since leaving the heart, and has therefore undergone a diastolic period in the aorta. In Figure 47 are shown spectra for similar conditions of flow in the arch and descending aorta of a single animal. The high frequency content in the arch is considerably increased over that in the descending aorta, which suggests that these are flow disturbances associated with the ejection of blood from the heart, and that they are damped out during diastole and are therefore much less marked in the descending aorta. However, this is not borne out by the results from dog 41, where both the ascending and descending aorta data is shown in Fig.48. Here the

ascending aorta sees first-beat blood, whilst the descending aorta sees second-beat blood. The control conditions match those described in the previous case, but following isoprenaline, high frequency disturbances occurred in the descending aorta; based on energy content above the 10th harmonic, this was in fact one of the most turbulent flows seen. Since diastole appeared quiescent, the disturbances in the descending aorta seem not to have been convected from the ascending aorta, but rather to have been generated locally in the blood flowing from the arch into the descending aorta on its second beat.

The implication of this is that transition to turbulence can occur in the descending aorta. It is possible to examine this proposition (and to provide a crude theoretical justification for the form of equation (1), which was derived experimentally) by applying boundary layer stability theory to the aortic wall boundary layer. This is done in Appendix C; there is general agreement with the data, and local transition is theoretically plausible.

The same applies to flow in the ascending aorta. In Figure 49, the data obtained in the ascending aorta is summarised. Again, an approximate demarcation line may be drawn between the undisturbed and the disturbed points, the resulting equation being

$$\hat{Re}_{crit} = 150\,\alpha \qquad (2)$$

In this case, the constant is almost a factor of two less than for the descending aorta. This is not unreasonable; the blood in this case is in its ejection stroke from the heart, and may already carry appreciable disturbances which might be expected to modify the critical Reynolds number of the wall boundary layer. Reductions of the order of two in critical Reynolds number due to free-stream disturbances were demonstrated by Dryden (1936).

Although these observations are compatible with boundary layer transition, there is obviously no proof, and there are other possible explanations for the origin of the observed disturbances. The most likely one is that disturbances originating in the ventricle or outflow tract, and interacting with each other, may in appropriate circumstances be strong enough to generate 'cascades' of smaller and smaller eddies before being damped out. These could give spectra of the observed form, at least in blood on its ejection stroke. In 'second-beat' blood, in the descending aorta, the mechanism could operate only if residual eddying was present in the arch region at the end of diastole. Some of the instantaneous profiles presented earlier (Figs.33, 38) show simultaneous forward and backward motion in diastole which may be a manifestation of this.

Finally, it should be noted that the earlier reported observations of Schultz et al and Ling et al were in good general agreement with those reported here, though enough detail is not given to allow their data to be included in Figs. 46 or 49.

CONCLUDING DISCUSSION

The observations presented here on velocity distribution confirm theoretical predictions in that boundary-layers both close to the left ventricle and far downstream in the descending aorta are shown to be thin. It is, however, clear that simple formulations of entrance-length, and of profiles in oscillating pipe-flow, are inappropriate; the most striking demonstration of this is the skewing which occurs in the distal ascending aorta under the influence of centrifugal force; the profile is still blunt, in the sense of having very thin boundary-layers, but the axial velocity at the edges of the boundary-layers on the inner and outer walls of the vessels may differ by 50% or more. Obviously any theory which ignores influences of this magnitude (i.e. straight pipe theory) is inadequate. The same is true for the effects of turbulence; even the more sophisticated theoretical developments, such as those of Womersley, assume laminar flow, and transition will inevitably modify boundary-layer behaviour.

The major influences which unsteadiness of the flow and transition to turbulence have in thinning aortic boundary-layers has meant that disappointingly little detail is revealed with the present probes; and boundary-layer exploration, even with much more miniaturised probes, would be a formidable undertaking. The aortic wall moves a millimetre or more radially in phase with pressure (Barnett et al, 1961); and the boundary-layer may be little thicker

than this. Measurements would almost certainly involve using a wall-mounted probe which could be traversed in fractions of a millimetre and discriminate spatially to that degree without interacting with the wall. It seems much more likely that information about the boundary-layer will come from 'remote' techniques like the very elegant 'gated' version of the ultrasonic Doppler flowmeter which is being developed by Perroneau et al (1969).

Despite the difficulties, more detail about boundary-layers is needed both to assess the magnitude of the shear-stresses to which the arterial wall is exposed, and to improve understanding of mechanisms of mass-transfer to the arterial wall. Fry (1968) demonstrated that the endothelial lining is sensitive to shear stress, and defined an 'acute yield stress', which lay between 300 and 540 dynes/cm^2 for the endothelium of the dog aorta; exposure to shear stresses whose time-averaged values exceeded these led to rapid deterioration and dissolution of the endothelial surface.

At the time when Fry reported these measurements, there was no information available about the magnitudes of wall shear stress which might occur in the normal circulation, and the situation is little better now. The present measurements have not defined the shape of the boundary-layer, so that calculations of wall shear stress involve assumptions about the velocity gradient at the wall and are very crude.

Assuming a boundary layer thickness of 2 mm., and a shape similar to that in steady flow over a flat plate, wall shear stress would reach 32 dynes/cm^2 for a systolic flow velocity of 100 cm/sec. Ling et al (1968) reported direct measurements made with a flush-mounted hot-film probe in a rigidly cuffed vessel in the descending aorta; peak shear stresses in systole reached 80-100 dynes/cm^2, and time-averaged values ranged from 16-32 dynes/cm^2.

These measurements, though direct, must be very approximate, as they will be extremely sensitive to the exact alignment of the probe surface flush with the endothelial surface. Rumberger et al (1972) have approached the problem differently, by examining the boundary-layer in the aorta of the horse (which is approximately 3 mm. thick); using a 1 mm. probe they have been able roughly to map it and estimate the velocity gradient at the wall. Their preliminary results give a peak shear-stress of 2-3 dynes/cm^2. These differ so greatly from those of Ling et al that it is clear that satisfactory measurements have yet to be made.

In addition to endothelial damage, Fry (1968) observed enhanced uptake of Evans' Blue dye into the arterial wall in regions of high shear stress. Similar observations were made by Caro et al (1971), and one of these illustrates extremely well how complex the flow behaviour may be close to vessel walls. One of the regions which showed marked uptake of Evans' Blue in Caro et al's experiments, when the dye was injected intravenously and allowed to circulate for

some time before examination of the vessels, was the anterior wall of the ascending aorta - i.e. the outer wall of the curvature into the arch. In the present experiments, the velocity of blood in the core of the flow close to this wall was shown to be lower than on the opposite wall, and since there was no evidence of different boundary-layer thickness, this would suggest a lower velocity gradient and shear-stress at the outer wall. This paradox is probably due to secondary motion, the faster-moving (outer) layers of the boundary-layer moving towards the wall under the influence of centrifugal force, effectively adding a component of flow towards the wall within the boundary-layer which would have a scouring effect. Again, local geometry appears to dictate the detailed form of the flow.

The observations reported by Caro et al demonstrated shear-dependence of mass transfer between the blood and the arterial wall, and led them to the hypothesis that this mechanism might be important in atherogenesis, by inhibiting efflux of materials like cholesterol in regions where the velocity gradient at the wall was low. Thus the lower limits of mean shear stress at arterial walls are also of interest, and are no better defined than the higher limits discussed above.

On a strictly practical level, velocity profiles in the aorta have relevance to other techniques of velocity and flow measurement in the aorta. Cuff electromagnetic flowmeters are sensitive to asymmetries in the velocity profile of the

flow through them; it is clear from the observations reported here that when they are used to measure aortic flow they should be located away from the curvature of the arch and wherever possible, calibrated in situ. It is also crucially important that they should not displace or angulate the vessel, since this can grossly distort the velocity profile locally. Catheter-tip velocity probes, whatever their mode of operation, can be expected to give reasonably representative time-averaged velocities for the broad core of the flow except when they are located very close to the wall (within 2 mm. for a hot-film catheter, 3-4 mm. for an electromagnetic catheter), but instantaneous values will not be reliable in the distal ascending aorta except very close to the centreline. In large vessels - such as the human ascending aorta - the mean core velocity should be within 10% of the true cross-sectional mean velocity, and it is potentially possible to measure cardiac output with reasonable accuracy if vessel diameter can be assessed angiographically.

The observations on turbulence have to be assessed carefully, since the fact that it can be precipitated in the aorta of the anaesthetised dog by manoeuvres like vagal stimulation or the administration of isoprenaline does not mean that it occurs under normal physiological conditions; indeed at first sight it rather suggests the opposite. It is, however, worth considering the matter a little further.

In order to use the conclusions reached above about transition predictively, it is necessary to know the normal range of $\hat{Re}$ and α , and the factors which may affect them. Measurements collected from the literature for a range of animal species (Fig.50) show that both $\hat{Re}$ and α increase with body size, and that these increases are roughly proportional. However, data is sparse for most species, and in the one species where it is reasonably abundant (the dog), there is very marked scatter, as is shown in Fig.51. There are several probable reasons for this, apart from experimental error, since the calculation of each point depends upon the assumption that viscosity is a constant, and upon three different measurements - vessel diameter, heart-rate, and peak velocity. The first and second will show body-size dependence; and the second and third will be strongly influenced by the nature and depth of anaesthesia. In Figure 51, for example, all the values of α above 17 were derived from animals under barbiturate anaesthesia, which regularly produces tachycardia. It also lowers peak velocity, and the lower values of Reynolds number are probably biassed downwards from this cause. The overall effect of anaesthesia will thus be to displace the points downwards and to the right, which the present observations would predict to be a stabilising influence. That this effect operates, particularly on Reynolds number, is confirmed by the data of Noble et al (1966), which was

obtained in resting, conscious animals. The Reynolds numbers are consistently at the high end of the range; it is possible that they are biassed upwards slightly because of local flow acceleration due to the constricting effect of the cuff probe; but even if this effect was very marked (say 20%), the points would still be at the high end of the range.

Many of the points in Fig.51 would lie above the demarcation lines in Figs.46 and 49, and might therefore be expected to represent transitional or turbulent flows; but since values of $\hat{Re}$ and α are anaesthetic-sensitive, it is of particular interest to examine their relationship in conscious animals and particularly man.

Relevant data is extremely sparse; the values derived from Noble et al are virtually the only ones available for the dog. For normal man, eight points can be derived from the results of Snell et al (1965), who used the pressure-gradient technique to measure velocity; and four points can be calculated from the data of Gabe et al (1969). These refer to four patients with ischaemic heart-disease, but since there was sinus rhythm without anatomical or valvular abnormality, it is perhaps reasonable to assume that normal fluid dynamic conditions existed. Finally, five values are calculable for normal man from the data of Prec et al (1949) on the assumption that peak velocity is twice mean systolic velocity - i.e. that the systolic flow waveform is triangular. All these points, which apply to the ascending aorta, are

plotted in Fig.52; and the line from Fig.49 which represents equation (2) is drawn in. It seems likely on the present assessment that almost all these flows would have been transitional or turbulent.

The situation in high output states such as exercise is even more speculative, since there does not appear to be any quantitative data available for conscious animals. Published electromagnetic flowmeter waveforms suggest that peak velocities (and therefore $\hat{Re}$) may be as much as 50% higher than resting values. Comparable changes in α would also occur due to tachycardia (doubling heart-rate would increase α by 40%), so that under physiological conditions, the $\hat{Re}$-α point might well reside above the demarcation line and move up and down parallel to it with changes in cardiac output.

The distance to which such turbulence in the ascending aorta might extend through the circulation is entirely speculative, and is an obvious subject for study with catheter-tip hot-film probes. Schultz et al observed simultaneous turbulence in the aorta and the brachiocephalic artery in one animal, but could not decide whether this was convected to the downstream site or locally generated; the amplitude of the turbulent velocity fluctuations was much lower in the brachiocephalic record. Both $\hat{Re}$ and α are, of course, directly proportional to vessel radius, and will fall with distance from the heart; but $\hat{Re}$ will also depend on local flow velocity, which may remain high at

least in the first generation of branches; beyond that it seems unlikely that transition could occur.

There is no apparent reason, from the fluid dynamic viewpoint, why turbulence should be undesirable, since the increased pressure drop over a laminar flow would be trivial compared to that caused by the peripheral resistance. There are, however, a number of interesting physiological implications. The first relates to sound production. It has been generally assumed in physiological and clinical circles that turbulence is what causes murmurs, and/therefore that in the normal circulation, it is usually absent; and the statement by McDonald (1960), that laminar flow is silent, has generally been accepted. Neither of these is necessarily true. There are a number of phenomena associated with laminar flow which may generate sound - the vortex shedding which is the mechanism of the Aeolian harp being the classical example; and Bruns(1959) has argued that such phenomena are the cause of intravascular murmurs. Similarly, there is no <u>a priori</u> reason why turbulent pressure fluctuations should always be detectable at the chest wall; there might well be a 'threshold' corresponding to an appreciable intensity of turbulence within the vessel.

No systematic attempt was made during these experiments to study sound generation. However, a loud, low-pitched systolic murmur was audible for the highly-disturbed flow conditions in dogs 41 and 42 when a stethoscope was applied to the aortic wall. These murmurs were not audible in the

neck, and possibly would not have been audible through the chest wall in a closed-chest animal. In the undisturbed control conditions in dog 41, no murmur was audible.

The presence of turbulence in a flow will modify conditions close to the wall through its effect on the shape of the boundary layer; if the mean flow-rate is not altered, the boundary-layer will be thinner in turbulent flow, and the velocity-gradient at the wall steeper. This effect will not always be gross, because the mean velocity outside the boundary-layer will fall. In steady flow, for example, at a fixed Reynolds number of 2000, transition from Poiseuille flow to turbulent flow will increase the velocity gradient at the wall by approximately 50%. In arterial flow, the effect would probably be greater, since the profile is blunt even before transition; but its magnitude would also depend upon the mechanism of transition, which is not yet clarified.

No long-term studies have been made of the effect of vibration on arterial walls, for obvious reasons; but Roach (1963) demonstrated that the onset of acute post-stenotic dilatation in vivo occurred only when a murmur and palpable thrill were present over the segment distal to a stenosis. More recently, she has shown (Boughner & Roach, 1970) that the changed elastic properties seen distal to a stenosis can also be produced by exposure of the vessel to small amplitude vibrations in the frequency range 30-400 Hz

for periods of several hours. This matches closely the frequency spectrum of velocity fluctuations detected during this work in turbulent flow. It is interesting to speculate that the dilatation of major arteries which takes place with age may be in response to prolonged low-amplitude vibration rather than intrinsic degenerative changes.

A great deal more needs to be done to define normal flow conditions within major arteries of animals and man, particularly close to boundaries, and it is clear that both new types of transducer, and a range of flow-visualisation techniques and mass-transfer studies, will be required both in vivo and in models to provide experimental information. The hot-film technique, however, may still have a good deal to offer; it is being applied to obtain more detailed descriptions of intra-arterial flow-patterns, both in larger animals (Rumberger et al, 1972), and, with probes of sub-millimetric dimensions (Francis, personal communication), in the dog. Obvious points to emerge from the present study are the need to establish normal values of Reynolds number and α in man, to find out whether turbulence is the normal regime of flow in the human aorta, and to examine the relationship between turbulence and the generation of audible murmurs. Work along these lines, with catheter-tip versions of the hot-film probe, is now in progress (Seed, 1972).

ACKNOWLEDGEMENTS

Thanks are due to many colleagues who helped this project. It began shortly after the Physiological Flow Studies Unit was established, and I am particularly indebted to Dr. C.G. Caro, Director of the Unit, both for the invitation to undertake it, and for the provision of many superb facilities.

Successful development and application of the probe would have been impossible without the long period of collaboration I enjoyed with a fluid-dynamicist, Dr. N.B. Wood. The observations on turbulence were in large part made with Dr. Robert Nerem during a short visit which he paid to the Unit.

Many colleagues gave their time freely in discussion. In particular, Drs. L.J.S. Bradbury, T.J. Pedley and K. Parker helped with fluid mechanics problems, and Messrs. B. Belcher and M. Gordon with questions involving electronics. Technical assistance was provided by Mr. P.W. Dytko, who made many of the probes, Messrs. M. Blackett and V. Bass, who constructed apparatus, and Mr. P. Ford, whose help was invaluable in the animal laboratory.

The work was supported by grants from the Wates and Nuffield Foundations and funds from the Medical Research Council. Personal support came from the latter, and from St. Thomas's Hospital Endowment Fund.

APPENDIX A: Frequency spectral analysis

In a turbulent flow, the random eddies which constitute turbulence will be 'seen' by a velocity probe as fluctuating velocity components superimposed upon the bulk flow velocity. Thus the velocity recorded at a point in a turbulent flow may be represented as U+u', where U is the mean velocity, and u' is the fluctuating or turbulent component. Since u' fluctuates randomly, its average value is zero. However, the value of u'^2 will not be zero, since squaring 'rectifies' the oscillations; so the mean square value of u', which is $\overline{u'^2}$, has a positive value, and this represents the mean kinetic energy of the fluctuating velocity, u'. For comparison between different flows, it is convenient to express velocity and energy components non-dimensionally, as ratios of the corresponding mean components; thus $\frac{\overline{u'^2}}{U^2}$ expresses the fluctuating (turbulent) kinetic energy as a fraction of the mean kinetic energy of the flow.

Because the eddies in turbulent flow are on every scale from large to small, and are carried with the mean flow, the fluctuating velocity components seen by the (stationary) probe will contain many frequencies, and a frequency distribution or spectrum of u' will exist, which can be characterised in a number of ways. For example, the amplitude of the fluctuating velocity component can be measured in a series of successive frequency bands; from this, fractional kinetic energy per cycle ($\frac{\overline{u'^2}}{U^2.\Delta f}$, where Δf is bandwidth) can be calculated and expressed as a function of frequency, f. Typically, this distribution

curve will be centred on some frequency, f_0, and will diminish in amplitude as frequency becomes both very large and very small about this value f_0. The value of f_0 will be dictated by the size of the largest eddies in the flow, and these will be on a scale, L, related to the geometry of the flow. In a pipe flow, for example, the largest eddies will have a diameter approximately that of the pipe, and thus the appropriate value of L will be pipe diameter. Thus f_0 will be approximately equal to U/L. The maximum amplitude occurring within this frequency spectrum will be dictated by a number of interacting and often complicated features of the flow, which may include such phenomena as local and upstream geometry, flow obstructions and fluid viscosity.

When the underlying flow is unsteady, as in an artery, the situation is more complicated, since frequency analysis of the velocity, U+u', will show the combined frequency distribution of the basic unsteady waveform and the turbulence. The former will be represented by a set of harmonics, falling in amplitude to, perhaps, 1% of peak velocity by the tenth - say 25 Hz in the dog. The frequency distribution of u' will be smooth, moving from virtually zero at low frequency through a peak and back towards zero at high frequencies. Thus the frequency spectrum will contain two patterns which may well overlap, though turbulent fluctuations at any frequency will be random from beat-to-

beat, whilst the harmonics of the underlying waveform will not. Thus even if quantitative spectra are available, distinctions between laminar and turbulent flows may be difficult.

As mentioned above, comparison between two turbulent spectra is facilitated by plotting energy ratios rather than absolute values, since the latter are likely to vary with Reynolds number, and therefore with U. In unsteady flow, comparability is further helped by plotting such ratios against harmonic number rather than frequency, since both axes are now non-dimensional and the parts of the spectra contributed by underlying flow harmonics should 'collapse' on to each other.

Such a format has been adopted in this work. Measurements of the velocity component in each frequency band were made by passing the arterial velocity signal through a frequency spectrum analyser (Brüel & Kjer Audio Frequency Spectrometer type 2112). This contains a switched series of narrow bandpass filters, with very sharply cut off upper and lower limits, which allow instantaneous analysis in one-third octave steps from a centre frequency of 25 Hz upwards. The sine-wave output therefore represents the instantaneous peak-to-peak amplitude of the signal for frequencies within one-third of an octave about the set frequency. An example of the output at a number of frequency settings is shown in Fig.44, together with the input

velocity signal. Spectral energy distributions were derived from these measurements as follows: the peak signal in each frequency band was averaged from a series of beats. Since this signal, which we call a, is a sine-wave, $a/\sqrt{2}$ is a root-mean-square value for the velocity fluctuation occurring during systole in that frequency band, and $\frac{a^2}{2}$ is the mean-square (i.e. energy) value. To convert this into fractional systolic energy, it was divided by $\hat{u}^2$, where $\hat{u}$ is peak systolic velocity. Finally, each value of this was divided by the number of harmonics within its frequency band, to give fractional systolic kinetic energy per harmonic (E). Thus for each waveform, a series of values of E was derived, each corresponding to a particular frequency - which itself was divided by heart-rate and expressed as a harmonic. In Figures 45, 47 and 48, E is plotted against harmonic number; each of these plots is thus a systolic energy spectrum over a particular harmonic range.

APPENDIX B: Velocity distribution of inviscid flow in a bend

In unsteady inviscid flow in a rigid pipe bend, the streamline patterns will be fixed and will be invariant with time, and by continuity so will all relative velocities. Therefore the derivation may be simplified by assuming steady flow.

Figure 53 shows the system being considered. Fluid is originating from a uniform stagnation region (1), representing the ventricle. Although the velocity in the ventricle is not zero throughout the cycle, the blood is probably sufficiently mixed for stagnation conditions there to be considered uniform at any instant. The fluid flows into a curved conduit and passes through a plane (2), which is orthogonal to the streamlines. Distance along the plane is denoted by s and velocity u_2 and pressure p_2 may vary along it.

Along any streamline, Bernouilli's theory relates pressure and velocity:

$$p_0 = p_2 + \tfrac{1}{2}\rho . u_2^2 \qquad (B.1)$$

(Where p_0 is the (uniform) stagnation pressure of the flow and p_2 is the static pressure in region (2).)

The centrifugal pressure gradient along s is given by

$$\frac{\partial p_2}{\partial s} = \frac{\rho . u_2^2}{r} \qquad (B.2)$$

where r is the radius of curvature of the streamline at the point along s considered.

Differentiating eq.(B.1) with respect to s,

$$0 = \frac{\partial p_2}{\partial s} + \rho . u_2 . \frac{\partial u_2}{\partial s} \qquad (B.3)$$

Substituting for $\frac{\partial p_2}{\partial s}$ from (B.2) and rearranging,

$$\frac{u_2}{r} = - \frac{\partial u_2}{\partial s} \qquad (B.4)$$

Since increments in r and s are identical, B.4 becomes

$$\frac{u_2}{r} = \frac{-du_2}{dr} \quad , \quad \text{i.e.} \quad \frac{dr}{r} = \frac{-du_2}{u_2} \qquad (B.5)$$

the solution of which is

$$\ln.r = -\ln.u_2 + \ln.c$$

where ln.c is a constant of integration,

$$\text{i.e.} \qquad r.u = \text{constant} \qquad (B.6)$$

Thus the velocity is inversely proportional to the radius of curvature of the streamline, and is therefore larger at the inside of the bend. The same mechanism will operate when the direction of flow is reversed. A consequence of this velocity distribution, by continuity, is

that the streamlines will be more concentrated at the inside of the bend, and more widely spaced at the outside; they will not in general be concentric. The extent of the skew which is produced will be inversely proportional to the radius of curvature; variations in this dimension are probably the cause of the variations in skew in different animals which are seen in Fig.30.

APPENDIX C: Boundary layer stability theory

Stability theory may be applied crudely to the aortic wall boundary layer by considering the forward flow in systole to be comparable to that associated with the instantaneous acceleration of flow over a flat plate. The velocity profile in this case is not unlike that of a steady flat-plate boundary layer and the critical Reynolds number criteria for a flat-plate based on the boundary layer thickness δ may be applied as a first approximation, i.e.

$$\hat{Re}_{crit} = \left(\frac{\hat{u}.\delta}{\nu}\right)_{crit} \simeq 1000 \qquad (C.1)$$

It is only necessary to estimate boundary layer thickness, and this can be done by using the accelerated flat-plate formula

$$\delta \simeq 4\sqrt{\nu.t} \qquad (C.2)$$

and defining t as $\frac{1}{4\omega}$ - the approximate duration of systole; then on substitution, equation C.2 becomes

$$\frac{\delta}{r} \simeq \frac{2}{\alpha} \qquad (C.3)$$

A similar result may be obtained by examining Womersley's solutions (1957) where the constant is estimated to be 8. The profiles presented by Ling et al give a value of approximately 5.5, and the results obtained in this study

(assuming a boundary layer thickness of 2 mm.) give values between 2 and 5.5. The choice is obviously somewhat arbitrary. However, if an equation of the form of C.3 is combined with C.1, the dependence of critical Reynolds number may be shown to be

$$Re_{crit} = \text{constant} \times \alpha \qquad (C.4)$$

where the constant of proportionality ranges from 250 to 1000 depending on which of the above values is used. The experimental correlation (equation (1)) has the same format as this, with a constant at the lower end of the range estimated above. This in fact would be expected, since the disturbances generally occur during flow deceleration in systole; decelerating flows such as this exhibit inflection points in their velocity profiles, and have been shown to be more unstable than steady or accelerating flows (Shen, 1961).

REFERENCES

Adams, D.B., Baccelli, G., Mancia, G. & Zanchetti, A. (1969) Cardiovascular changes during naturally elicited fighting behaviour in the cat. American Journal of Physiology 216, 1226-1235.

Atabek, H.B. & Chang, C.C. (1961) Oscillatory flow near the entry of a circular tube. Zeitschrift für angewandte Mathematik und Physik, 12, 185-201.

Barnett, G.O., Mallos, A.J. & Shapiro, A. (1961) Relationship of aortic pressure and diameter in the dog. Journal of Applied Physiology 16, 545-548.

Baxter, I.G. & Pearce, J.W. (1951) Simultaneous measurement of pulmonary arterial flow and pressure using consenser manometers. Journal of Physiology 115, 410-429.

Bellhouse, B.J. (1970) Fluid mechanics of a model mitral valve. Journal of Physiology 208, 72-73P.

Bellhouse, B.J. & Rasmussen, C.G. (1968) Low-frequency characteristics of hot-film anemometers. DISA Information, No.6, 3-10. DISA, Herlev, Denmark.

Bergel, D.H., Clark, C., Schultz, D.L. & Tunstall-Pedoe, D.S. (1970) The measurement of instantaneous blood velocity and a calculation of total mechanical energy expenditure

in ventricular pumping. AGARD Conference Proceedings No.65, Session 3, paper 19, 1-15.

Bergel, D.H. & Gessner, U. (1966) The electromagnetic flowmeter. In: Methods in Medical Research 11, 70-82. Ed.: R.F. Rushmer, Yearbook Medical Publishers, Chicago.

Boughner, D.R. & Roach, M.R. (1970) The effect of low-frequency vibration on arterial wall elastin. AGARD Conference Proceedings No.65, Session 2, paper 9, 1-8.

Bruns, D.L. (1959) A general theory of the causes of murmurs in the cardiovascular system. American Journal of Medicine 27, 360-374.

Caro, C.G., Fitz-Gerald, J.M. & Schroter, R.C. (1971) Atheroma and arterial wall shear: Observation, correlation and proposal of a shear dependent mass transfer mechanism for atherogenesis. Proceedings of Royal Society of London B, 177, 109-159.

Dryden, H.L. (1936) Air flow in the boundary layer near a plate. National Advisory Committee for Aeronautics Report No.562. Superintendent of Documents, Washington, D.C.

Ferguson, D.J. & Wells, H.S. (1959) Frequencies in pulsatile flow and response of magnetic meter. Circulation Research 7, 336-341.

Francis, G.P., Kiser, K.M. & Falsetti, H.L. (1972) An experimental study of velocity profile development in the aorta. Proceedings of DISA conference on fluid-dynamic measurements in the industrial and medical environments, 305-313. Ed: D.J. Cockrell, Leicester University Press.

Frank, O. (1928) Der Ablauf der Geschwindigkeit in der Aorta. Sitzungsberichte Gesellschaft Morphologie und Physiologie, Munich, 38, 1-7.

Fry, D.L. (1968) Acute vascular endothelial changes associated with increased blood velocity gradients. Circulation Research 22, 165-197.

Fry, D.L., Mallos, A.J. & Casper, A.G.T. (1956) A catheter tip method for measurement of the instantaneous aortic blood velocity. Circulation Research 4, 627-632.

Gabe, I.T., Gault, J.H., Ross, J., Jnr., Mason, D.T., Mills, C.J., Shillingford, J.T. & Braunwald, E. (1969) Measurements of instantaneous blood flow velocity and pressure in conscious man with a catheter-tip probe. Circulation 40, 603-614.

Goldstein, S. (1938) Modern Developments in Fluid Dynamics, Volume I, Chapter 2. Clarendon Press, Oxford.

Gordon, M. (1972) A modular instrumentation system. Journal of Physiology 223, 13-14P.

Grahn, A.R., Paul, M.H. & Wessel, H.U. (1968) Design and evaluation of a new linear thermistor velocity probe. Journal of Applied Physiology 24, 236-246.

Grahn, A.R., Paul, M.H. & Wessel, H.U. (1969) A new direction-sensitive probe for catheter-tip thermal velocity measurements. Journal of Applied Physiology 27, 407-412.

Ham, T.H., Shen, S.C., Fleming, E.M. & Castle, W.B. (1948) Studies on the destruction of red blood cells. Thermal injury: action of heat in causing increased spheroidicity, osmotic and mechanical fragilities and hemolysis of erythrocytes: observations on the mechanisms of destruction of such erythrocytes in dogs and in a patient with a fatal burn. Blood 3, 373-403.

Jones, A.S. (1970) Wall shear in pulsatile flow. Applied Mathematics Preprint, University of Queensland, No.35.

Katsura, S., Weiss, R., Baker, D. & Rushmer, R.F. (1959) Isothermal blood flow velocity probe. I.R.E. Transactions on Medical Electronics, ME6, 283-285.

King, L.V. (1914) On the convection of heat from small cylinders in a stream of fluid: Determination of the convection constants of small platinum wires with applications to hot-wire anemometry. Philosophical Transactions of the Royal Society of London, A214, 373-432.

Kirkebø, A. (1968) Cardiovascular investigations on hedgehogs during arousal from hibernating state. Acta Physiologica Scandinavica 73, 394-406.

Kuchar, N.R. & Ostrach, S. (1967) Unsteady entrance flows in elastic tubes with application to the vascular system. Case Western Reserve University Report F.T.A.S./T.R.-67-25.

Laufer, J. (1954) The structure of turbulence in fully-developed pipe flow. N.A.C.A. Technical Report No.1174.

Lighthill, M.J. (1954) The response of laminar skin friction and heat transfer to fluctuations in the stream velocity. Proceedings of the Royal Society of London, A224, 1-23.

Ling, S.C. (1960) Heat transfer characteristics of hot-film sensing elements used in flow measurement. Trans. ASME. Journal of Basic Engineering 82, 629.

Ling, S.C., Atabek, H.B. & Carmody, J.J. (1969) Pulsatile flow in arteries. Proceedings of 12th International Congress on Applied Mathematics, 277-291. Ed: M. Hetényi & W.G. Vincenti. Springer-Verlag, Berlin.

Ling, S.C., Atabek, H.B., Fry, D.L., Patel, D.J. & Janicki, J.S. (1968) Application of heated-film velocity and shear probes to hemodynamic studies. Circulation Research 23, 789-801.

Machella, T.E. (1936) The velocity of blood flow in arteries in animals. American Journal of Physiology 115, 632-644.

McDonald, D.A. (1952) The velocity of blood flow in the rabbit aorta. Journal of Physiology 118, 328-339.

McDonald, D.A. (1952) The occurrence of turbulent flow in the rabbit aorta. Journal of Physiology 118, 340-347.

McDonald, D.A. (1955) The relation of pulsatile pressure to flow in arteries. Journal of Physiology 127, 533-552.

McDonald, D.A. (1960) Blood flow in arteries. Monographs of the Physiological Society No.7. Edward Arnold, London.

McFarlane, R.G. (1960) The blood coagulation system. In: The Plasma Proteins, Volume 2, 137-181. Ed: F.N. Putnam, Academic Press, New York.

Mills, C.J. (1966) A catheter tip electromagnetic velocity probe. Physics in Medicine & Biology 11, 323-324.

Mills, C.J. & Shillingford, J.P. (1967) A catheter tip electromagnetic velocity probe and its evaluation. Cardiovascular Research I, 263-273.

Mixter, G., Jnr. (1953) Respiratory augmentation of inferior vena caval flow demonstrated by a low-resistance phasic flowmeter. American Journal of Physiology 172, 446-461.

Müller, A. (1954) Über die Verwendung des Pitot-Rohres zur Geschwindigkeitsmessung. Helvetica physiologica et pharmacologica acta 12, 98-111.

Nikuradse, J. (1934) In: Applied Hydro- and Aeromechanics. Quoted by L. Prandtl & O.G. Tietjens. McGraw-Hill, New York.

Noble, M.I.M., Trenchard, D. & Guz, A. (1966) Left ventricular ejection in conscious dogs: 1. Measurement and significance of the maximum acceleration of blood from the left ventricle. Circulation Research 19, 139-147.

Ohlsson, N-M. (1962) Left heart and aortic blood flow in the dog. Acta Radiologica, Supplement 213, 1-80.

Pedley, T.J. (1972) On the forced heat transfer from a hot film embedded in the wall in two-dimensional unsteady flow. Journal of Fluid Mechanics 55, 329-358.

Perroneau, P., Hinglais, J., Pellet, M., Leger, F. & Schwartz, P.Y. (1970) Vélocimètre sanguin par effet Doppler à émission ultra-sonore pulsée. L'Onde Electrique 50, 369-389.

Pfeffer, M.A. & Frohlich, E.D. (1972) Electromagnetic flowmetry in anaesthetised rats. Journal of Applied Physiology 33, 137-140.

Porje, I.G. & Rudewald, B. (1961) Haemodynamic studies with differential pressure technique. Acta Physiologica Scandinavica 51, 116-135.

Prandtl, L. (1952) Essentials of Fluid Dynamics. Blackie, London.

Prec, O., Katz, L.N., Sennett, L., Roseman, R.H., Fishman, A.P. & Hwang, W. (1949) Determination of the kinetic energy of the heart in man. American Journal of Physiology 159, 483-491.

Richardson, P.D. (1967) Heat transfer from a circular cylinder by acoustic streaming. Journal of Fluid Mechanics 30, 337-355.

Roach, M.R. (1963) Experimental study of the production and time-course of post stenotic dilatation in the femoral and carotid arteries of adult dogs. Circulation Research 13, 537-551.

Rumberger, J.A., Gross, D.R., Muir, W.W. III, Geiger, G.L., Nerem, R.M. & Hamlin, R.L. (1972) Exploratory measurements of arterial flow in horses. Proceedings 25th Annual Conference on Engineering in Medicine & Biology, p.152.

Sarpkaya, T. (1966) Experimental determination of the critical Reynolds number for pulsating Poiseuille flow. Transactions of the American Society for Mechanical Engineers, Series D. Journal of Basic Engineering 88, 589-598.

Schlichting, H. (1932) Berechnung ebener periodischer Grenzschichtströmungen. Physikalische Zeitschrift 33, 327-335.

Schlichting, H. (1968) Boundary-Layer Theory. Translated by J. Kestin. McGraw-Hill, Maidenhead.

Schröter, R.C. & Sudlow, M.F. (1969) Flow patterns in models of human bronchial airways. Respiration Physiology 7, 341-355.

Schultz, D.L., Tunstall-Pedoe, D.S., Lee, G. de J., Gunning, A.J. & Bellhouse, B.J. (1969) Velocity distribution and transition in the arterial system. In: Circulatory and Respiratory Mass Transport. A Ciba Foundation Symposium, 172-202. Ed: G.E.W. Wolstenholme & J. Knight. Churchill, London.

Seed, W.A. (1972) Hot-film anemometry in the human aorta. In: Blood flow measurement. Ed: C. Roberts, 147-150. Sector Publishing Ltd., London.

Shen, S.F. (1961) Some considerations on the laminar stability of time-dependent basic flows. Journal of Aerospace Sciences 28, 397-417.

Shercliffe, J.A. (1962) The Theory of Electromagnetic Flow-Measurement. University Press, Cambridge.

Snell, R.E., Clements, J.M., Patel, D.J., Fry, D.L. & Luchsinger, P.C. (1965) Instantaneous blood flow in the human aorta. Journal of Applied Physiology 20, 691-695.

Spencer, M.P. & Greiss, F.C. (1962) Dynamics of ventricular ejection. Circulation Research 10, 274-279.

Spencer, M.P., Johnston, F.R. & Denison, A.B., Jr. (1958) Dynamics of the normal aorta. 'Inertiance' and 'compliance' of the arterial system which transforms the cardiac ejection pulse. Circulation Research 6, 491-500.

Stoker, J.J. (1957) Water waves. Interscience Publishers, Inc., New York.

Taylor, D.E.M. & Wade, J.D. (1970) The pattern of flow around the atrioventricular valves during diastolic filling. Journal of Physiology 207, 71-72P.

Taylor, D.E.M. & Whamond, J.S. (1972) Measurement of energy and flow distribution within heart-chambers in vivo. Proceedings of DISA conference on fluid-dynamic measurements in the industrial and medical environments, 340-343. Ed: D.J. Cockrell, Leicester University Press.

Vidal, R.J. & Golian, T.C. (1967) Heat-transfer measurements with a catalytic flat plate in dissociated oxygen. American Institute of Aeronautics and Astronautics Journal 5, 1579-1588.

Wessel, H.U., James, G.W. & Paul, M.H. (1966) Effects of respiration and circulation on central blood temperature of the dog. American Journal of Physiology 211, 1403-1412.

Womersley, J.R. (1955) Method for the calculation of velocity, rate of flow and viscous drag in arteries when the pressure gradient is known. Journal of Physiology 127, 553-563.

Womersley, J.R. (1957) The mathematical analysis of the arterial circulation in a state of oscillatory motion. Technical Report WADC TR 56-614. Wright Air Development Center, Ohio.

Yellin, E.L. (1966) Laminar-turbulent transition process in pulsatile flow. Circulation Research 19, 791-804.

Young, D.F. & Cholvin, N.R. (1966) Application of the concept of similitude to pulsatile blood flow studies. Biomedical Fluid Mechanics Symposium, 78-88. American Society of Mechanical Engineers.

Supplement

Published papers which have content in common with this thesis

Seed, W.A. (1969) Fabrication of thin-film microcircuits on curved substrates. Journal of Scientific Instruments, Series 2, 2, 206.

Seed, W.A. & Wood, N.B. (1969) An apparatus for calibrating velocity probes in liquids. Journal of Scientific Instruments 2, 896-898.

Seed, W.A. & Wood, N.B. (1970a) Development and evaluation of a hot-film velocity probe for cardiovascular studies. Cardiovascular Research 4, 253-263.

Seed, W.A. & Wood, N.B. (1970b) Use of a hot-film velocity probe for cardiovascular studies. Journal of Physics E. Scientific Instruments, Series 2, 3, 377-384.

Seed, W.A. & Wood, N.B. (1971) Velocity patterns in the aorta. Cardiovascular Research 5, 319-330.

Nerem, R.M. & Seed, W.A. (1972) An in vivo study of aortic flow disturbances. Cardiovascular Research 6, 1-14.

TABLE

Summary of data for flow conditions

Dog	Aortic site	Diameter (cm)	Experimental condition*	Heart rate (Hz)	Peak velocity (cm/sec)	$\hat{Re}$	α	Flow state
35	Descending	1.0	Control	1.47	95	2,700	8.2	Disturbed
			Vagal stimulation	0.76	69	1,960	5.75	Disturbed
			Isoprenaline	3.58	80	2,270	12.75	Undisturbed
			Control	2.0	71	2,050	9.5	Disturbed
			Isoprenaline	3.58	65	1,860	12.75	Undisturbed
38	Descending	0.8	Control	0.95	154	3,500	5.2	Highly disturbed
			Propranolol+ pentobarbitone	1.64	101	2,320	6.8	Disturbed
39	Descending	1.0	Control	1.75	56	1,600	8.6	Undisturbed
			Isoprenaline	3.42	127	3,630	12.4	Highly disturbed
			Control	1.82	72	2,060	9.0	Undisturbed
40	Arch	1.6	Isoprenaline	3.46	107	4,890	19.8	Disturbed
	Descending	1.3	Isoprenaline	3.46	112	4,160	16.2	Disturbed
41	Ascending	1.5	Control	2.0	75	3,230	14.2	Disturbed
			Isoprenaline	4.1	93	3,980	20.2	Disturbed
			Control	2.35	72	3,090	15.5	Disturbed
	Descending	0.75	Control	2.98	58	1,240	8.6	Undisturbed
			Isoprenaline	4.0	160	3,430	10.0	Highly disturbed
42	Descending	0.8	Control	3.23	252	5,400	9.0	Highly disturbed

*The term 'control' implies morphine + pentobarbitone anaesthesia but no other intervention; it has no implication concerning the flow state.

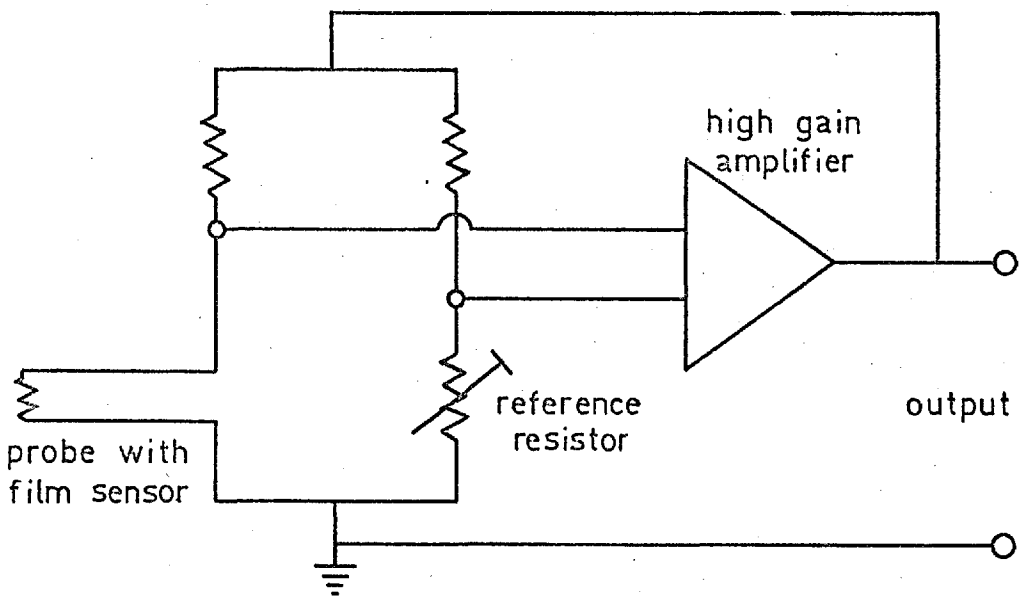

Fig.1 Basic anemometer circuit

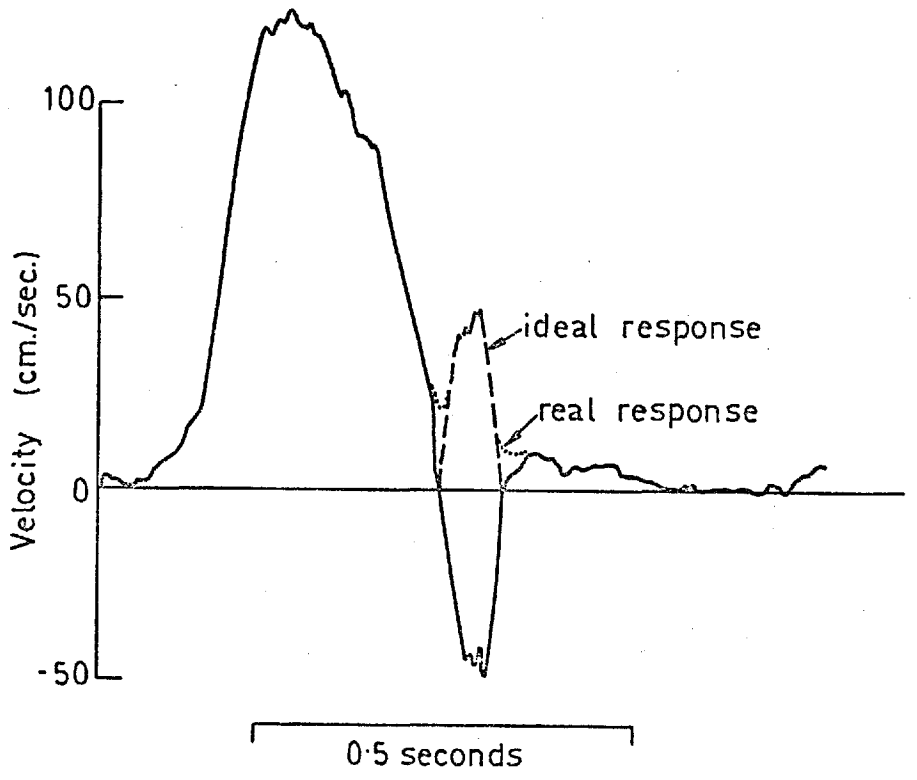

Fig.2 Aortic velocity waveform showing ideal hot-film response (- - - - -) and predicted actual response (....) distorted by boundary-layer phase-lags.

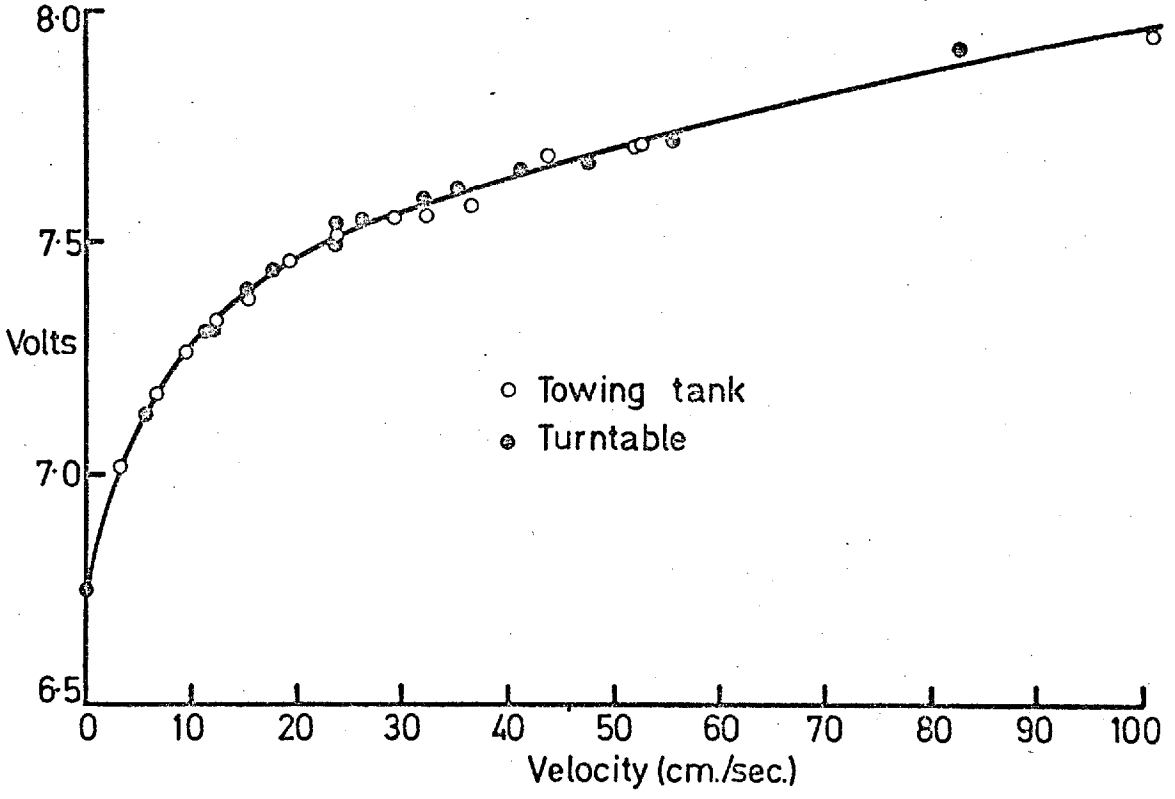

Fig.3 Steady calibrations: comparison between turntable and towing tank.

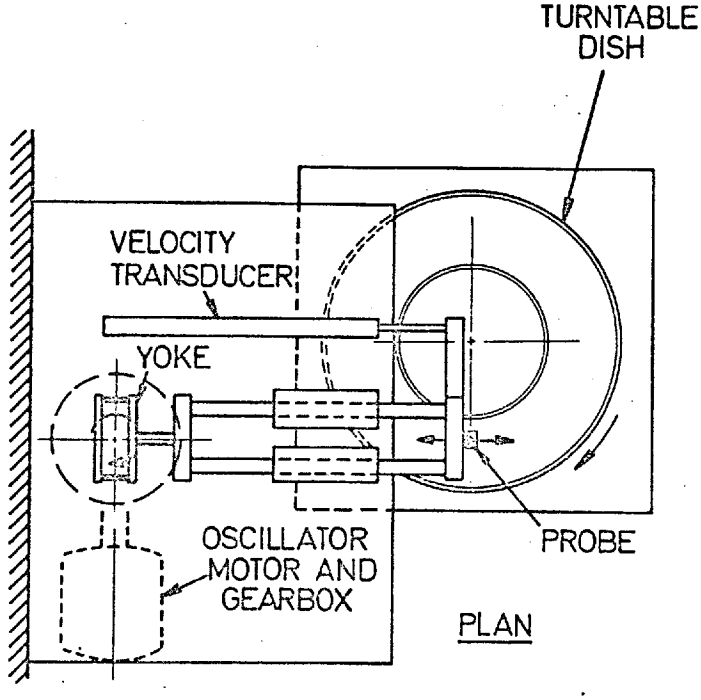

Fig.4 Schematic diagram of apparatus for steady and oscillatory flow calibration of hot-film probes.

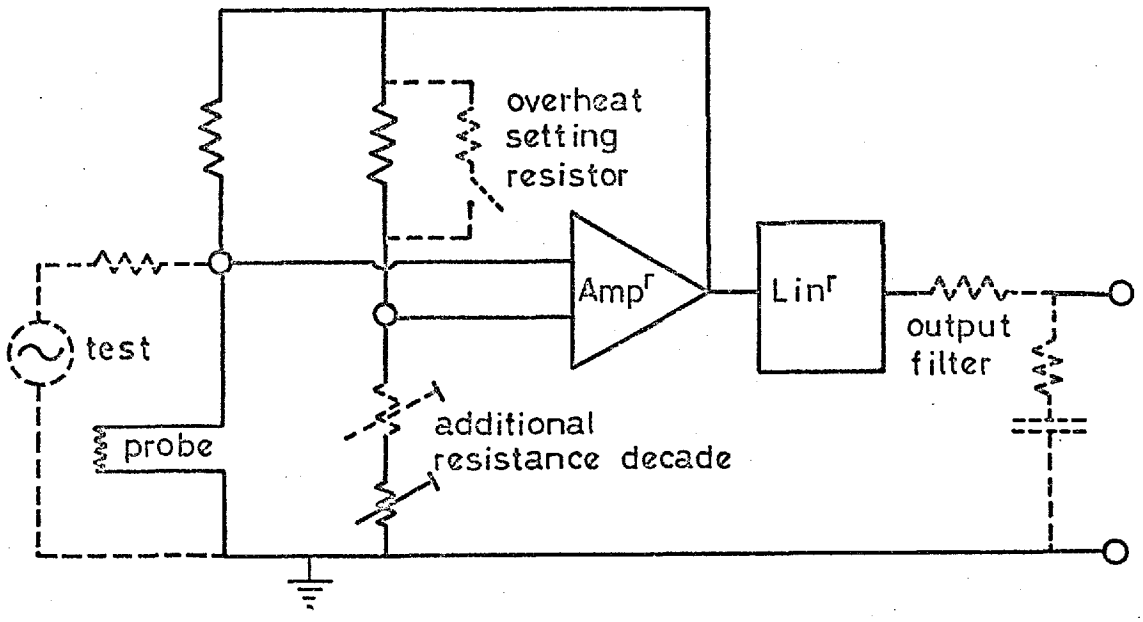

Fig.5 Anemometer circuit modified for use at 1% overheat, and showing circuit for electrical frequency-response testing (left).

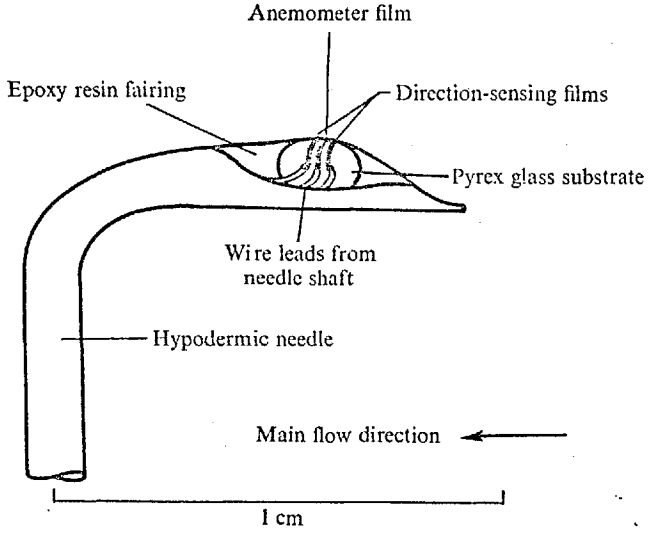

Fig.6 Final hot-film probe design.

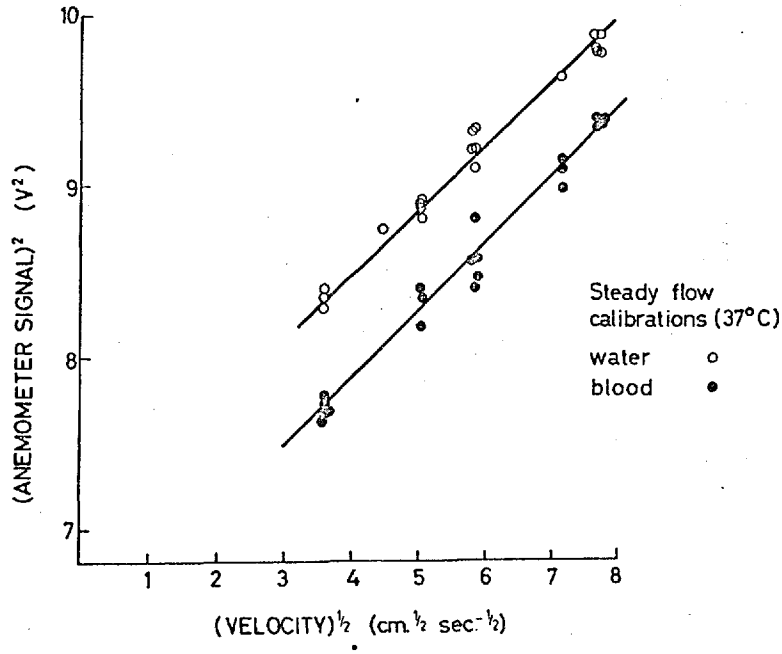

Fig.7 Relative sensitivity of probe to blood and water; paired calibrations, performed in steady flow and linearised numerically.

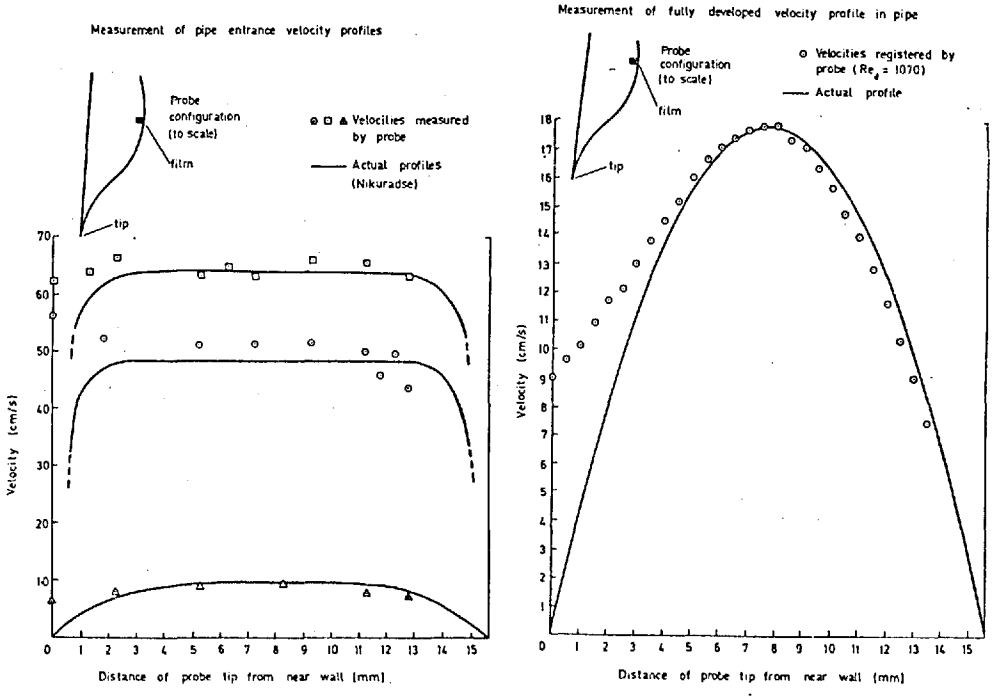

(a) (b)

Fig.8 Velocity measurements in steady pipe flow. Predicted (full line) and measured velocity distributions
a) in entrance region; results for three different flow rates (Reynolds numbers 726, 4840, 6520).
b) fully developed flow far downstream (Reynolds number 10 0.

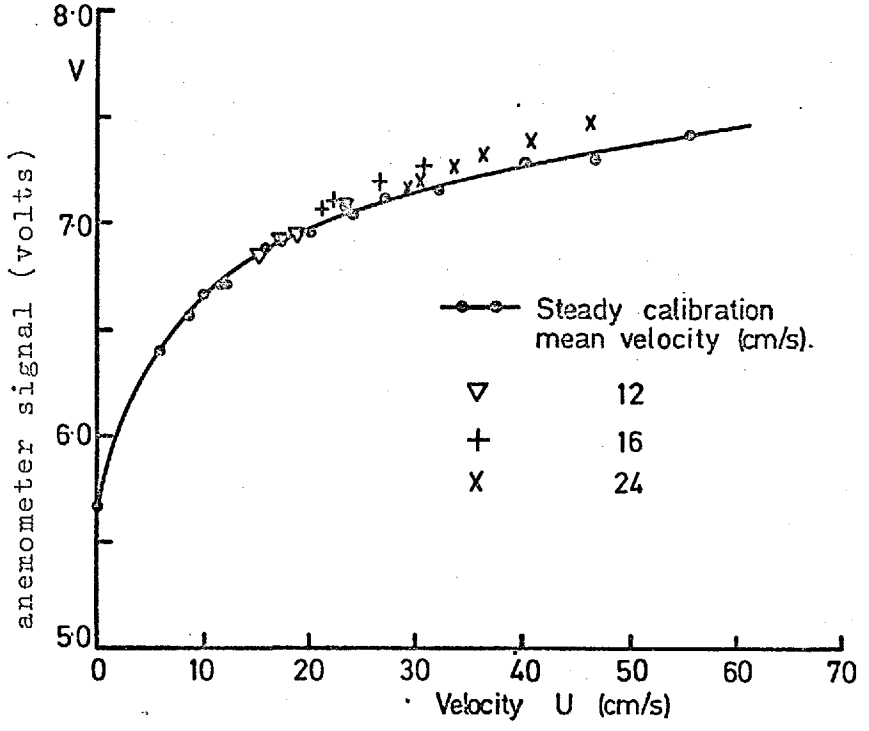

Fig.9(a) Calibration points obtained by unidirectional oscillation of probe in steady mean flow (three runs at indicated steady velocities) compared to steady flow calibration.

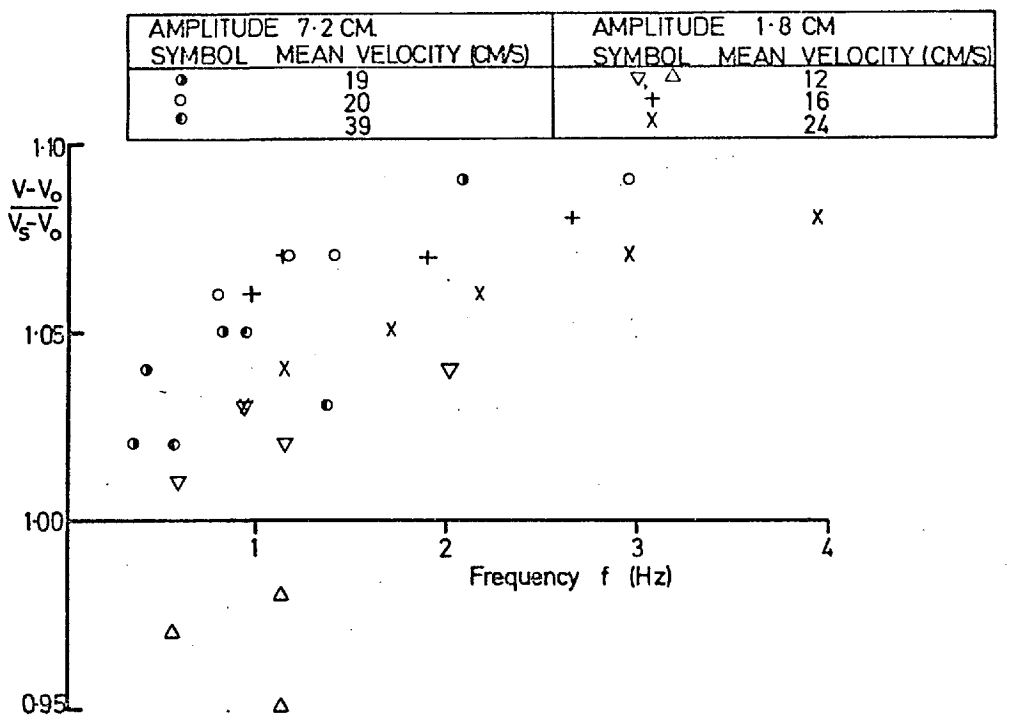

Fig.9(b) Results of a number of unidirectional oscillatory calibration runs plotted in frequency response form. V is unsteady signal, and V_S is steady signal at the same instantaneous velocity; V_O is signal at zero flow.

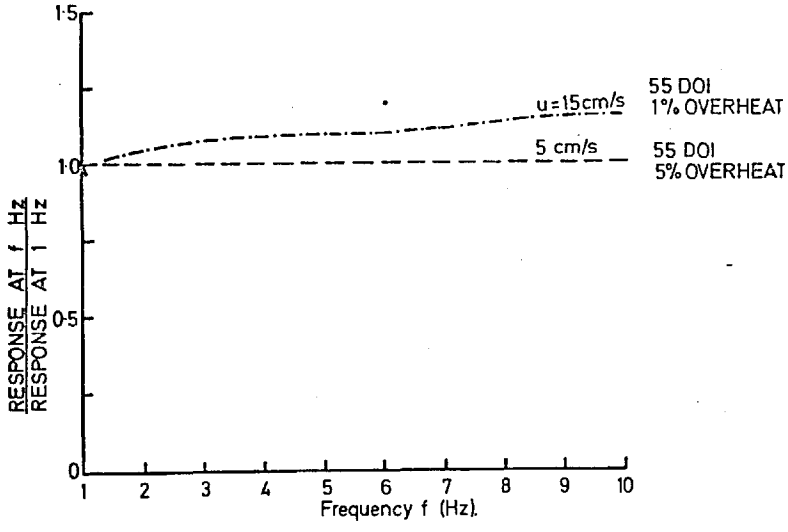

Fig.10 Frequency response of the system at 1% and 5% overheats to electrical testing.

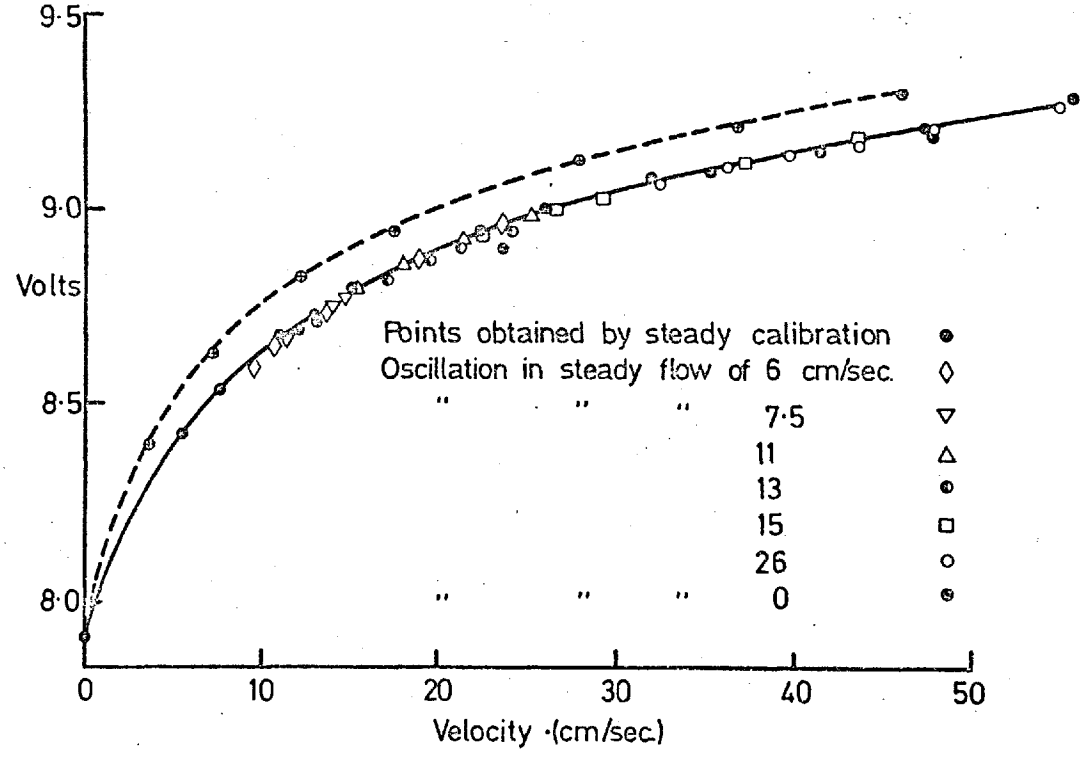

Fig.11(a) Calibration points obtained by oscillation of probe in stated steady mean flows: 5% overheat.

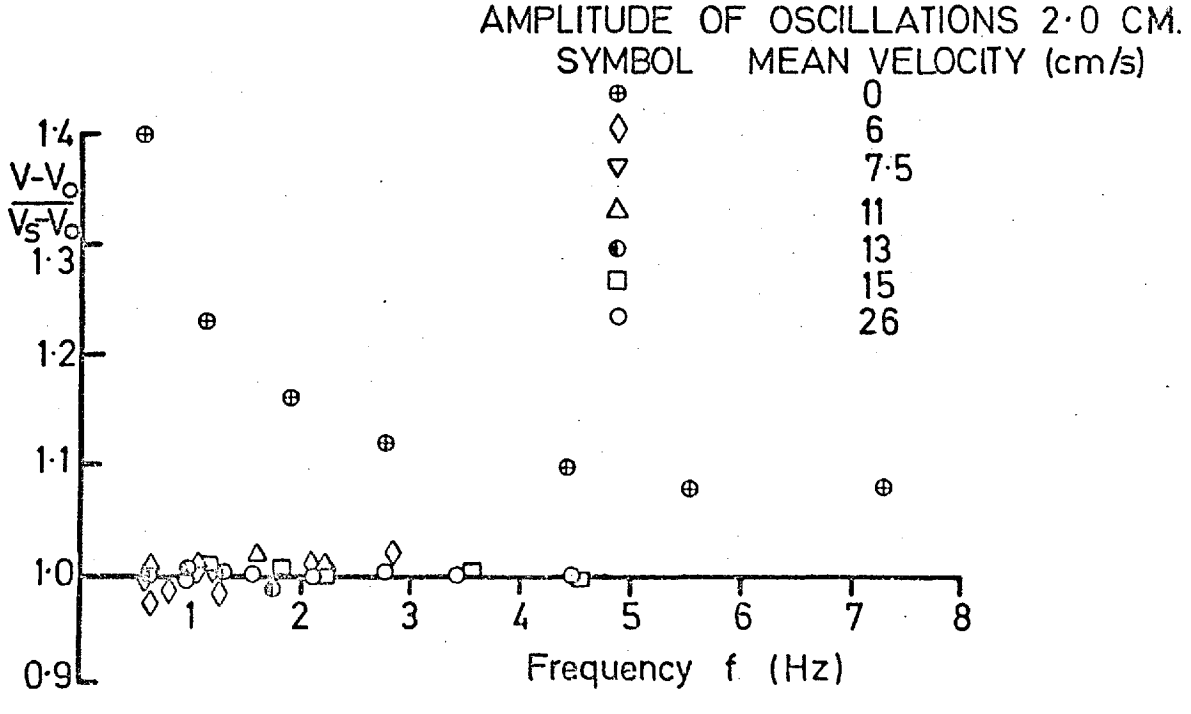

Fig.11(b) Above results expressed in frequency response form.

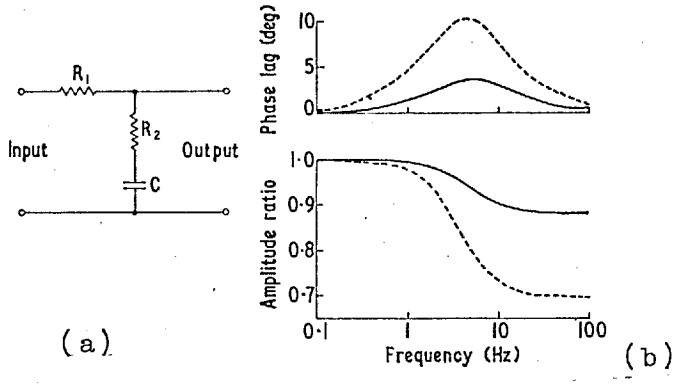

Fig.12(a) Anemometer output filter
(b) Amplitude and phase characteristics at two different values of R_1.

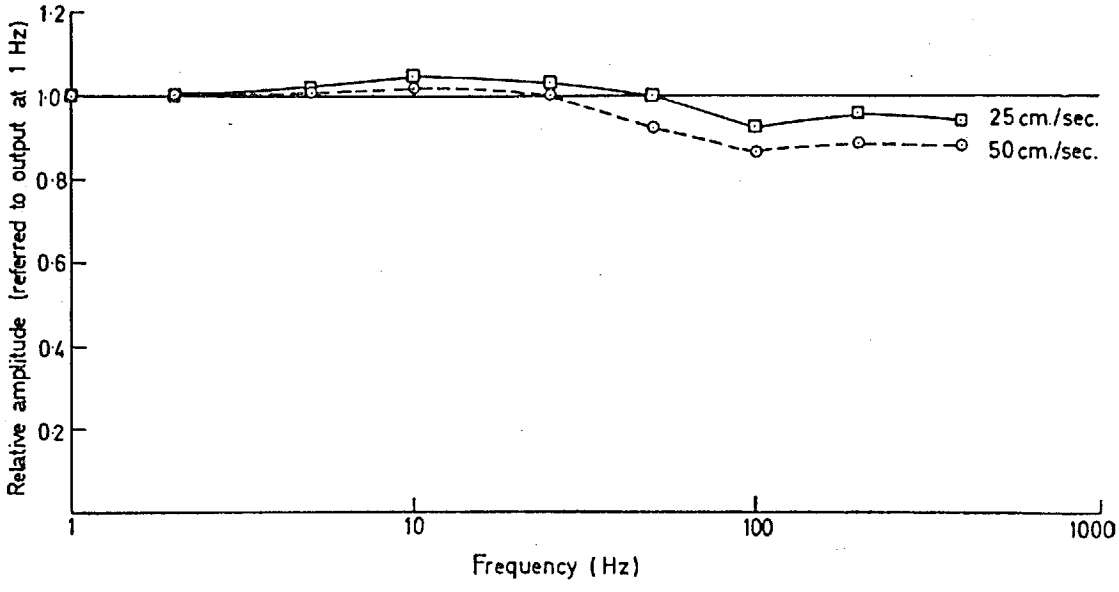

Fig.13 Frequency response of filtered system at 1% overheat to electrical testing; measured at two steady velocities.

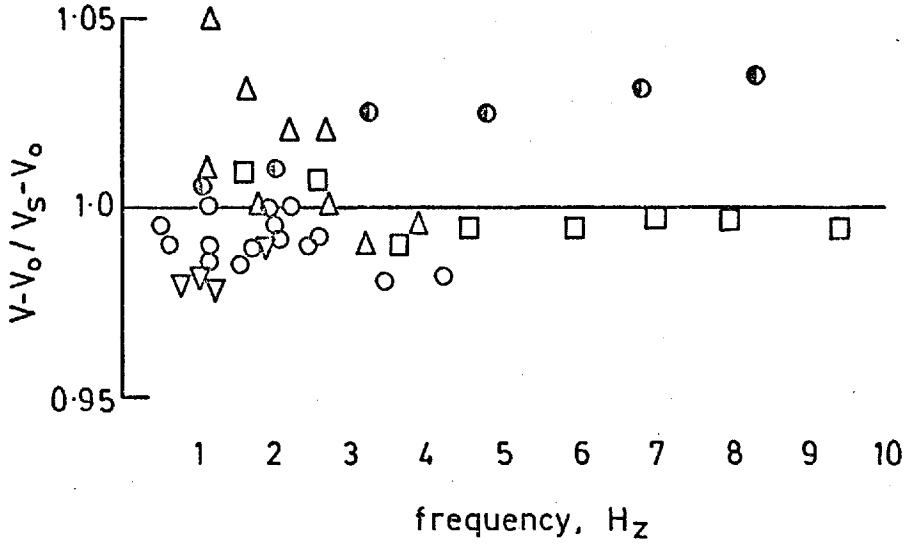

Fig.14 Frequency response of filtered system at 1% overheat to oscillatory flow testing. Axes as Fig.9(b). Results of unidirectional oscillation in steady flows of:

▽ 6 cm/sec.
○ 12 "
△ 18 "
□ 24 "
◐ 26 "

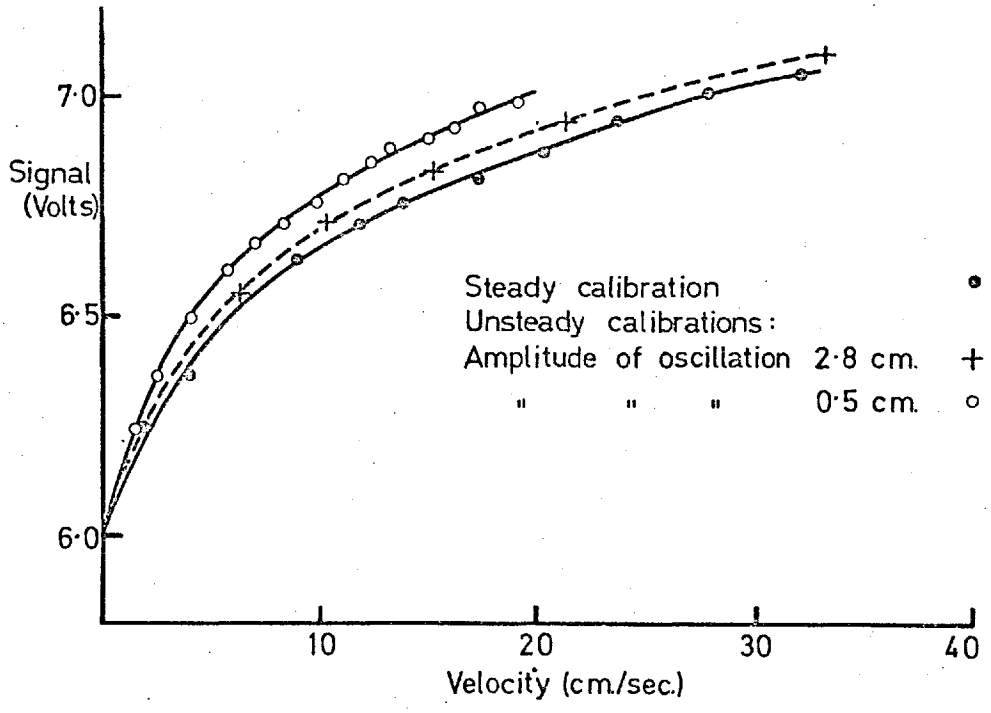

Fig.15(a) Calibration points obtained by oscillation of probe in still water (two runs at stated amplitudes of oscillation) compared to steady flow calibration.

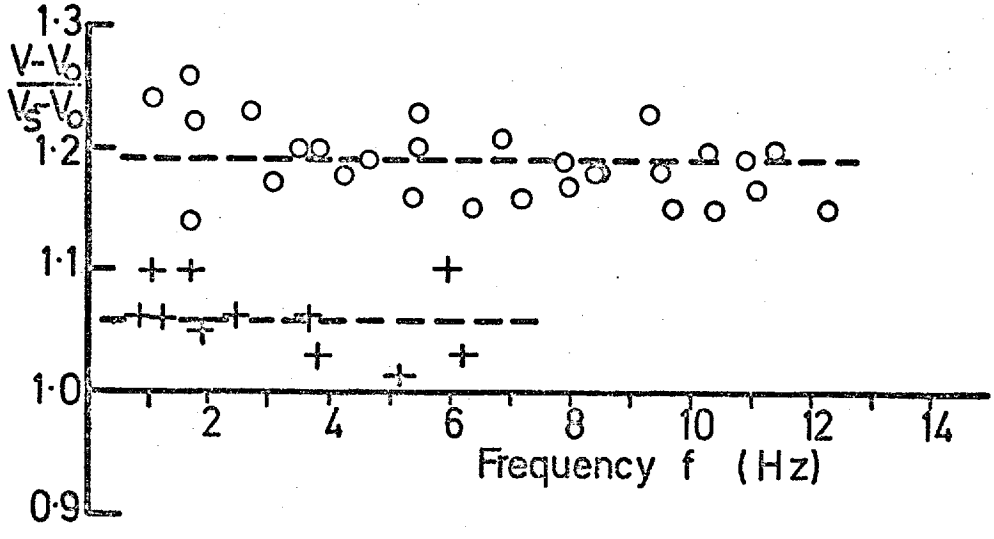

Fig.15(b) Results of above and further runs expressed in frequency response form.

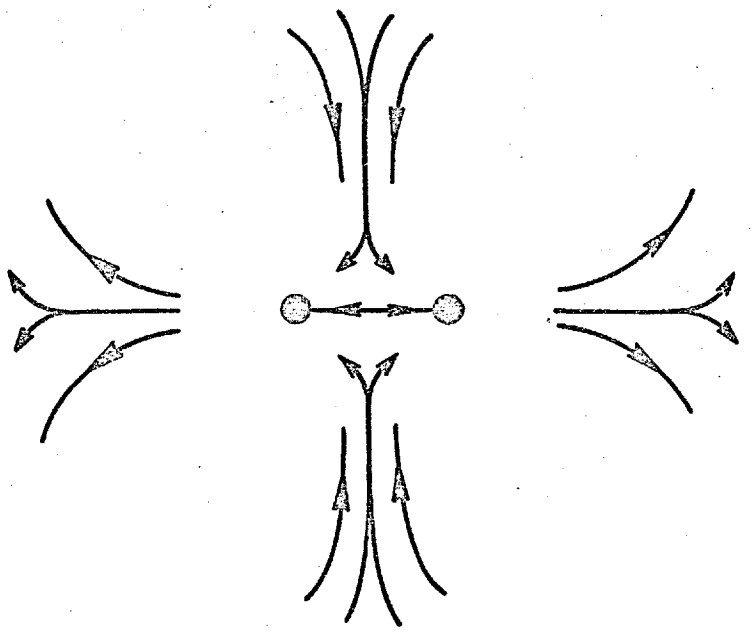

Fig.16 Sketch illustrating the motion observed in small particles on the liquid surface near the probe during oscillation of the probe in initially still liquid.

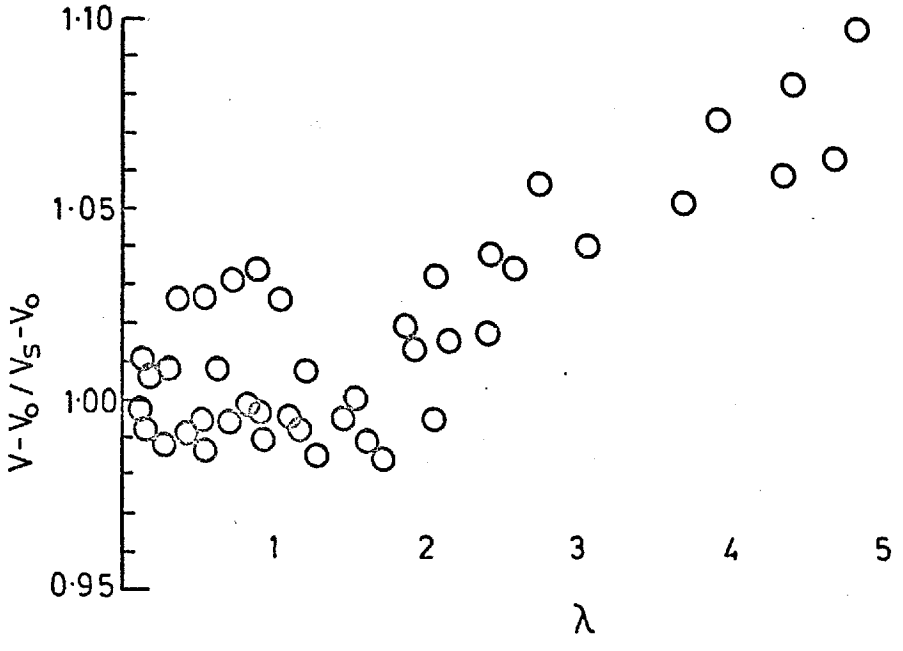

Fig.17 Effect of progressively increasing periods of wake reflux in each cycle of oscillatory motion on probe response. λ is ratio of unsteady to steady velocity (see p.52).

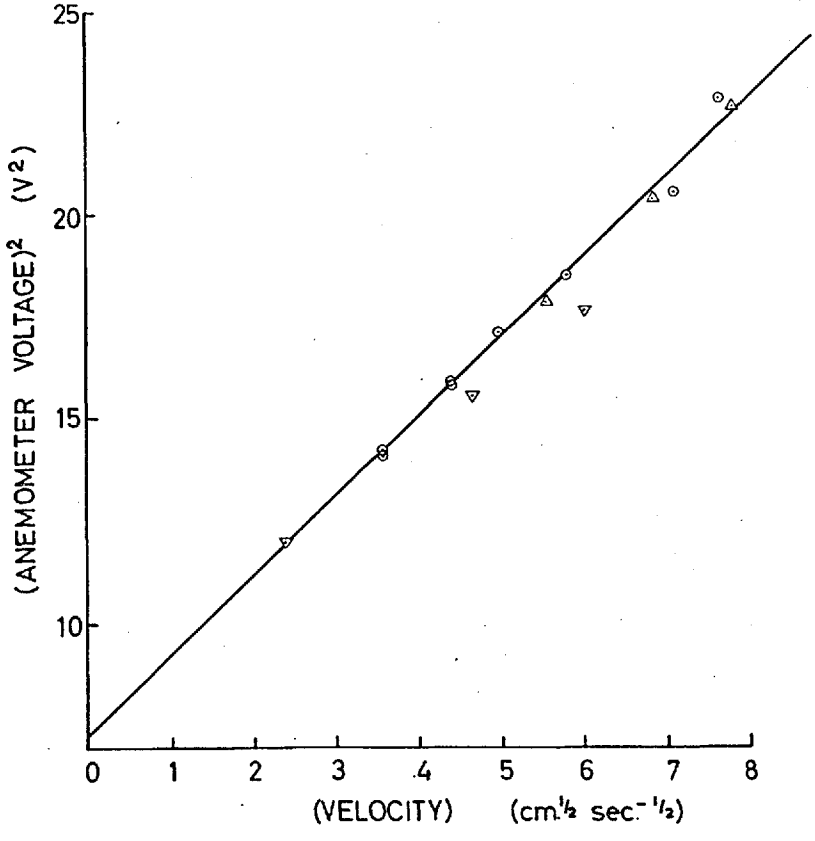

Fig.18 Static and dynamic calibrations of probe in canine blood at 37°C, linearised numerically.
○ steady flow
△ peak forward velocity) during oscillation
▽ peak backward velocity) at three frequencies in steady flow.

Stroke of Oscillations (2a) 2.1 cm.

Symbol	Mean Velocity (cm. s^{-1})	Frequency (Hz)	λ
●	18	2.6	0.98
▽	18	1.1	0.41
◐	6	2.4	2.80
◇	8	2.8	1.45

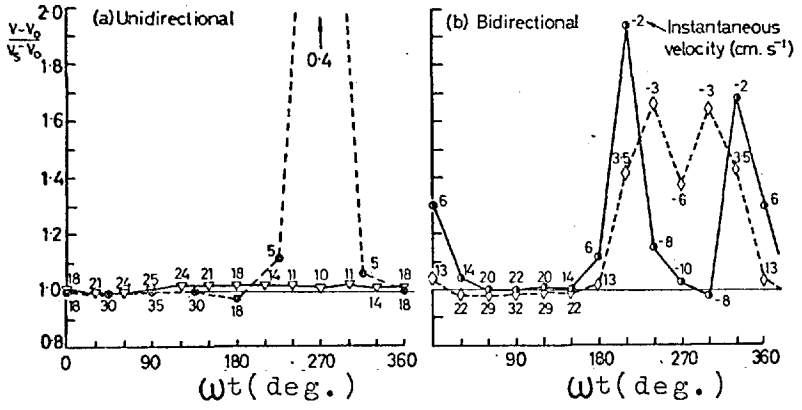

Fig.19 Comparison of unsteady results with steady calibrations. Complete cycles of oscillatory flow. The numbers opposite each plotted point indicate the true velocity at that instant and allow calculation of the absolute error. The two flows in (a) are unidirectional: those in (b) reverse.

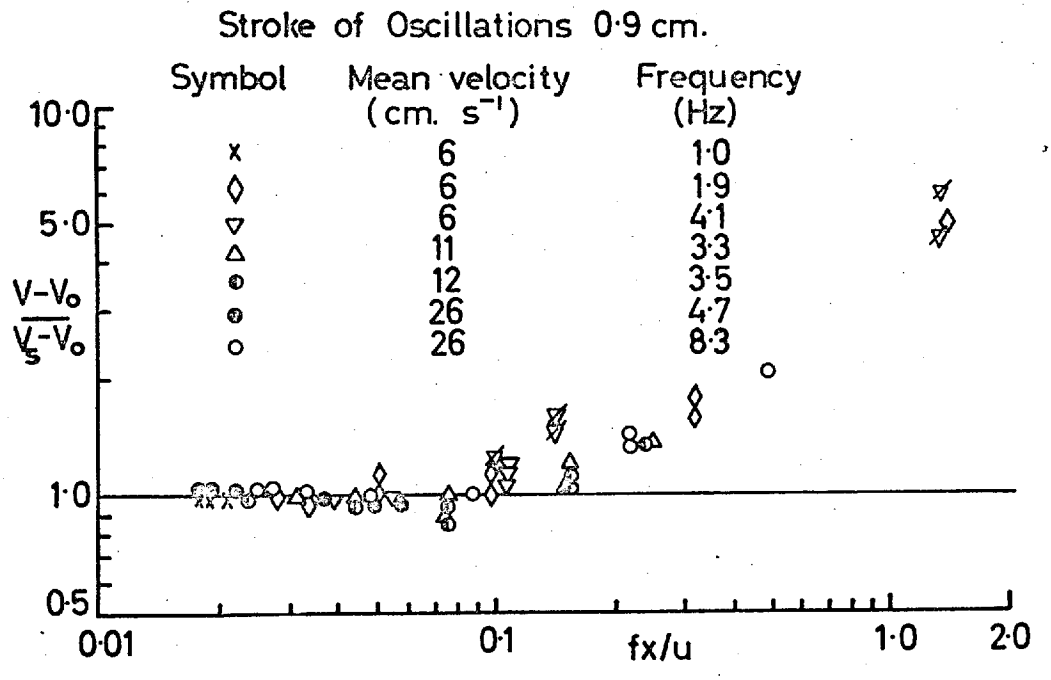

Fig.20 Comparison of unsteady results with steady calibrations; points plotted against boundary layer phase-lag parameter fx/u. Points with an oblique line obtained in reverse flow.

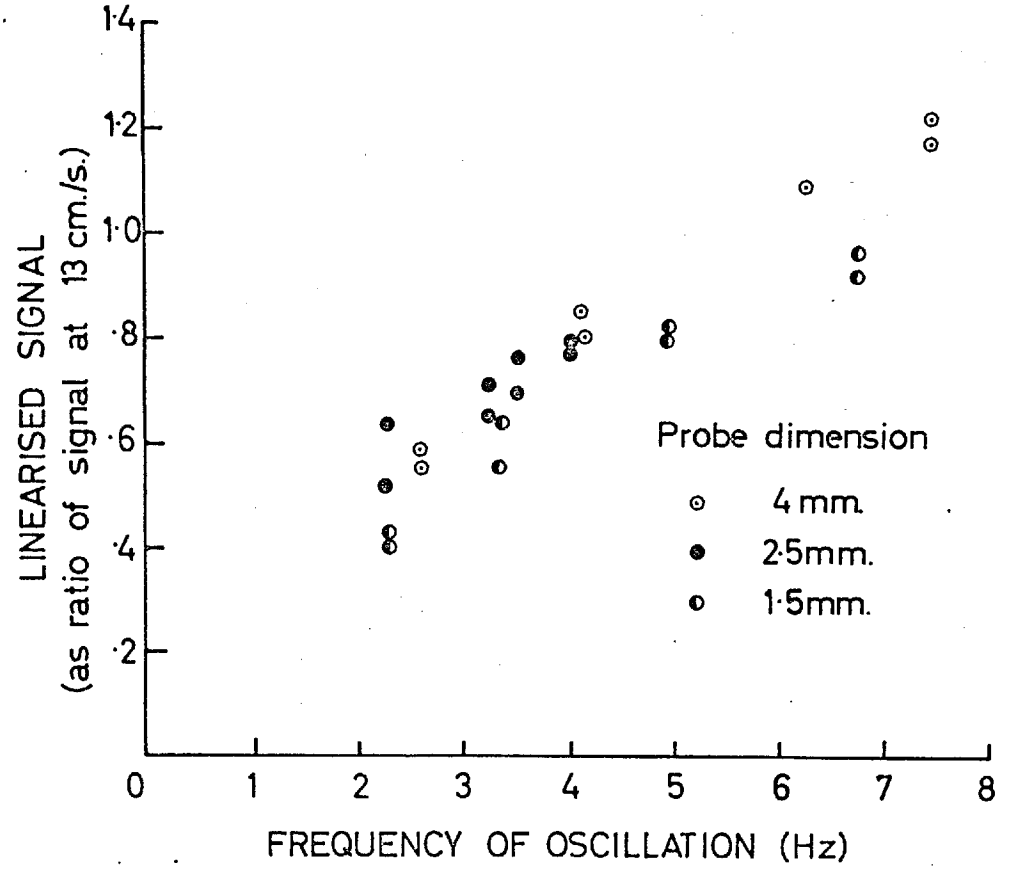

Fig.21 Effect of frequency on 'lift-off' of zero flow signal in reversing flow; results for three probes of different size.

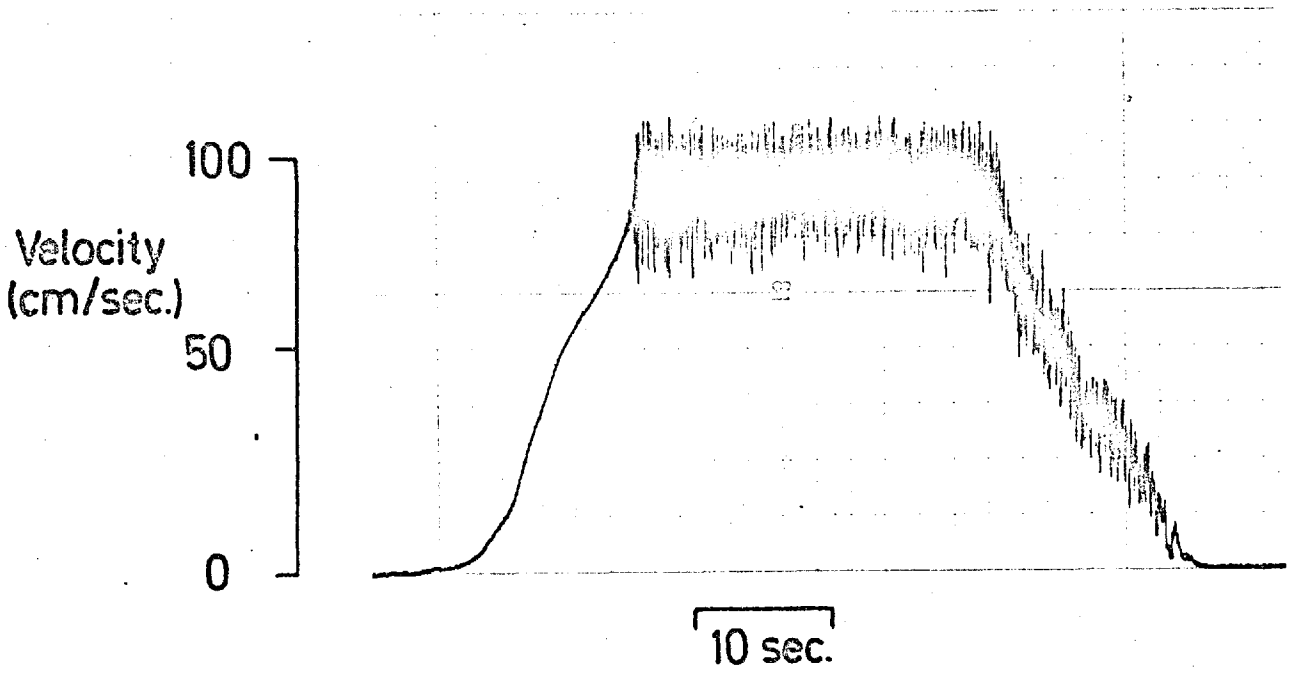

Fig.22 Signal from probe in pipe-flow. The flow was slowly increased until turbulence occurred, and later stopped. Peak Reynolds number 9500.

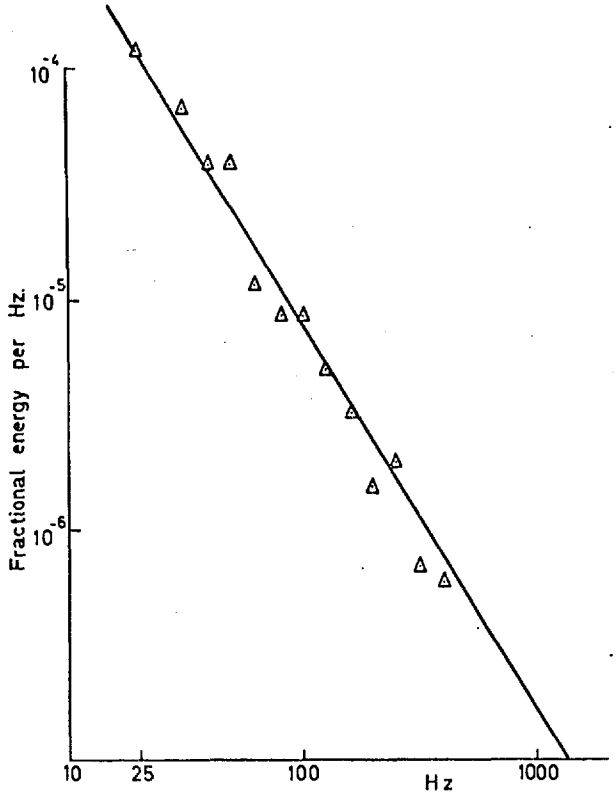

Fig.23 Frequency distribution of turbulent energy in pipe flow. The points are measured with the hot-film probe; the line is calculated from theory and from the hot-wire robe measurements of Laufer (1954).

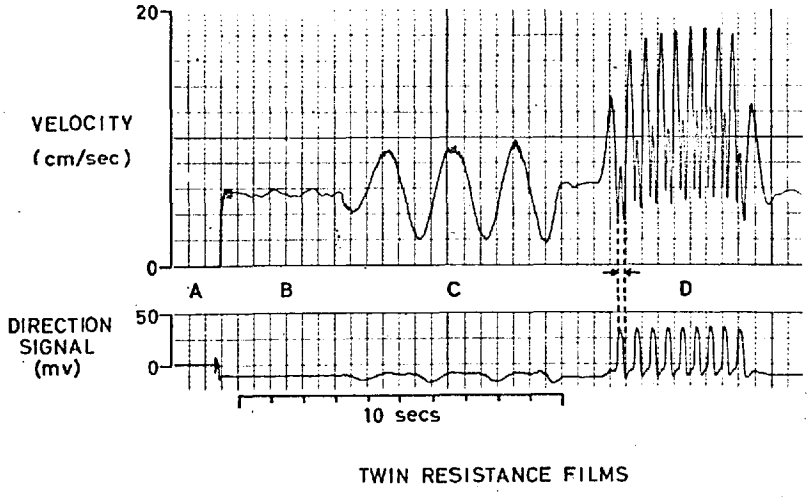

Fig.24 Flow direction sensing, tested in calibration rig.
A: balance position, zero flow.
B: steady flow.
C: unidirectional oscillating flow.
D: reversing flow (indicated during one cycle by arrows).

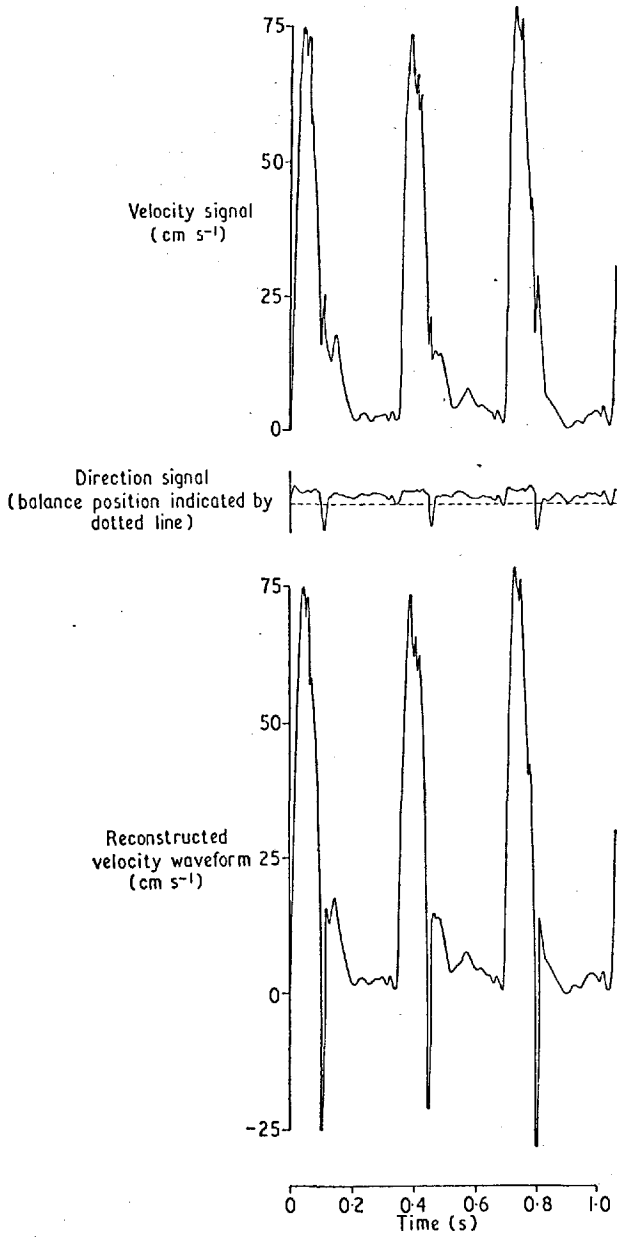

Fig.25 Original velocity and direction signals recorded in the ascending aorta, and (bottom) reconstructed waveform.

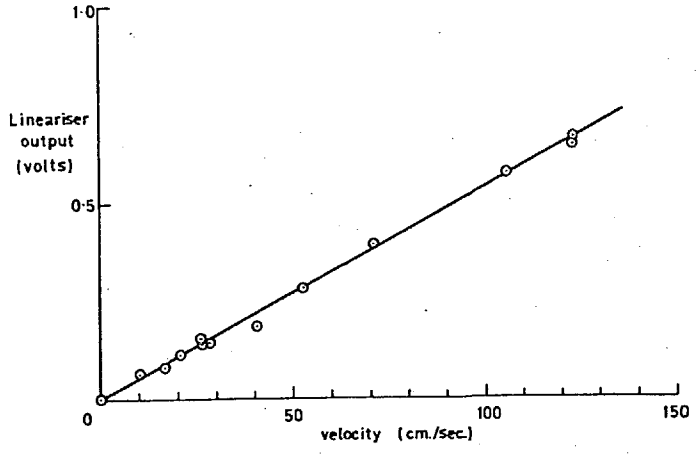

Fig.26 Linearised steady flow calibration obtained in blood at 37°C.

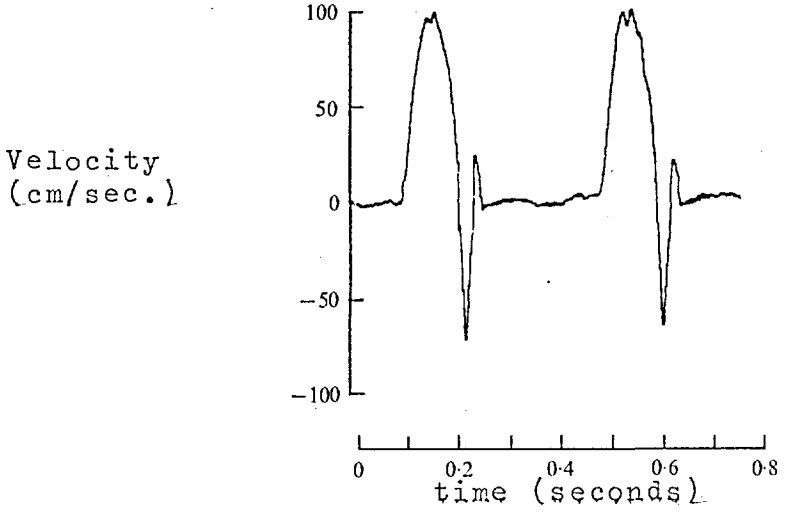

Fig.27 Averaged waveforms obtained from many beats recorded in the ascending aorta.

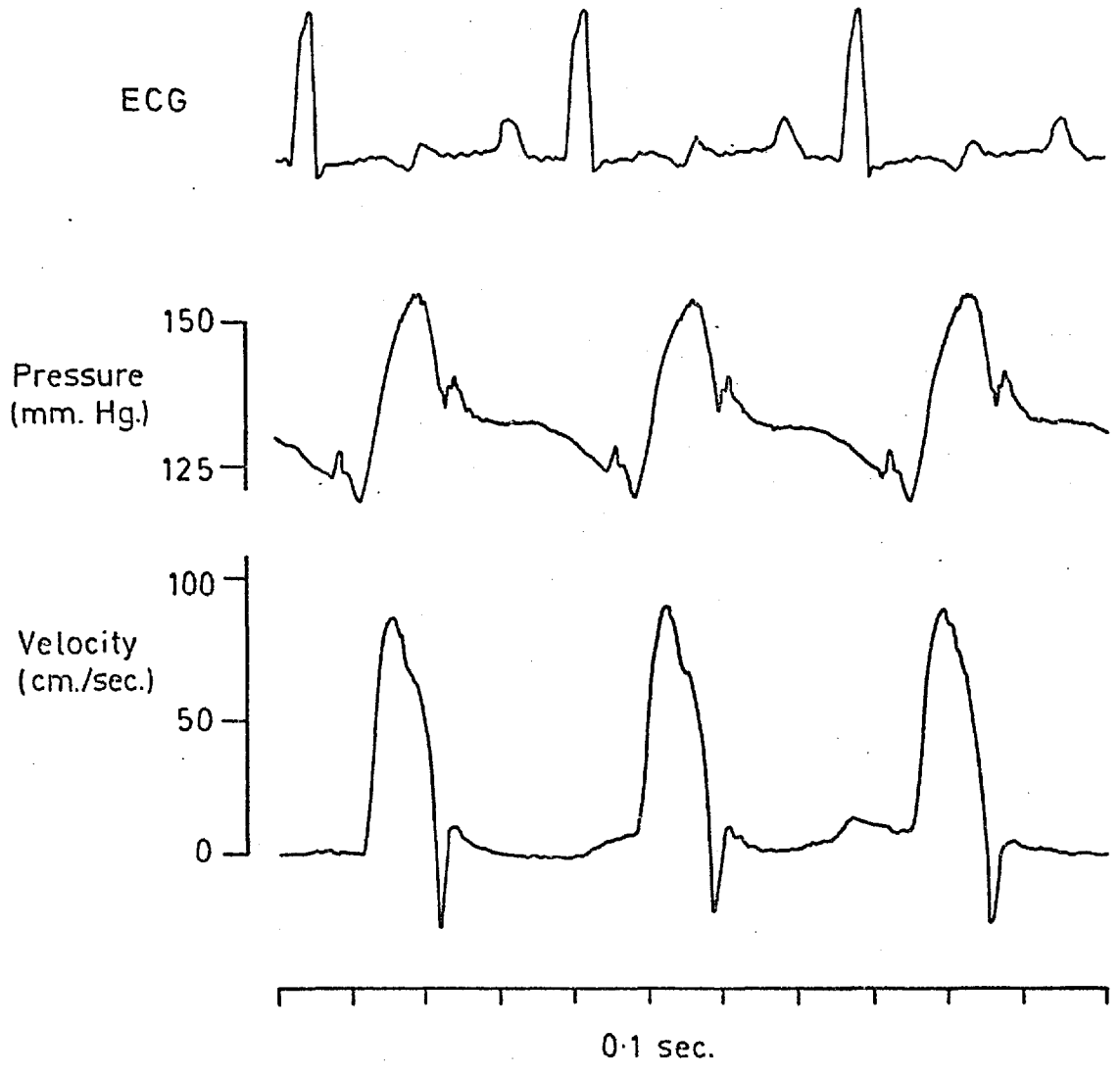

Fig.28 ECG, centreline velocity in the ascending aorta, and aortic arch pressure. Tracing from original UV record.

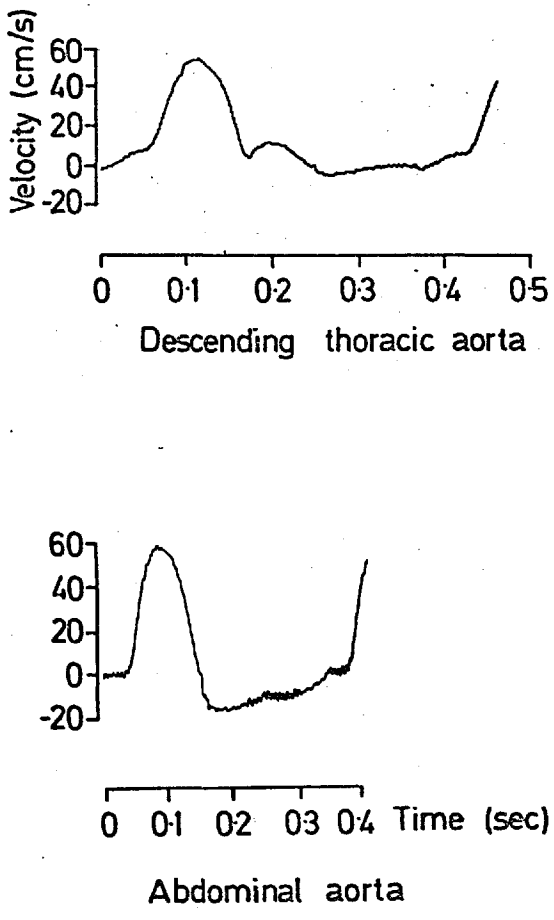

Fig.29 Averaged waveforms from different sites in the aorta.

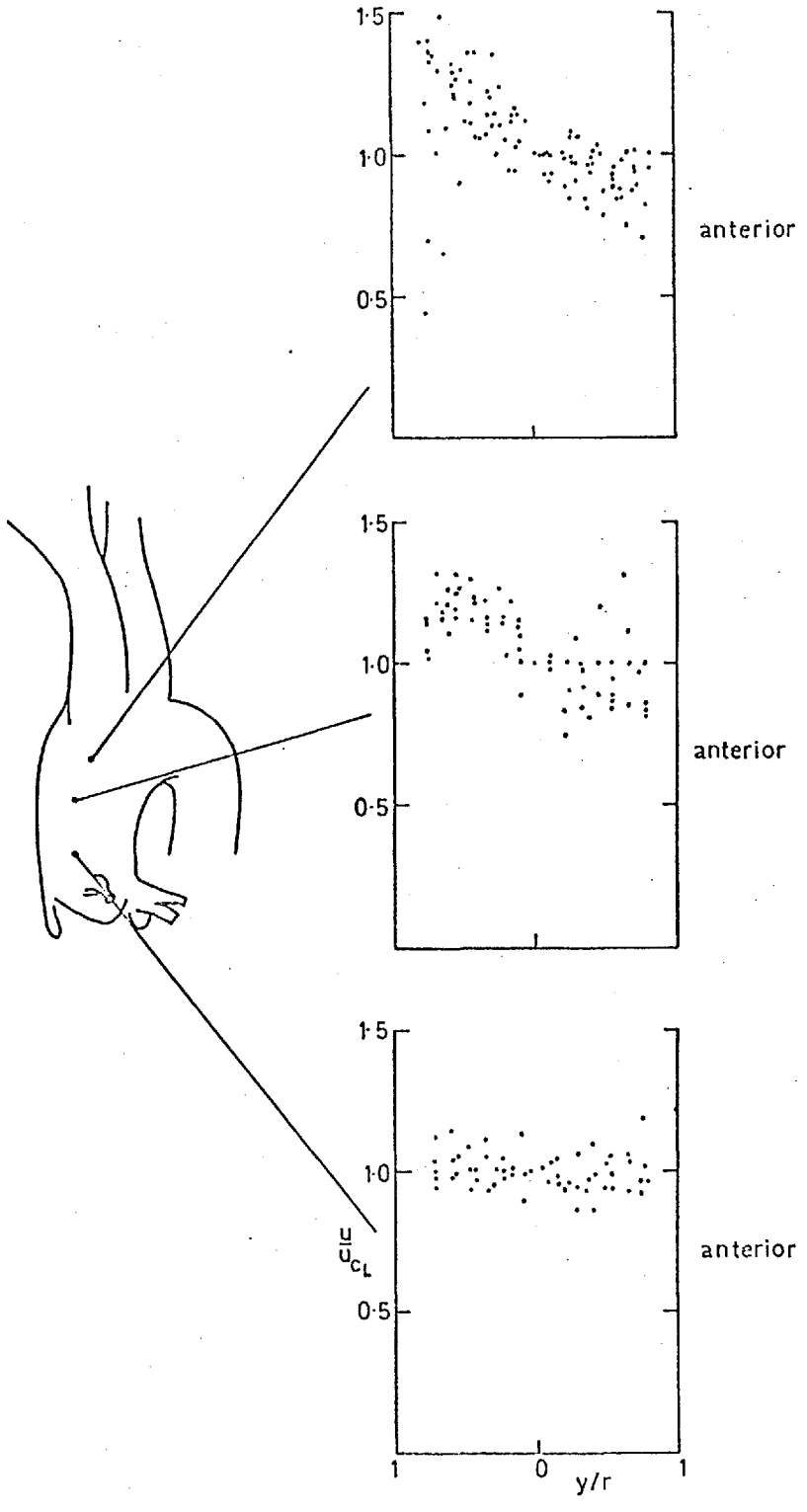

Fig. 30. Peak systolic velocity distribution at three indicated levels in the ascending aorta. All velocities expressed as a fraction of centreline velocity, and all radial positions as a fraction of radius. Each 'box' contains data from several animals. All traverses are in the plane of the arch.

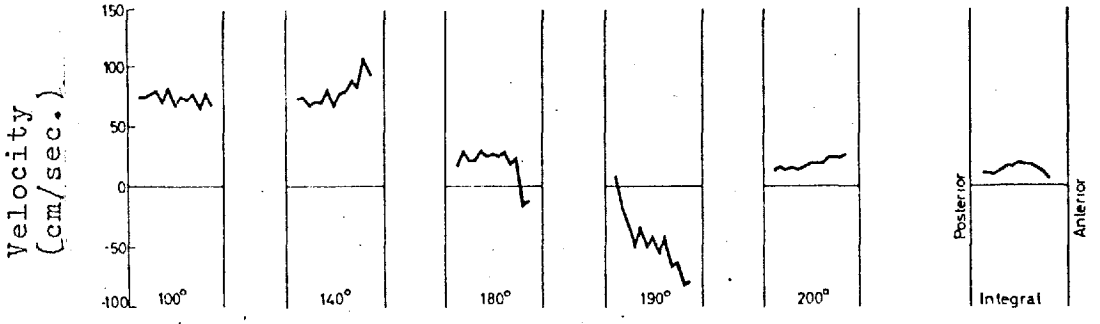

Fig.31 Instantaneous velocity profiles close to the aortic valve. In this, and subsequent similar figures, the origin (0°) is the R wave of the ECG, and profiles at five instants in the cycle are illustrated; the time-averaged profile is shown on the right. Antero-posterior plane. Diameter 16 mm., heart-rate 194/min.

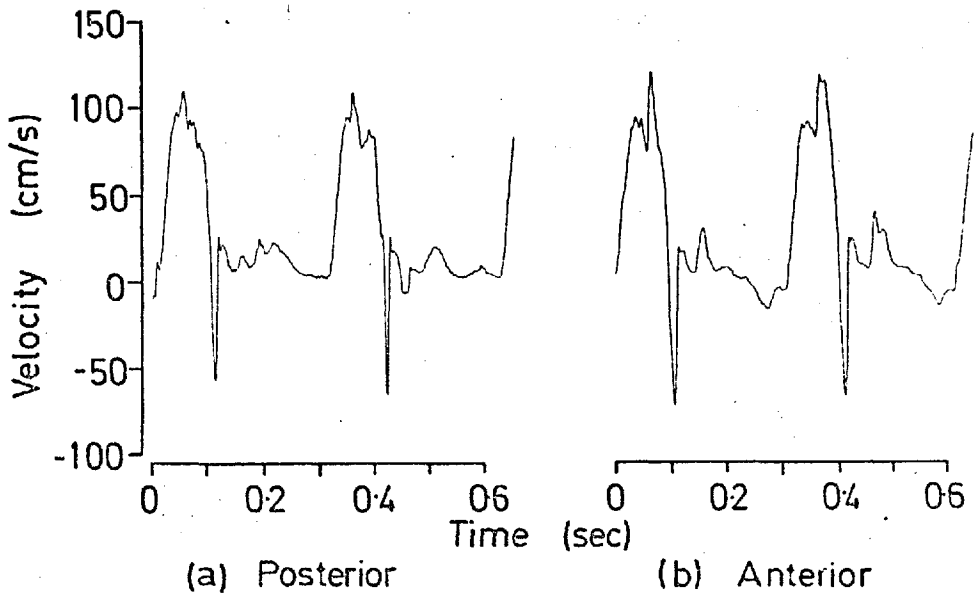

Fig.32 Individual velocity waveforms in the proximal ascending aorta, demonstrating the cause of the late systolic skew in the profile shown in Fig.31.

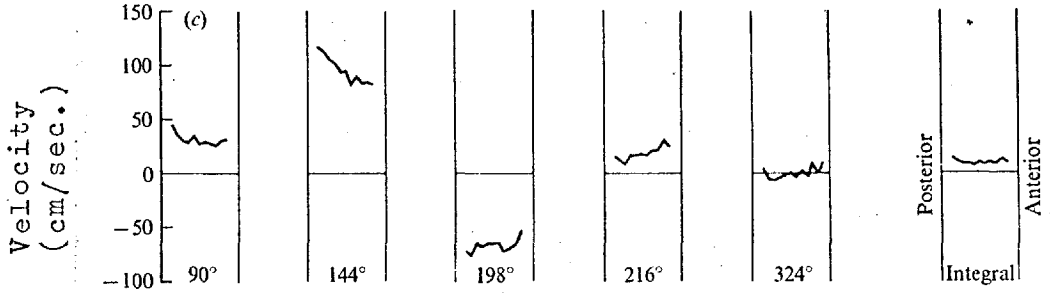

Fig.33 Instantaneous profiles in antero-posterior plane, distal ascending aorta. Diameter 14 mm., heart-rate 194.

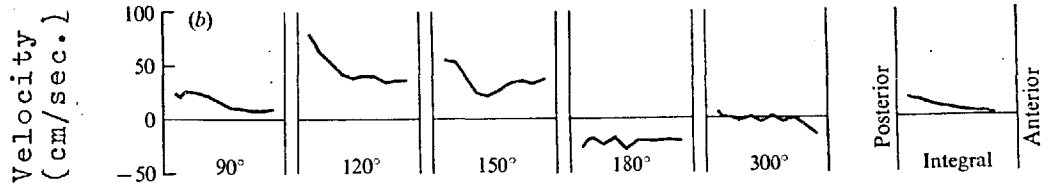

Fig.34 Instantaneous profiles in antero-posterior plane, middle site in ascending aorta. Diameter 22 mm., heart-rate 163.

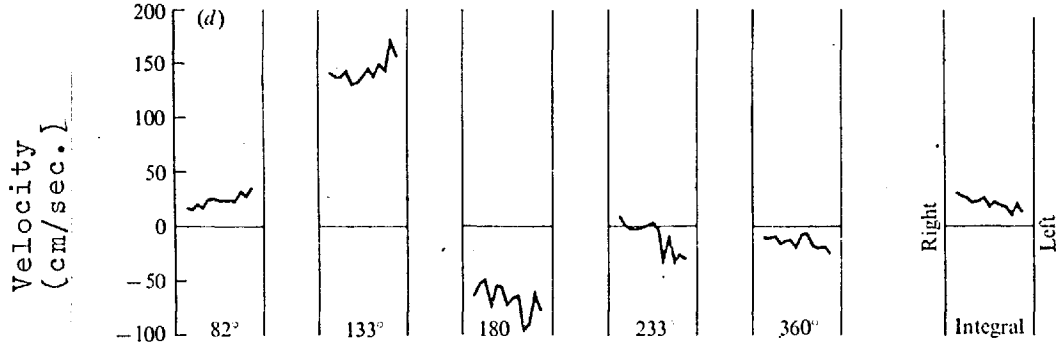

Fig.35 Instantaneous profiles in left-right plane, distal ascending aorta. Diameter 16 mm., heart-rate 190.

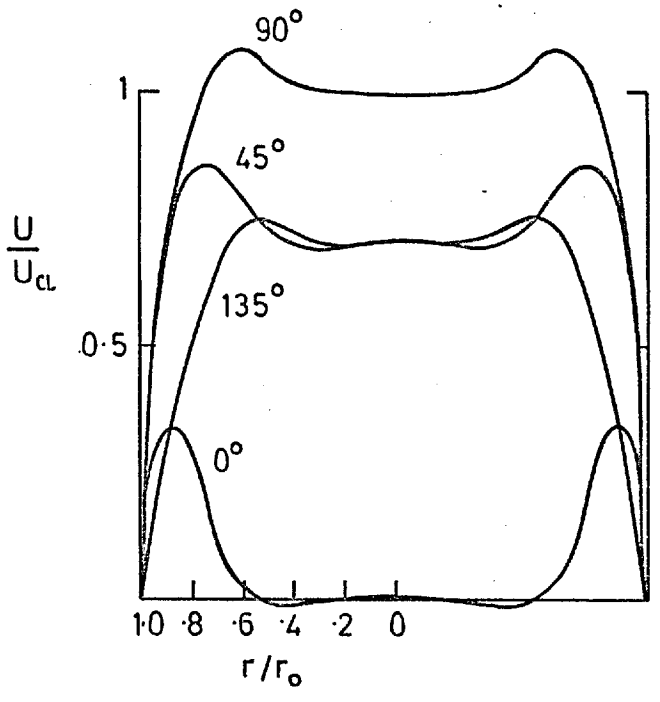

Fig.36 Instantaneous velocity profiles calculated from theory for oscillating pipe flow with $\alpha = 10$. Profiles from 180° to 360° are mirror images.

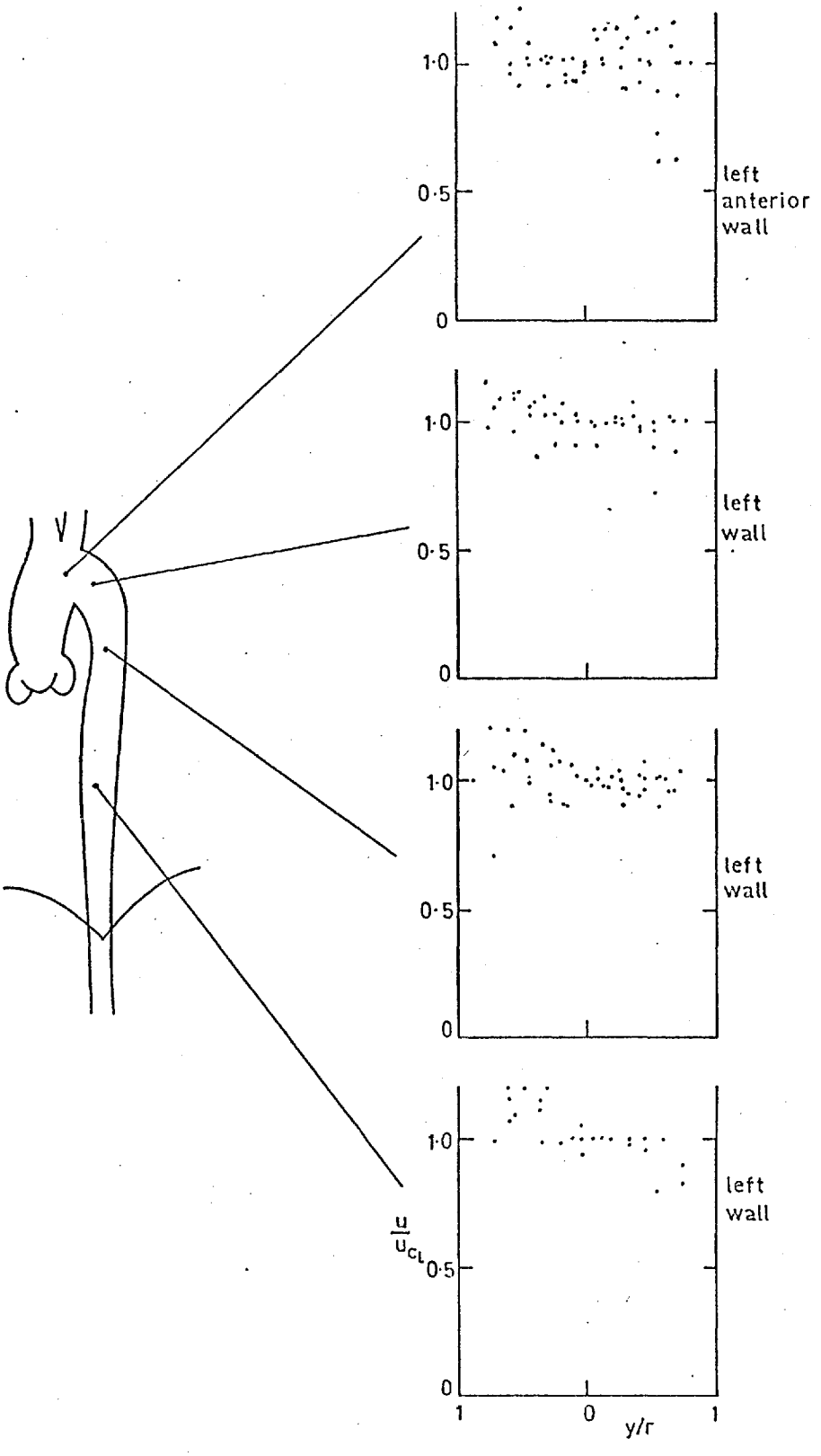

Fig. 37. Peak systolic velocity distribution at indicated sites in the arch and descending thoracic aorta. Points calculated as in fig. 30.

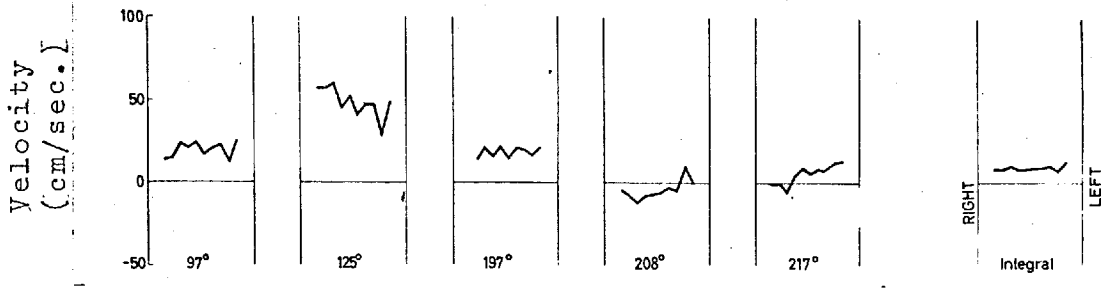

Fig.38 Instantaneous profiles in left-right plane, upper descending thoracic aorta, 2.5 cm. from the origin of the left subclavian artery. Diameter 13 mm. Heart-rate 150.

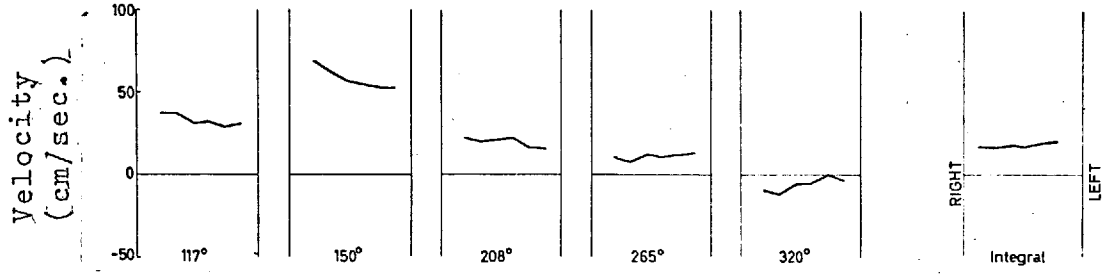

Fig.39 Instantaneous profiles in left-right plane, lower descending thoracic aorta, 10 cm. from left subclavian artery. Diameter 15 mm., heart-rate 160.

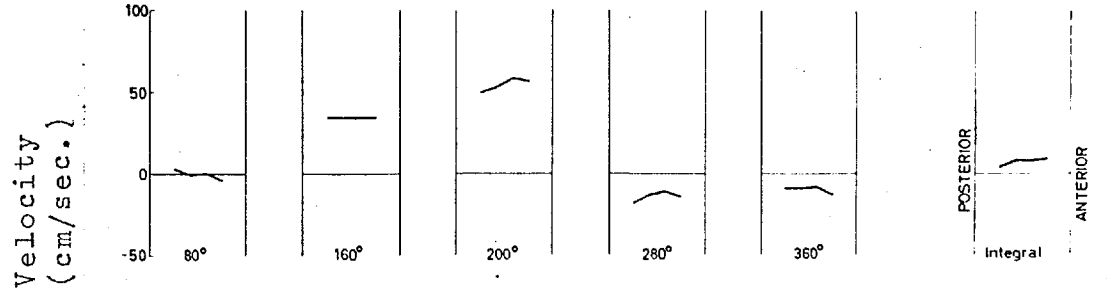

Fig.40 Instantaneous profiles in R-antero-L-posterior plane, abdominal aorta 2.5 cm. from its termination. Diameter 12 mm., heart-rate 180.

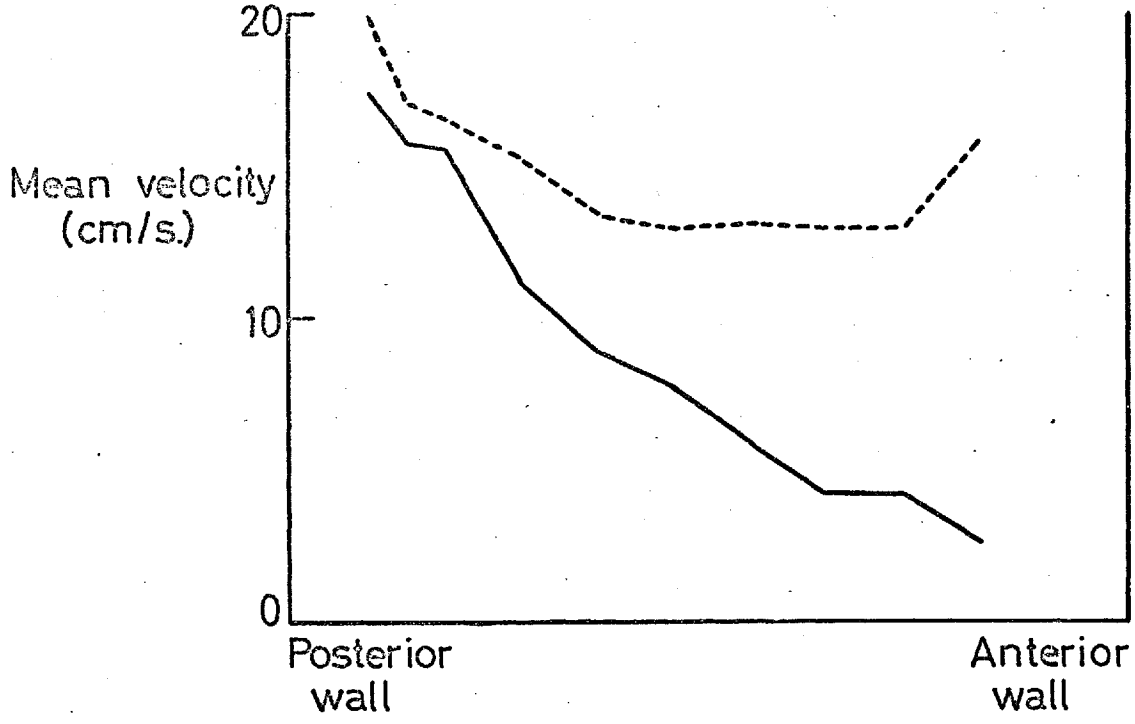

Fig.41 Time-integrated velocity profiles in ascending aorta.
----- waveform integrated in rectified form;
——— waveform integrated after switching to assign negative polarity to reversed flow phases of the signal.

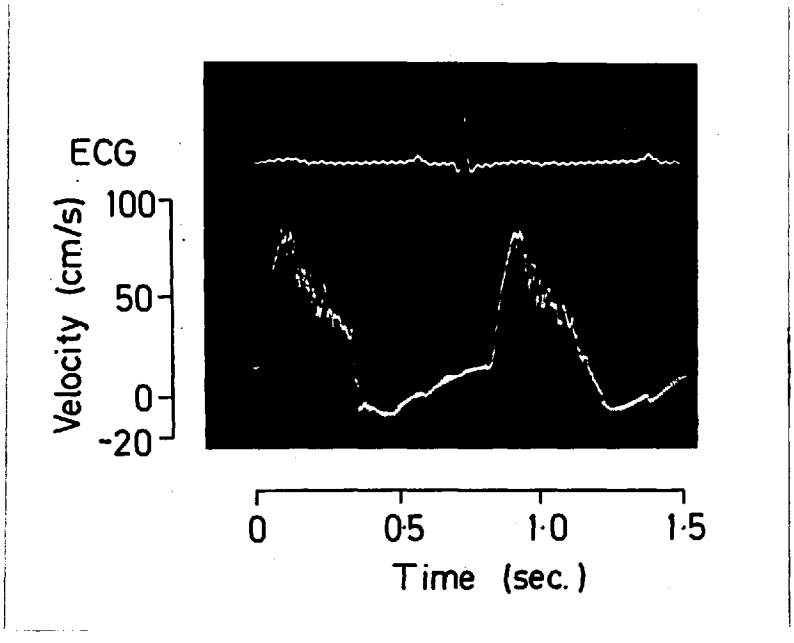

Fig.42 Velocity waveforms showing high-frequency flow-disturbances during deceleration of systolic flow.

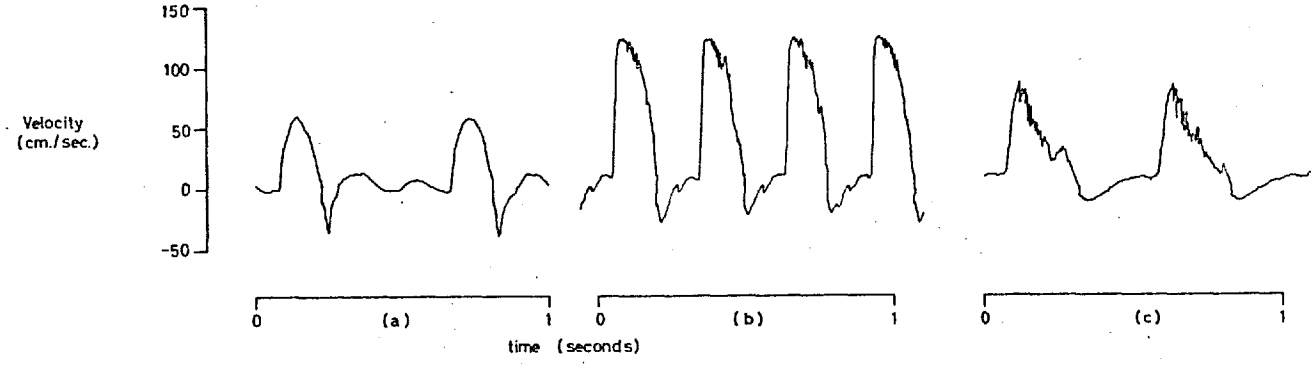

Fig.43 Velocity waveforms recorded in the descending thoracic aorta.
a) undisturbed; b) disturbed; c) highly disturbed.

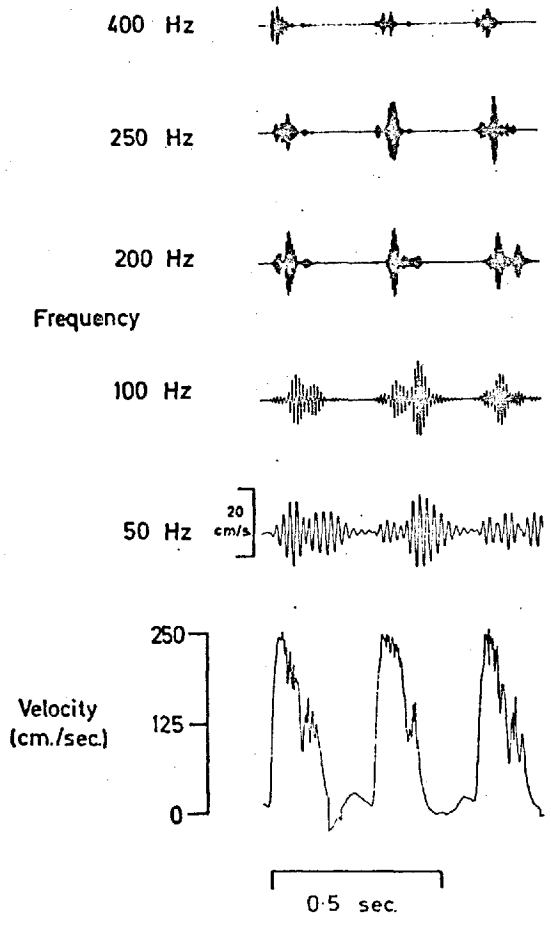

Fig.44 Frequency analyser output for highly disturbed flow in the descending aorta. The input waveform is shown at the bottom. The velocity scale opposite the 50 Hz signal applies at all frequencies.

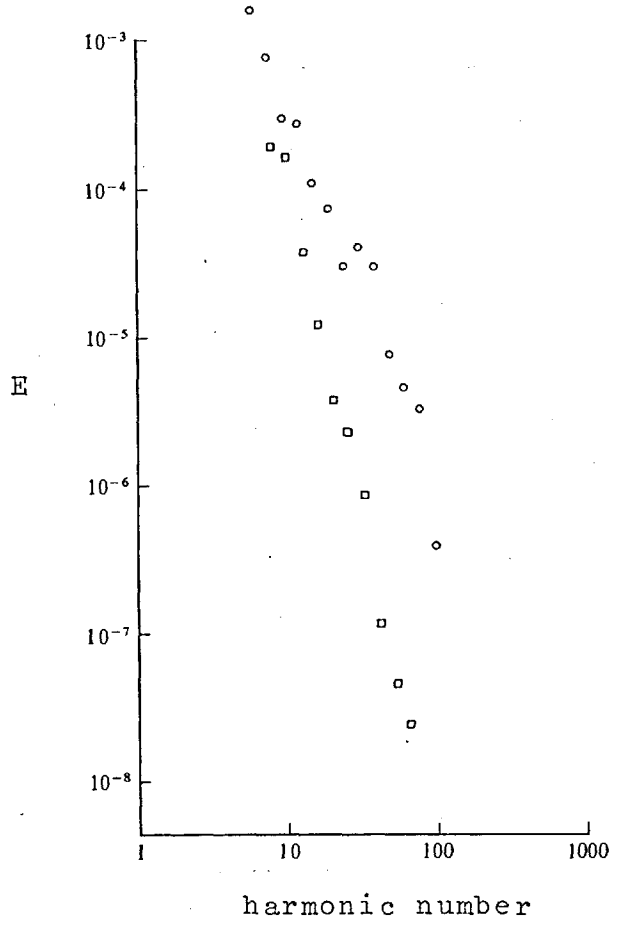

Fig.45 Energy spectra (derived as in Appendix A) for high frequency components of flow in the descending aorta.
○ dog 41, isoprenaline infusion - highly disturbed;
□ dog 41, control - undisturbed.

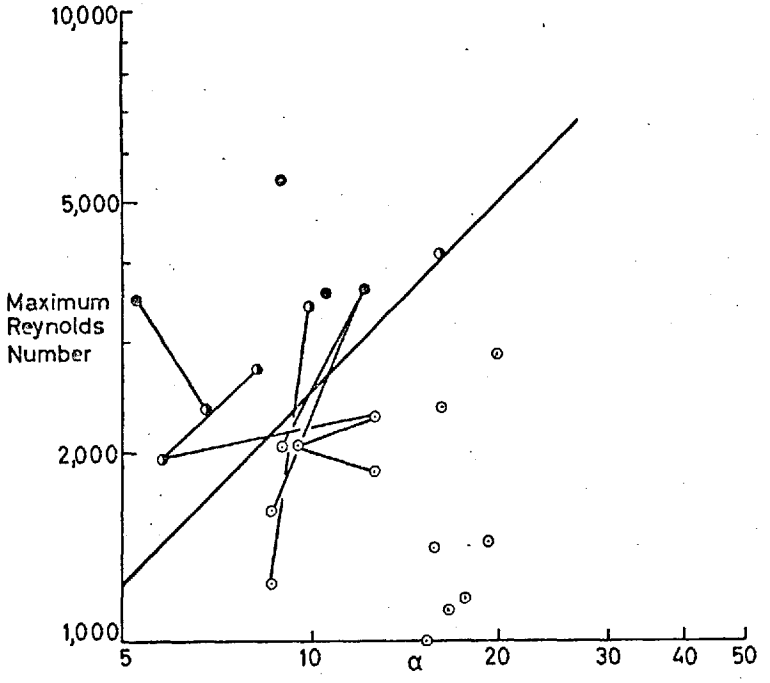

Fig.46 Reynolds number and α for the descending aorta.
○ undisturbed flow
◐ disturbed flow
◉ highly disturbed flow.
The line corresponds to equation(1) in the text.

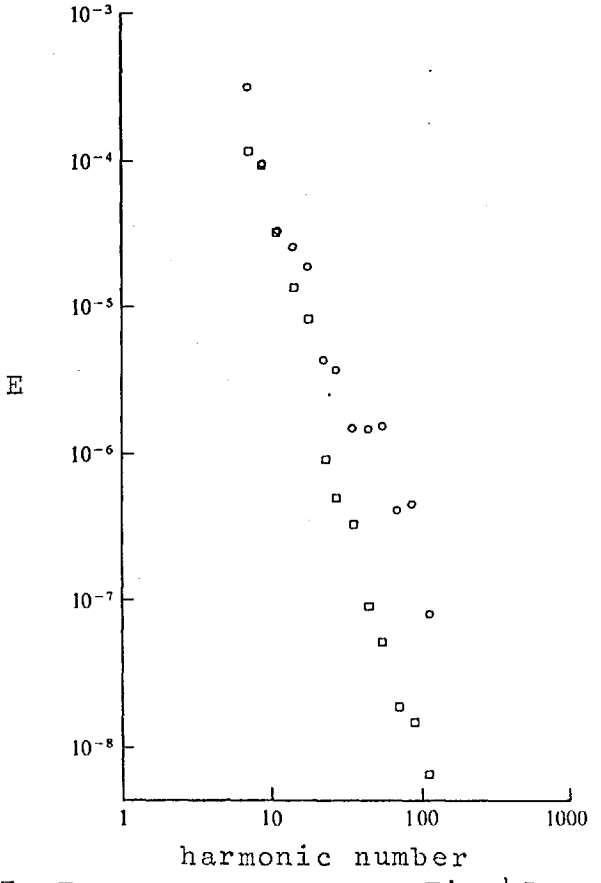

Fig.47 Energy spectra, as Fig.45.
○ aortic arch) dog 40,
□ descending aorta) isoprenaline infusion.

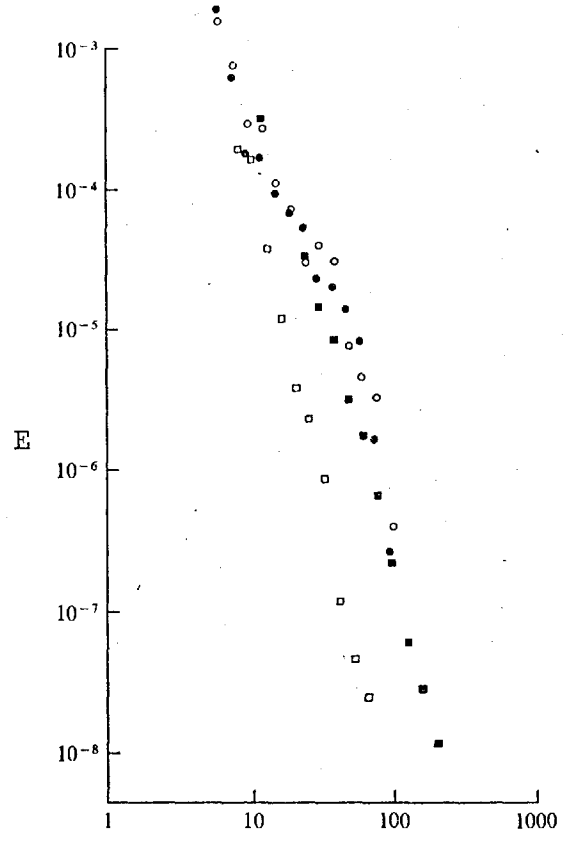

Fig.48 Energy spectra, as Fig.45. Dog 41.

▣ ascending aorta, control
□ descending aorta, control
◎ ascending aorta, isoprenaline
○ descending aorta, isoprenaline.

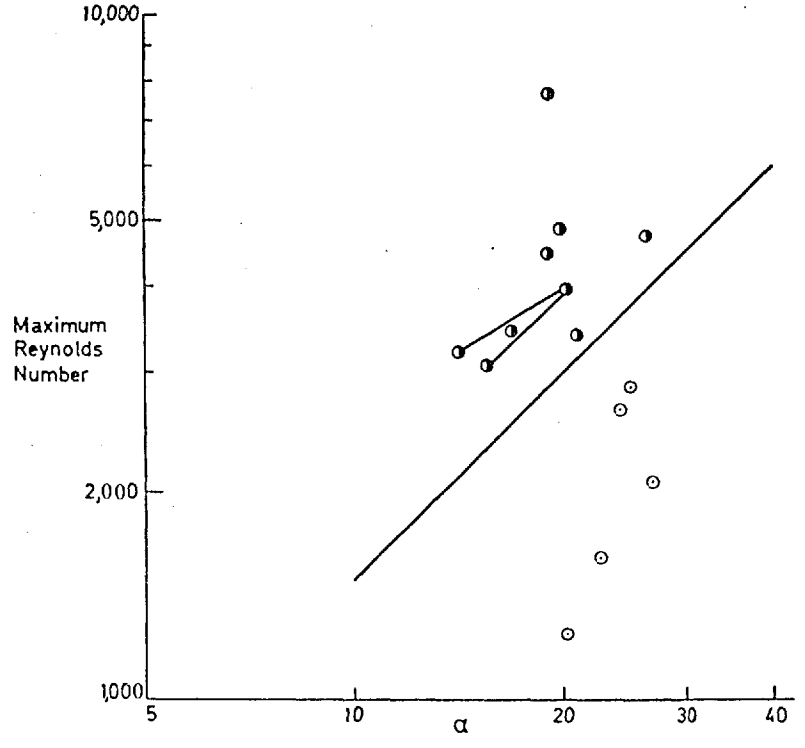

Fig.49 Reynolds number and α for the ascending aorta. Symbols as Fig.46. The line represents equation (2) in the text.

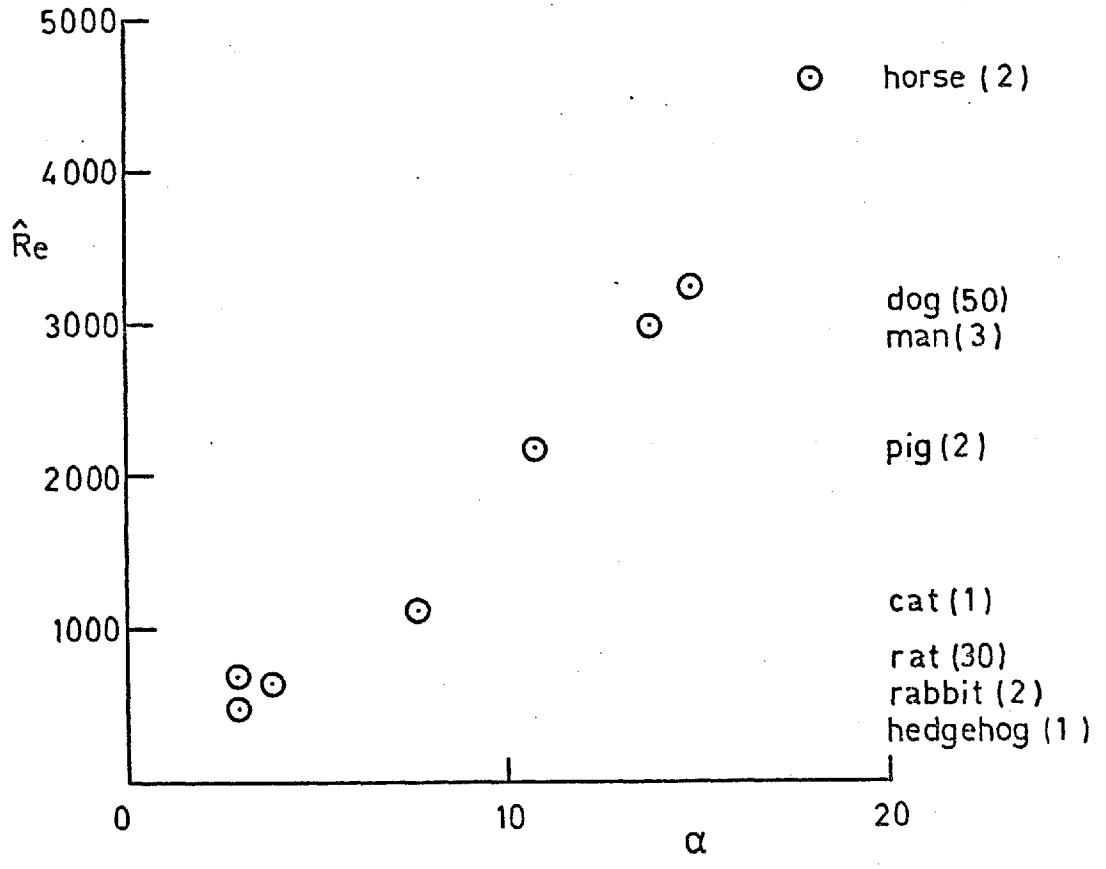

Fig.50 Reynolds number and α for the aorta in a range of animal species. The number of measurements for each species is given, and the points are derived by averaging. Sources for the dog are cited with Fig.51. Other sources are:

Adams et al (1969) - cat
Kirkebø (1968) - hedgehog
Ling et al (1969) - pig
McDonald (1952) - rabbit
Pfeffer & Frohlich (1972) - rat
Rumberger et al (1972) - horse

The measurements were all made in animals under anaesthesia.

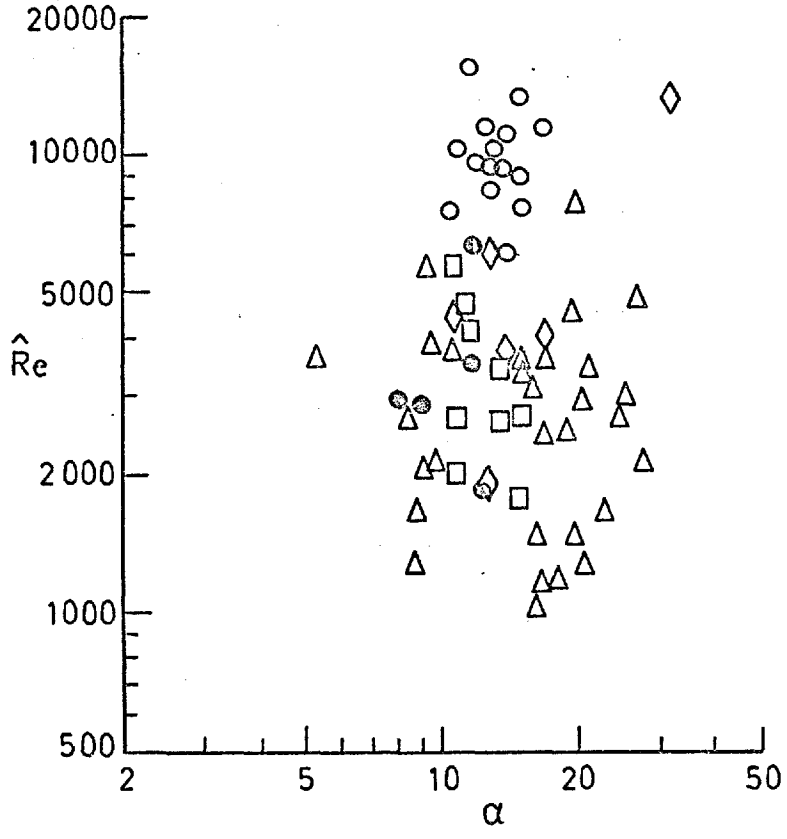

Fig.51 Reynolds number and α for the dog aorta. Sources are:

- ◉ Ling et al (1969)
- ○ Noble et al (1966) - resting, conscious dogs
- ◇ Schultz et al (1969)
- □ Spencer & Greiss (1962)
- ◐ Spencer, Johnston & Denison (1958)
- △ This study.

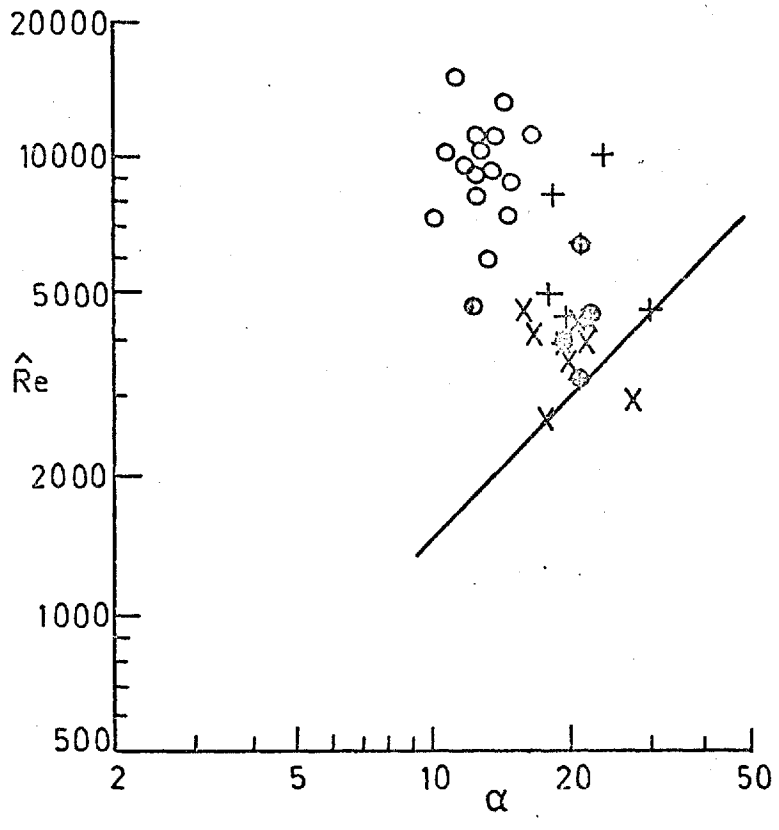

Fig.52 Reynolds number and α for the ascending aorta of conscious dogs and man. The line corresponds to equation (2) in the text. Sources are:

dog: ○ Noble et al (1966)
◐ Spencer, Johnston & Denison (1958)

man: + Prec et al (1949)
× Snell et al (1965)
⊕ Gabe et al (1969)

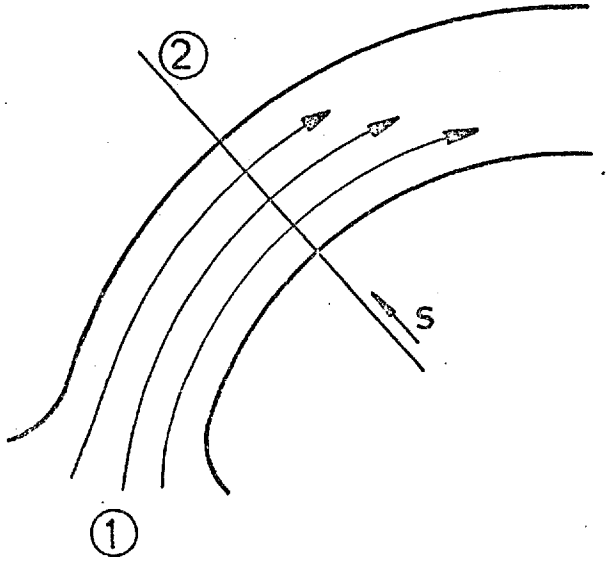

Fig.53 Schematic drawing of flow in the proximal aorta.